Universidade de Aveiro Departamento de Física
2017

Cátia Sofia Jorge Leitão

Sensores de fibra ótica como tecnologia não-invasiva para avaliação da pressão arterial central

Optical fibre sensors as a non-invasive technology to the central arterial pressure assessment

Universidade de Aveiro Departamento de Física
2017

Cátia Sofia Jorge Leitão

Sensores de fibra ótica como tecnologia não-invasiva para avaliação da pressão arterial central

Optical fibre sensors as a non-invasive technology to the central arterial pressure assessment

Tese apresentada à Universidade de Aveiro para cumprimento dos requisitos necessários à obtenção do grau de Doutor em Engenharia Física, realizada sob a orientação científica do Doutor João de Lemos Pinto, Professor Catedrático do Departamento de Física da Universidade de Aveiro, do Doutor Paulo Sérgio de Brito André, Professor Associado do Departamento de Engenharia Eletrotécnica e de Computadores do Instituto Superior Técnico da Universidade de Lisboa e do Doutor José Adelino Mesquita Bastos, Professor Adjunto Convidado da Escola Superior de Saúde da Universidade de Aveiro e Médico Cardiologista do Centro Hospitalar do Baixo Vouga.

Apoio financeiro da FCT e do FSE no âmbito do III Quadro Comunitário de Apoio (bolsa de doutoramento SFRH/BD/84076/2012)

Ao André
Aos meus pais e irmão

o júri

Presidente

Doutora Ana Isabel Couto Neto da Silva Miranda
professora catedrática do Departamento de Ambiente e Ordenamento da Universidade de Aveiro

Doutor Carlos Manuel Bolota Alexandre Correia
professor catedrático do Departamento de Física da Universidade de Coimbra

Doutor Pierre Boutouyrie
professor de farmacologia da Universidade Paris Descartes

Doutora Ana Luísa Nobre Fred
professora associada do Departamento de Bioengenharia do Instituto Superior Técnico da Universidade de Lisboa.

Doutora Margarida Maria Resende Vieira Facão
professora auxiliar do Departamento de Física da Universidade de Aveiro

Doutor João de Lemos Pinto
professor catedrático do Departamento de Física da Universidade de Aveiro

agradecimentos

Como autora deste trabalho, sinto que este não é apenas meu, mas de todos aqueles que me ajudaram e apoiaram neste percurso. Começo por agradecer aos meus orientadores. Ao Prof. Lemos Pinto pela oportunidade de poder realizar este trabalho, incentivando-me sempre a dar o meu melhor. Ao Prof. Mesquita Bastos, pelos conselhos e extraordinárias oportunidades que me proporcionou durante estes quatro anos. Ao Prof. Paulo André, que apesar na distância física, nunca fez notar a sua ausência, estando sempre disponível para me ajudar.

Aos meus colegas e amigos do Departamento de Física e Instituto de Telecomunicações, pelas conversas e boa disposição! Agradeço ao Carlos Marques, pela gravação das redes de Bragg utilizadas neste trabalho. Ao Steve Gonçalves pela valiosa contribuição na execução da interface gráfica para análise de dados. Um agradecimento muito especial ao Paulo Antunes, pelo companheirismo e pelo papel fundamental na realização deste trabalho, assim como à Nélia Alberto, pela amizade, compreensão e pela leitura deste documento. Aos docentes e funcionários, pela disponibilidade e amizade, especialmente ao Sr. Ivo Mateus e Miguel Rocha por todo o trabalho realizado na oficina de metalomecânica.

À Doutora Vera Afreixo, pelo apoio à análise de dados.

Ao grupo de Eletrónica e Instrumentação do Departamento de Física da Universidade de Coimbra, liderado pelo prof. Carlos Correia, por todo o apoio no início deste trabalho.

À equipa *Pathophysiology, Pharmacology and Imaging of Large Arteries* do *Paris – Cardiovascular Research Center* do *European Georges Pompidou Hospital* quero expressar a minha gratidão pela forma como fui recebida por todos, foi um verdadeiro privilégio. Um agradecimento especial aos Profs. Stephane Laurent e Pierre Boutouyrie, Dr. Hakim Kettab e Eng. Louise Marais.

Ao serviço de Cardiologia do Centro Hospitalar do Baixo Vouga, deixo os mais sinceros agradecimentos pela amabilidade com que sempre me receberam, assim como pelo apoio prestado. Agradeço especialmente ao Dr. José António, chefe do Serviço de Cardiologia, à Dra. Catarina Gabriel e Dra. Verónica Ribau, pela constante disponibilidade.

Agradeço também a colaboração extraordinária de toda a equipa da Unidade de Intervenção Cardiovascular do Hospital Geral do Centro Hospitalar e Universitário de Coimbra, em particular ao Dr. Marco Costa, Dra. Raquel Fernandes, Dr. Romeu Cação, Dra. Susana Margalho, Dr. Luís Paiva, Dr. Toni de Sousa, Dr. Joana Silva, Dra. Rafaela Ramos e Prof. Lino Gonçalves, foi verdadeiramente um prazer conhecer-vos e partilhar um pouco do vosso conhecimento!

A todos os voluntários que participaram nos estudos apresentados nesta dissertação, pela disponibilidade e boa vontade.

À Fundação para a Ciência e Tecnologia, por tornar financeiramente viável este trabalho. Ao Instituto de Nanoestruturas, Nanomodelação e Nanofabricação, Departamento de Física e Instituto de Telecomunicações pelas condições de acolhimento proporcionadas no desenvolvimento do trabalho apresentado nesta dissertação.

A todos os meus amigos, que estão comigo nas vitórias e me amparam nas derrotas, por acreditarem em mim, por vezes mais que eu mesma. Um agradecimento especial à Catarina, companheira de ensino secundário e de doutoramento, pela alegria contagiante e amizade. À Joana, que pela sua genuinidade e amizade, me inspira todos os dias, obrigada por todo o apoio, inclusive na leitura desta tese.

À minha família, especialmente aos meus pais e irmão, pelos valores que me incutiram desde cedo e por terem facilitado o meu percurso académico.

Ao André, pelo apoio, disponibilidade, e serenidade que me proporcionou durante a execução deste trabalho.

O meu sincero obrigada a todos.

palavras-chave

Sensores de fibra ótica, pressão arterial central, análise da onda de pulso, hipertensão, POF, FBG, sensores baseados em intensidade

resumo

Com o presente trabalho pretendeu-se explorar soluções de fibra ótica na aquisição da onda de pulso na artéria carótida, para análise da sua morfologia e cálculo da pressão arterial central.

Foram desenvolvidos três sistemas, dois baseados em redes de Bragg, gravadas em fibra de sílica, e outro em modulação de intensidade, usando fibra ótica de plástico.

O primeiro sensor foi desenvolvido com o objetivo de testar a exequibilidade da utilização de fibra ótica nesta aplicação. Após resultados promissores da sua caracterização e testes em sujeitos, o desenvolvimento dos dois sensores consequentes teve por objetivo o aumento da sensibilidade e facilidade de utilização das sondas, pela melhoria da sua forma, portabilidade e autonomia.

A solução baseada em intensidade mostrou-se ainda como um sistema que coligava desempenho a baixo custo, tendo por isso sido submetida a um estudo pré-clínico, comparando o seu desempenho ao de um dispositivo comercial, de natureza eletromecânica, numa pequena coorte de indivíduos saudáveis. Este estudo teve como objetivo investigar a correlação dos resultados obtidos com a sonda de fibra ótica e o dispositivo comercial. Tendo-se obtido uma correlação muito forte entre as duas técnicas, o dispositivo foi proposto para avaliação clínica. O desempenho da sonda foi assim comparado a um dispositivo comercial, numa coorte de indivíduos hipertensos. Foram também levados a cabo testes invasivos, usando como referência ondas de pressão obtidas no lúmen da artéria aorta em contexto de cateterismo cardíaco. Em ambos os estudos clínicos foram obtidos coeficientes de correlação muito fortes e diferenças de pressão média na gama obtida para dispositivos comerciais. Conclui-se assim que o dispositivo baseado em modulação de intensidade surge como uma promissora alternativa de baixo custo aos dispositivos eletromecânicos de avaliação de pressão arterial central disponíveis no mercado.

keywords

Optical fibre sensors, central arterial pressure, pulse wave analysis, hypertension, POF, FBG, intensity based sensors

abstract

The present study aimed to explore fibre optic solutions in the acquisition of the pulse wave in the carotid artery, to its morphology analysis and central arterial pressure calculation.

Three systems were developed, two based on Bragg gratings, engraved in silica fibre, and another on intensity modulation, using plastic optical fibre.

The first sensor was developed in order to test the feasibility of the fibre optics use in this application. After promising results in the characterization and small tests in subjects, the development of the consequent two sensors had as main goals increasing the probes sensitivity and user-friendliness, by improving its shape, portability and autonomy.

The intensity-based solution proved to be the system that best combined performance to low cost, and thus was subjected to a pre-clinical study, comparing its performance to a commercial device in a small cohort of healthy individuals. This study aimed to investigate the correlation between the results obtained with the fibre optic probe and the commercial device.

Having been obtained a very strong correlation between the two techniques, the device was proposed for clinical evaluation. The probe's performance was therefore compared to a non-invasive commercial device, in a cohort of hypertensive individuals. Invasive testing was also performed, using as reference pressure waves obtained in the lumen of the aortic artery in cardiac catheterization context.

In both trials very strong correlation coefficients were obtained, as well as medium pressure differences in the range verified for commercial devices. It is concluded that the device based on intensity modulation arises as promising low cost alternative to central arterial pressure assessment electromechanical devices available in the market.

symbols and constants

α	Thermal expansion coefficient of the fibre
α_a	Wall rigidity coefficient
A_{cs}	Arterial cross-sectional area
A_{diast}	Diastolic arterial cross-sectional area
a_d	Vessel diameter
a_h	Vessel wall thickness
a_l	Vessel length
a_r	Vessel radius
Δ	Difference
Δcf	Direct difference between superficial carotid and femoral locations
$\Delta\lambda_B$	Bragg wavelength variation
Δl	Mechanical perturbation
ΔP	Pressure difference
Δs	Distance between two arterial sites
ΔT	Temperature variation
Δt	Time delay of two arterial pulses assessed in two different locations
d	Distance
ε_z	Longitudinal strain
E	Young's modulus
F	Blood flow
f_{length}	Fibre length
f_r	Fibre radius
ζ	Thermo-optic coefficient
η	Blood viscosity

h	Distance between the fibre centre and the extremity of the emission cone
θ_c	Critical angle
θ_i	Angle of incidence
θ_{max}	Maximum angle of a ray to enter the fibre
θ_t	Maximum angle of a transmitted ray
I_C	Collected intensity
Λ	Bragg grating period
λ	Light wavelength
λ_B	Bragg wavelength
n_{core}	Refractive index of the fibre core
n_{clad}	Refractive index of the fibre cladding
n_{eff}	Effective refractive index
n_{medium}	Refractive index a determined medium
n_{out}	Refractive index of the fibre exterior medium
π	3.14159265359
ρ	Blood density
p	Significance level
$P1$	Pressure at the artery's onset
p_{11}	Component of the strain-optic tension
p_{12}	Component of the strain-optic tension
$P2$	Pressure at the artery's end
P_E	Emitted power
P_e	External pressure
p_e	Effective strain-optic constant
P_i	Internal pressure
p_{length}	Propagation length

P_t	Transmural pressure
p_{wave}	Pressure wave function
$p_{wavetest}$	Pulse wave values obtained with the tested technique
$p_{waveref}$	Pulse wave values obtained with the reference technique
R	Resistance
r	Correlation coefficient
r^2	Determination coefficient
T	Arterial wall tension
$t_{Diastole}$	Systole duration
$t_{Systole}$	Diastole duration
ν	Poisson's ratio
V	V-parameter

acronyms

A	Afternoon
AA	Afternoon average pulse
AAMI	Association for the advancement of medical instrumentation
ABPM24	24-hour ambulatory blood pressure monitoring
ADC	Analog-to-digital converter
AE	Immediately after exercising
AE2	2 minutes after exercising
AE4	4 minutes after exercising
AIx	Augmentation index
AIx%	Augmentation index in percentage
AM	Morning average pulse
a. u.	Arbitrary units
BMI	Body mass index
BP	Blood pressure
BPM	Beats per minute
CHBV	Centro Hospitalar do Baixo Vouga
CHUC-HG	Centro Hospitalar e Universitário de Coimbra – Hospital Geral
cPP	Central pulse pressure
cSP	Central systolic pressure
CV	Cardiovascular
CVD	Cardiovascular disease
D	Significantly different
DP	Diastolic arterial pressure
ESC	European Society of Cardiology

ESH	European Society of Hypertension
FBG	Fibre Bragg grating
FF	Form factor
FF%	Form factor as percentage
FW	Forward wave
GTF	Generalized transfer function
GUI	Graphical user interface
HDL	High Density Lipoprotein
HR	Heart rate
HT	Hypertension
HVPZT	High-voltage piezoelectric amplifier
ICC	Intraclass correlation coefficient
IFS	Intensity fibre sensors
IMT	*Intima-media* thickness
IR	Infra-red
KrF	Krypton fluoride
LDL	Low density lipoprotein
M	Morning
MAP	Mean arterial pressure
MRI	Magnetic resonance imaging
NA	Numeric aperture
ND	Non-significantly different
n_p	Number of points
ns	Non-significant
n_{sub}	Number of subjects
OFS	Optical fibre sensors
PCC	Pearson correlation coefficient

PD	Photodetector
PMMA	Poly(methyl 2-methylpropenoate) / poly(methyl methacrylate)
POF	Plastic optical fibre
PP	Pulse pressure
PPG	Photoplethysmography
pSP	Peripheral systolic pressure
PWA	Pulse wave analysis
PWV	Pulse wave velocity
PZT	Piezoelectric
R	Resting
RMSD	Root-mean-square deviation
RMSD%	Root-mean-square deviation in percentage
RW	Reflected wave
SCC	Spearman correlation coefficient
SCORE	Systematic coronary risk evaluation
SD	Standard deviation
SOF	Silica optical fibre
SP	Systolic arterial pressure
UV	Ultraviolet
y	Years old

index of contents

1

Introduction

1.1. Motivation

Cardiovascular diseases (CVDs) are the prime cause of death in developed countries, and consequently worldwide organizations have been gathering efforts to evolve strategies to counteract this trend. In the 2016 “European guidelines on cardiovascular disease prevention in clinical practice”, cardiovascular (CV) prevention is defined as a coordinated set of actions at the population level or targeted at an individual, that aim to eliminate or minimize the impact of CVDs and their related disabilities (Piepoli *et al*. 2016). When the subject-matter is CVDs, prevention has a key role in reducing its prevalence, being not only important to identify the predominant risk factors, as much as make sure that the preventive measures are implemented as stated and are translated in death rate decreasing. The European task force working on cardiovascular prevention, states that the elimination of health risk behaviours would make it possible to prevent at least 80 % of CVDs and 40 % of cancers (Piepoli *et al.* 2016). Portugal is no exception when it comes to CVDs, as it can be observed in Fig. 1.1, in the top 10 death causes of 2013, CVDs prevail as the main cause (DGS 2015).

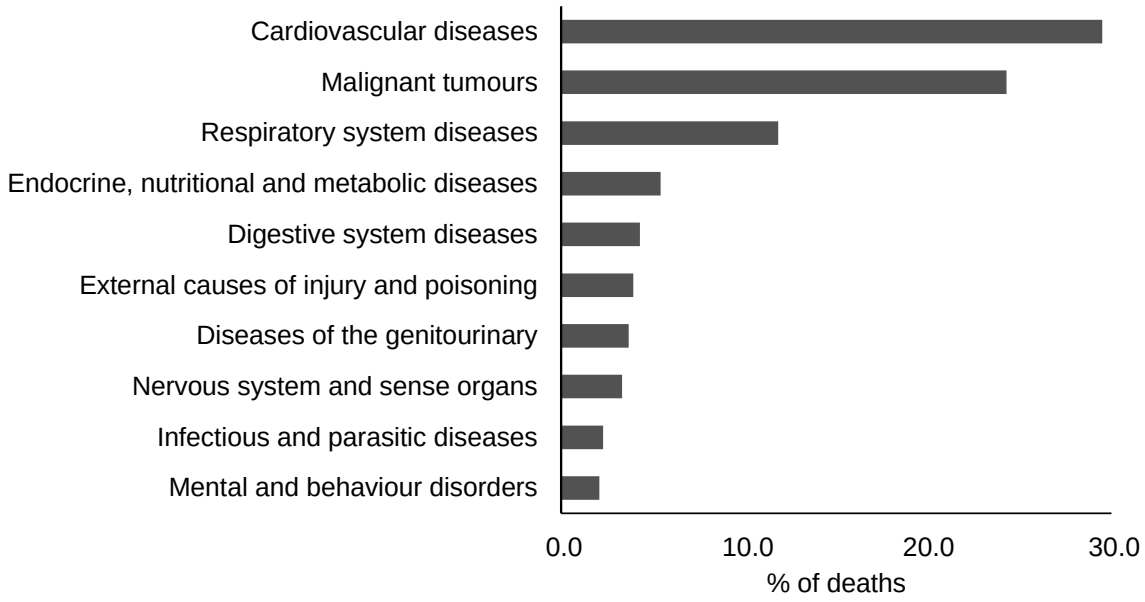

Figure 1.1. Top ten causes of death in Portugal of 2013 (data from DGS 2015).

The World Heart Federation stated that the majority of CVDs is caused by risk factors that can be controlled, treated or modified, such as high blood pressure (BP), cholesterol levels and body mass index (BMI), as well as, smoking habits, sedentary lifestyle and diabetes. In terms of attributable deaths, the leading CVD risk factor is high BP (with 13 % of global deaths attributed), followed by tobacco use (9 %), raised blood glucose (6 %),

physical inactivity (6 %) and overweight, and obesity (5 %). On the other hand, there are also major CVD risk factors that cannot be controlled, such as, age, gender and family history (WHO 2011).

Hypertension (HT) is the leading cause of CVDs worldwide, and it is estimated that in 2025, 1.56 billion adults will be living with HT (WHO 2016). Risk stratification is of extreme importance, since only a small fraction of the hypertensive population has a BP elevation alone, with its majority exhibiting additional CV risk factors. Moreover, when concomitantly present, HT and other CV risk factors have not a simple additive effect, they potentiate each other in an exponential way, leading to a total CV risk that is greater than the sum of its individual components. The cardiovascular risk factors, besides HT, are presented on Fig. 1.2, being male gender (at younger age), age, smoking habits, high levels of cholesterol and triglycerides, diabetes, obesity and family history (Mancia *et al.* 2013).

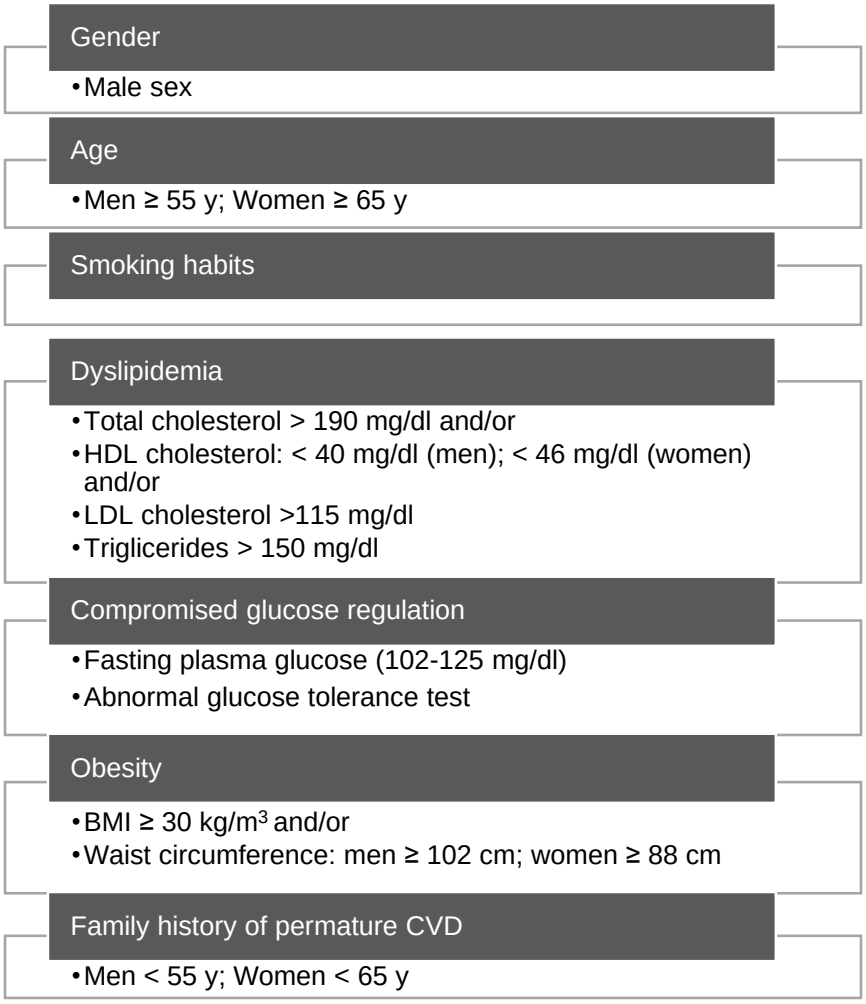

Figure 1.2. Risk factors, besides HT, influencing CVD prognosis (HDL - high density lipoprotein, LDL - low density lipoprotein, y - years) (data from Mancia *et al.* 2013).

An ideal scenario would be for all adults to have their CVD risk assessed, however that is not always practicable. Physicians evaluate cardiovascular risk every day and risk charts are important to standardize the risk assessment process. Apparently healthy subjects' total risk should be assessed by using the systematic coronary risk evaluation (SCORE) charts. On the other hand, people with established CVDs are already at very high risk of further events and need rapid intervention on all risk factors (Piepoli *et al.* 2016). SCORE is a risk chart with the aim to estimate the 10-year risk of a first fatal atherosclerotic event, whether heart attack, stroke, aneurysm of the aorta, or other. Distinction is made between countries with high and low CV risk, being the latter the case of Portugal. The SCORE charts for low risk European countries are presented in Fig. 1.3. The charts retrieve the 10-year CV risk, taking in consideration the subject's age, smoking status, cholesterol level and brachial systolic arterial pressure (SP), attributing the percentage in the square corresponding to the overall subject's parameters.

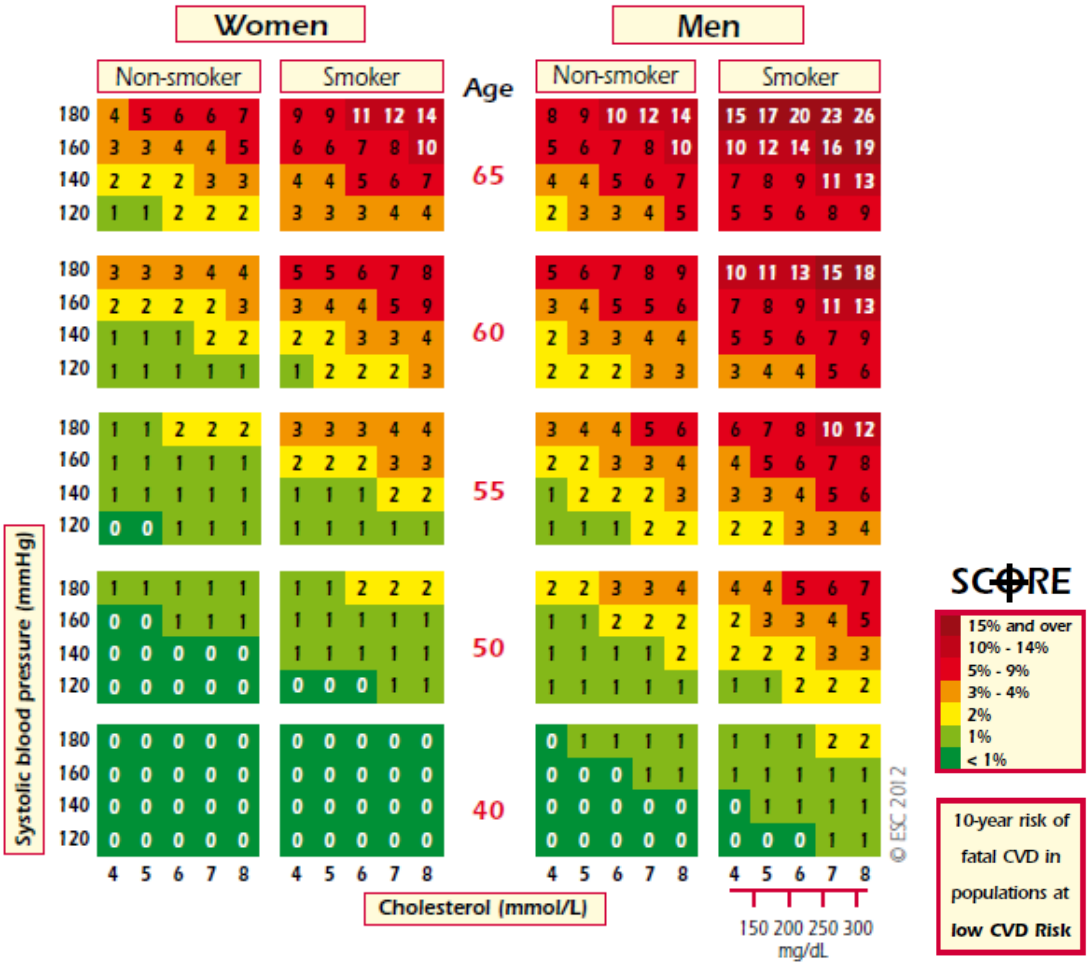

Figure 1.3. SCORE chart for 10-year risk of fatal CVD in countries with low CVD risk (adapted from the *European SCORE Memocard*).

A key factor on cardiovascular prevention is thus HT control, once it is responsible for a great part of cardiovascular events, such as cerebrovascular accidents and ischemic heart disease (Safar *et al.* 2003). The last "European Guidelines for the management of arterial hypertension" report an overall prevalence of HT in around 30 to 45 % of the general population, increasing sharply with age. HT is known as the "silent killer" and therefore many people who suffer from this condition are unaware of it. As stroke major cause, HT prevalence in different countries is usually assessed using its mortality rate as surrogate (Mancia *et al.* 2013).

The approaches for HT monitoring and treatment have changed over time. The first accurate description of how blood is pumped throughout the body by the heart was made by William Harvey in 1628, in his book entitled "Exercitatio Anatomica de Motu Cordis et Sanguinis in Animalibus" ("An Anatomical Study of the Motion of the Heart and of the Blood in Animals") (BBC 2016). More than a century later, Stephen Hales (1677-1761) reported the first direct invasive measurement of blood pressure on animals (Lewis 1994).

Another century passed until, in 1863, Étienne-Jules Marey introduced the first graphic method for arterial pulse wave recording (Fig. 1.4a). The created device used a mechanical membrane and a lever system to write the radial pulse waveform directly on smoked paper (Marey 1863; Avolio *et al.* 2010). In his studies, Marey remarked pulse characteristic differences between young and old subjects, having verified a prominent late systolic augmentation in the latter.

The pulse wave changes, from the youth to older age, were later confirmed by Mahomed in the 1870s, noticing similar pulse waveform changes between asymptomatic subjects with elevated arterial pressure and the elderly (Mahomed 1872). In the beginning of the twentieth century, arterial pulse wave morphology was used by life insurance companies to accept or decline applicants, on the basis of their arterial conditions (O'Rourke and Nichols 2005). The non-invasive measure of brachial pressure was enabled in 1896 by Riva-Rocci, who published the invention of the mercury sphygmomanometer, schematically showed in Fig. 1.4b (Riva-Rocci 1896).

During the third decade of the past century, the development of the electrocardiogram and occlusive cuffs for blood pressure measurement, lead clinicians to focus on the extreme values of blood pressure (Vlachopoulos *et al.* 2000; Avolio *et al.* 2010).

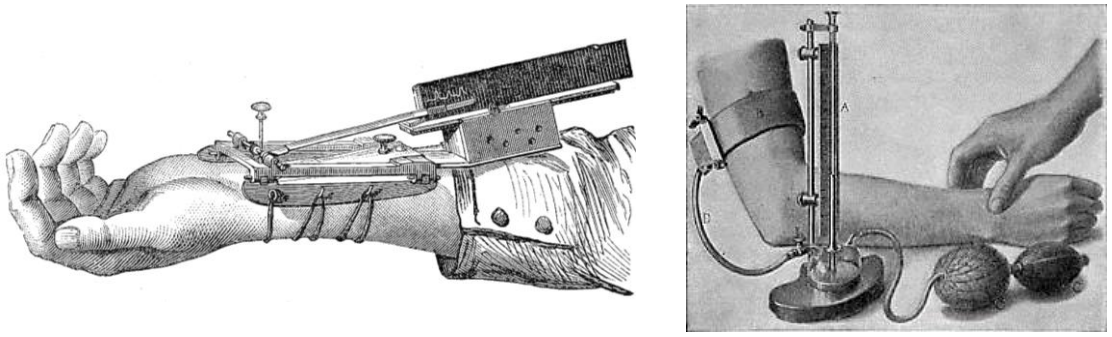

a) b)

Figure 1.4. Diagrams of: a) Marey's device for arterial pulse assessment (Marey 1863) and b) Riva-Rocci's mercury sphygmomanometer (Janeway 1904).

For the subsequent decades, diastolic arterial pressure (DP) values were considered best predictors of cardiovascular diseases. The resistance that the heart had to overcome was measured by DP, while SP represented the cardiac strength. At that time, the high SP was considered to have a positive CV outcome, whereas it is now known that SP value represents the pressure that the left ventricle have to overcome in each systole.

Only in the seventies and eighties, Kannel *et al.* demonstrated that SP was a better predictor for coronary and stroke events, changing completely the hypertension treatment paradigm (Kannel *et al.* 1971; 1981). Another interesting turn key moment happened in 1989, when Darne *et al.* drew attention to pulse pressure (PP - difference between diastolic and systolic pressures) as an important CVD risk factor (Darne *et al.* 1989). Since then, growing evidence has emerged, indicating that this index of the pulsatile component of blood pressure was a strong predictor of CV events. Associated with that concept, it was also found that in older patients, the lower the DP, the higher the event rate (Vlachopoulos *et al.* 2000).

In the past two decades, blood pressure measurement and HT diagnosis and control have been made by assessing the extreme values of peripheral arterial pressure (SP and DP) using sphygmomanometers. Currently, a subject is considered hypertensive when presenting office BP values of SP ≥ 140 mmHg and/or DP ≥ 90 mmHg, within at least two BP measures taken in sitting position in two separate visits, using a validated device. The different BP categories currently considered are presented on Table 1.1.

Several other studies have shown that HT diagnosis should not be performed only based in the standard office BP measurements, but also by taking in consideration out-of-office

BP values or, if available, 24-hour ambulatory BP monitoring (ABPM24) data, whose thresholds are presented on Table 1.2 (Mancia *et al.* 2013).

Table 1.1. HT categories accordingly to office BP levels (data from Mancia *et al.* 2013)

Category	SP (mmHg)		DP (mmHg)
Optimal	< 120	and	< 80
Normal	120 -129	and/or	80-84
High normal	130 -139	and/or	85-89
Grade I HT	140 -159	and/or	90-99
Grade II HT	160 -179	and/or	100-109
Grade III HT	≥ 180	and/or	≥ 110
Isolated systolic HT	≥ 140	and	< 90

Table 1.2. HT diagnosis thresholds accordingly to office, ABPM24 and home BP values (data from Mancia *et al.* 2013)

Category	SP (mmHg)		DP (mmHg)
Office BP	≥ 140	and/or	≥ 90
Home BP	≥ 135	and/or	≥ 85
ABPM24			
Day time (or awake)	≥ 135	and/or	≥ 85
Night time (or asleep)	≥ 120	and/or	≥ 70
24-hours	≥ 130	and/or	≥ 80

AMBP24 involves measuring BP at regular intervals (usually every 15 and 30 minutes, in day and night time, respectively) over a 24-hour period, while patients undergo normal daily activities, including sleep. This ambulatory monitoring technique has the advantages of excluding white coat and masked HT, allowing also the monitoring of the BP decrease/increase patterns during night, day, and sleep/awake transition. The cut-off value for home BP (or daytime ambulatory BP) is 135/85 mmHg. ABMP24 had become the gold-standard in HT diagnosis and is now widely applied (Mesquita-Bastos *et al.* 2010).

Concurrently, several studies have been demonstrating that the arterial systolic pressure in aorta, usually known as central systolic pressure (cSP), cannot be directly inferred from brachial values (O'Rourke 1990; Roman *et al.* 2007). The publication of the "Conduit

Artery Function Evaluation" study had a major impact on hypertension approach, since it was the first report demonstrating significant differences in cSP reduction, between patient groups treated with different antihypertensive regimens, even though brachial SP was comparably lowered (Williams *et al.* 2006; Miyashita *et al.* 2012). This study showed that the effects of antihypertensive drug treatments on brachial BP do not invariably reflect those seen on central pressure. Consequently, the research on hypertension monitoring and treatment have been changing, clarifying the importance of cSP and arterial stiffness assessment for a proper risk stratification in the hypertensive population (Avolio *et al.* 2010).

It can be concluded, as exposed by the European Societies of Hypertension (ESH) and Cardiology (ESC), as well as by several scientific studies (Avolio *et al.* 2009; Mesquita-Bastos *et al.* 2010; Benetos *et al.* 2011; Chirinos *et al.* 2012; Mancia *et al.* 2013), that HT monitoring, should be performed by self-measurements at home, ABPM24, central arterial stiffness evaluation with the assessment of aortic pulse wave velocity (PWV) and analysis (PWA), cSP, cPP and central-to-peripheral pressure amplification.

The guidelines acknowledged the non-invasive methods for the assessment of central hemodynamic parameters, but highlighted the need for large scale interventional studies for further confirmation of the prognostic importance of central blood pressure. cSP evaluation is not set in clinical practice, even though its clinical evidence as predictive value for CVDs (Roman *et al.* 2007; Pini *et al.* 2008; McEniery *et al.* 2014). The main motives that can be pointed out for the overall reluctance in performing those measurements are: the amount of training need to perform the measurements correctly, the lack of stablished threshold values for some pulse wave parameters and the overall high cost of pulse acquisition devices. For all the mentioned, it is safe to say that the development of easy to use, robust and low cost devices to assess central haemodynamic parameters is a need in the cardiology field. In the present work, it was studied the feasibility of optical fibre sensors as new sensitive and low cost methods for arterial pulse wave acquisition.

Modern optical fibre sensors (OFSs) owe their development to two of the great scientific advances made in the 1960s: the laser (1960), by Theodore Maiman, and the optical fibre (1966), originality created for telecommunications, by Charles Kao. The first experiments on low loss optical fibres being used for sensing purposes, go back to the 1970s (Grattan and Sun 2000). To the present, several worldwide research groups investigate new configurations of optical fibre devices for sensing and measurement, using a multiplicity of

fibres and configurations. Although several decades have passed since the introduction of OFSs, and despite their advantages with respect to other mature technologies, only since the last decade OFS had their market growing notably, thanks to the improvement of key optical components and to the decrease of the associated costs (Taffoni *et al.* 2013).

OFS have great advantages when compared with conventional transducers, especially for biomedical applications, due to its high accuracy, robustness, small size and light weight, electrical isolation from the patient, which makes them intrinsically safer than electronic sensors; immunity to electromagnetic interference, being also biocompatible and easy to sterilize (Silvestri and Schena 2011; Alberto *et al.* 2013).

Their unique features make them promising sensors for biomedical applications, namely using fibre Bragg gratings (FBG), written in silica optical fibres (SOF), and intensity modulation, with plastic optical fibres (POF), as reported in several publications (Mishra *et al.* 2011; Roriz *et al.* 2013; Poeggel *et al.* 2015).

Optical fibres began to be applied in the biomedical field with the purpose of illuminating internal organs during endoscopic procedures. During the years, the same technology has been adopted to perform other tasks like laser treatments, and to develop transducers for monitoring parameters of interest for both therapeutic and diagnostic purposes (Taffoni *et al.* 2013). OFS are now widely studied and applied in numerous medical applications, from non-invasive (Quandt *et al.* 2015) and minimally-invasive monitoring (O'Keeffe 2015) of physical properties, such as heart and respiratory rates (Petrovic *et al.* 2014), to more specific biochemical sensing, such as DNA (Giannetti *et al.* 2015).

1.2. Main goals and methodology

The present work had the main goal of testing the feasibility of optical fibre technology application to central arterial pulse wave acquisition. After the first applicability tests using FBGs, the work progression was planned towards the development and validation of a low cost, reliable and robust solution to central arterial pulse acquisition for PWA and cSP evaluations.

The arterial pulse causes distension movements in the order of the 300-400 μm (Benetos *et al*. 1993; Krejza *et al.* 2006). In this work, it was specified a goal resolution of at least 1-5 μm. Each developed sensor that met this requirement was tested in human individuals to assess the sensors performance and accuracy, root-mean-square deviation (RMSD)

was evaluated, regularly also presented in percentage (RMSD%). Only solutions able to assess arterial pulses sequences with at least 6 stable pulses, differing less than 10 % between them, were considered to fulfil the required performance.

A second goal was the manufacturing cost optimization, for which intensity based sensors were developed and tested. Once obtained a low cost solution with sensitivity and resolution according to the requirements, the probe was submitted to a small test comparing it with a commercial non-invasive electromechanical device in young individuals, in order to gather data supporting the optical probe implementation in clinical environment. In this work this testing stage is denominated as pre-clinical study.

After this study, which retrieved supporting data to the probe proposal for clinical evaluation. The intensity based solution was lastly clinically evaluated by testing it against a non-invasive electromechanical commercial device and invasive central pressure data acquired in the ascending aorta.

1.3. Thesis organization

This document is divided in eight chapters describing the process of development and testing of the fibre optic solutions for central hemodynamic monitoring, as well as, it is also presented the results from the clinical evaluation of the probe with the best manufacturing cost/reliability relation, accordingly with the proposed PhD work plan. In the current chapter is described the work context, the motivation for its development, the thesis structure and organization, finalizing with the main scientific contributions.

In Chapter 2, the main principles on central haemodynamics, arterial stiffness indexes and central pressure assessment commercial devices are presented. The theoretical background continues through the Chapter 3, where the fundamentals on optical fibre sensors, more specifically using FBG and intensity configuration, are described.

The developed probes are presented on Chapter 4, being divided in three parts respecting to each developed solution. The first section (4.1) regards the first feasibility test with FBGs, for which a probe named FBGbox was developed. In the section 4.2, an improved version of the FBG solution is presented. This second probe, designated as FBGpen, presented improvements in the shape, to a more user-friendly approach, in sensitivity and portability. After developing these two solutions, the research progressed towards the manufacturing cost reduction, applying an intensity configuration using POF, resulting in

the probe referred to as POFpen, which is presented in section 4.3. The contents on this chapter were previously published as:

- Leitão C, Bilro L, Alberto N, Antunes P, Lima H, *et al.*, "Feasibility studies of Bragg probe for non-invasive carotid pulse waveform assessment," *Journal of Biomedical Optics*, 18:017006, 2013 (section 4.1);
- Leitão C, Antunes P, André P, Pinto J, Bastos J, "Central arterial pulse waveform acquisition with a portable pen-like optical fibre sensor", *Blood Pressure Monitoring Journal*, 20 (1):43-6, 2015 (section 4.2);
- Leitão C, Antunes P, Bastos J, Pinto J, André P, "Plastic Optical Fibre Sensor for Noninvasive Arterial Pulse Waveform Monitoring", *IEEE Sensors Journal*, 15 (1):14-18, 2015 (section 4.3);
- Leitão C, Gonçalves S, Antunes P, Pinto J, Bastos J, André P, "Central arterial pressure assessment with intensity POF sensor", Proc. SPIE, *24th International Conference on Optical Fibre Sensors*, 9634:963424, 2015 (section 4.3);
- Leitão C, Antunes P, Pinto J, Bastos J, André P, "Optical fiber sensors for central arterial pressure monitoring", *Optical and Quantum Electronics*, 48 (3):218, 2016 (section 4.3).

In Chapter 5, the POFpen pre-clinical testing results are presented, which aimed to study its aptitude to be introduced in broader clinical studies, by analysing its accuracy, applicability and correlation with the results of a commercial device. Only POFpen was proposed to be clinically tested because it was the most advantageous probe in terms of working principle and manufacturing costs. The contents of this chapter were published as:

- Leitão C, Antunes P, Pinto J, Bastos J, André P, "Carotid distension waves acquired with a fiber sensor as an alternative to tonometry for central arterial systolic pressure assessment in young subjects", *Measurement*, 95:45-49, 2017.

Chapter 6 reports the non-invasive clinical evaluation of POFpen, performed in the cardiology service of "Centro Hospitalar do Baixo Vouga" (CHBV), using as reference a commercially available and widely used piezoelectric device. Following, the invasive validation performed in the "Unidade de Intervenção Cardiovascular" of "Centro Hospitalar e Universitário de Coimbra – Hospital Geral" (CHUC-HG) is described in Chapter 7. The contents of both chapters will be submitted to publication as:

- Leitão C, Ribau V, Afreixo V, Antunes P, André P, Pinto J, Boutouyrie P, Laurent S, Bastos J, "Clinical evaluation of an optical fibre sensor in the assessment of the central arterial pulse waves", to be submitted to *Journal of Hypertension*.

The content of chapter 7 has already been partially published as:

- Leitão C, Antunes P, Afreixo V, Andre P, Pinto L, Fernandes R, Costa M, Bastos J, "Comparison study of carotid distension waves measured with a non-invasive optical fibre sensor and aortic invasive pressure waves", *26th European Meeting on Hypertension and Cardiovascular Protection*, *Journal of Hypertension*, Vol 34, e-Supplement 2, Paris, September 2016.

In Chapter 8, the final remarks are presented, in which the main conclusions and future work perspectives are discussed.

The references and the publications and communications, made within the scope of this work, are accessible in the end of the document.

1.4. Main contributions

The main contributions of the developed work within this PhD thesis were the design, conception and testing of novel sensors for arterial pulse assessment based on optical fibre technology, and can be summarized as follows:

- Development of two working prototypes, based on FBGs, for the assessment of carotid pulses and calculation of arterial stiffness indexes and central systolic pressure (Chapter 4);
- Development of a simple, robust, portable and low cost solution based on intensity modulation (Chapter 4);
- Pre-clinical studies to ascertain the aptitude of POFpen introduction in broad clinical trials (Chapter 5);
- Non-invasive POFpen clinical evaluation against a reference device used worldwide for arterial pulse assessment, obtaining highly correlated results to the commercial device (Chapter 6);
- Invasive evaluation of POFpen, using as reference intra-aortic pressure waves acquired in catheterization context (Chapter 7).

2

Principles on central haemodynamics and pressure assessment devices

The main goal of this work was to develop optical fibre sensors to perform central haemodynamics assessment through the evaluation of pulse morphology and cSP. In order to fully understand the measured parameters, in this section the fundamentals on arterial anatomy and haemodynamic concepts such as flow, resistance and pressure are presented. This theoretical background will then focus on the effects of arterial stiffening at the central arterial level, and its impact on arterial pulse waveform and cSP. The contents are remarked with the state-of-the-art of commercial devices for arterial pulse acquisition as well as the methods used in their comparison and clinical evaluation.

2.1. Cardiovascular system and arterial anatomy

The cardiovascular system, also known as circulatory system, is a closed circuit composed by three fundamental components: heart, blood and vessels (arteries, veins and capillaries). The heart is a hollow muscular contractile organ divided in four chambers, two atria and two ventricles. The left side of the heart has the role of maintaining the pressure gradient needed for systemic circulation, while the right side is responsible for the pulmonary circulation.

For the systemic circulation, oxygenated blood is ejected from the left ventricle, flowing throughout the arteries and arterioles, to the capillaries located in the multiple body tissues. From the tissue capillaries, the deoxygenated blood returns, by the venous system, to the right atrium of the heart. After what in the pulmonary circulation, blood flows to the right ventricle, being pumped throughout the pulmonary artery to be oxygenated in the alveoli capillary beds. The oxygenated blood returns to the heart, entering the left atrium by the pulmonary vein, beginning a new circulatory cycle (Marieb and Hoehn 2012). The arteries always transport blood away from the heart and veins carry blood towards the heart. In Fig. 2.1, the higher calibre arteries and veins can be schematically seen. Within the scope of this work, the theoretic background is focused only in the systemic circulation.

Each cardiac cycle is divided in two main moments, systole (ventricular contraction and blood ejection) and diastole (ventricular relaxation and blood filling). At the beginning of the systole, pressure rises rapidly in the left ventricle, exceeding the aortic pressure in a very short period of time. When that happens, the aortic valve opens, the blood is ejected, and the aortic pressure rises. About half way through ejection, both pressures equalize, creating an adverse pressure gradient across the aortic valve, being maintained as both pressures start to fall, until the aortic valve closure (Bortolotto and Safar 2006). At this point, and due to its elastic nature, the pressure in the aorta falls slower than in the ventricle, as it acts as a reservoir during systole, storing ejected blood that is then forced out into the peripheral vessels during diastole (Safar 2007).

Both arteries and veins have three distinct layers, or *tunicas*, around the vessel's lumen. The *tunica intima* contains the endothelium, which forms a continuous surface that aims to minimize friction between the blood and the vessels' wall. The second layer is the *tunica media*, mostly composed by smooth muscle cells and elastin. The activity of the smooth muscle is regulated by sympathetic autonomic nervous system and biochemical reactions.

The vasodilation/contraction activities of the *tunica media* are critical in regulating the circulatory dynamics, where small changes in vessel diameter greatly influence blood flow and pressure. Lastly, the *tunica externa* or *adventitia* (the outmost layer), is largely composed by collagen fibres, which have the functions of protecting and reinforcing the vessels, as well as anchoring them to the surrounding structures (Marieb and Hoehn 2012).

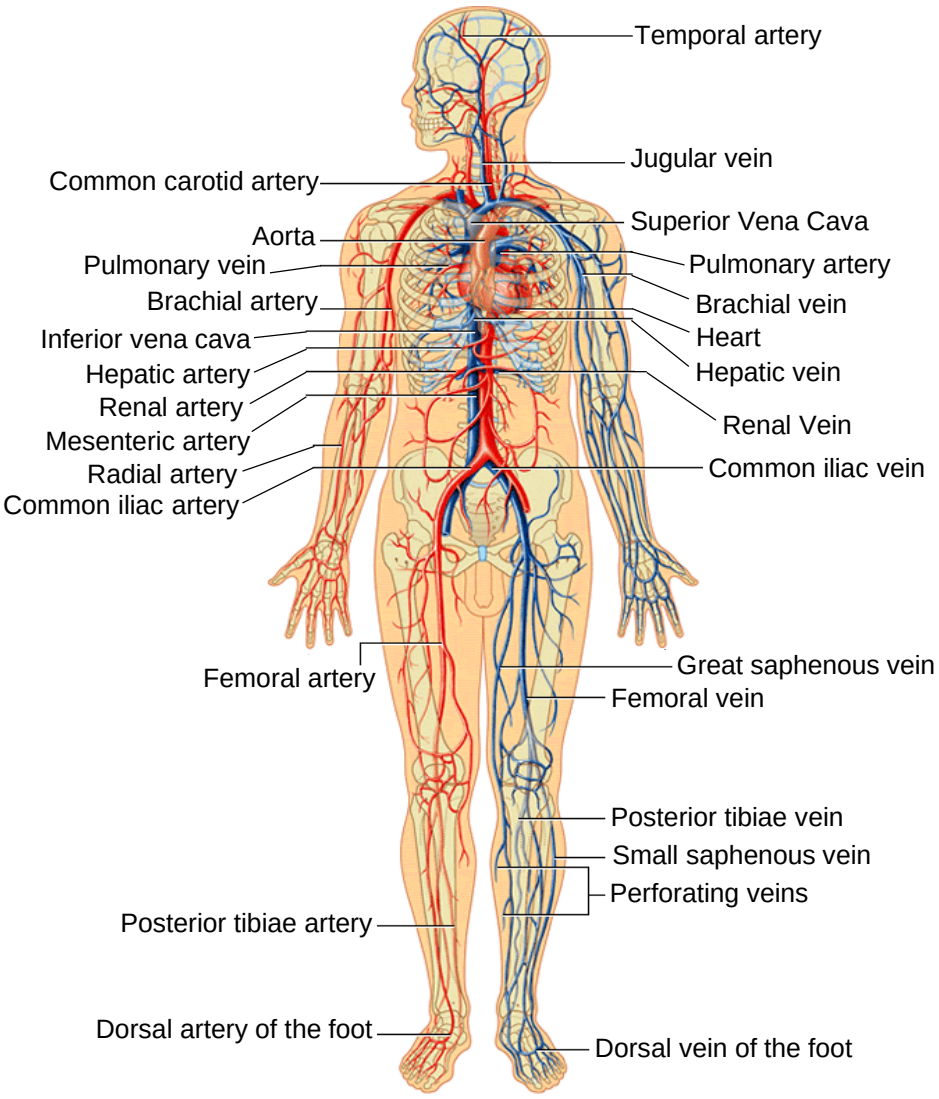

Figure 2.1. Main calibre veins and arteries (adapted from Aviva 2010).

Considering the arterial features from the heart to the peripheral circulatory system, such as calibre, wall structure and function, the arteries can be divided in: elastic, muscular and arterioles (see Fig. 2.2). The elastic central arteries have large lumens, making them low-resistance pathways that conduct blood from the heart to the medium-sized arteries, being for that reason usually referred to as “conducting arteries”. The *tunica media* of

elastic arteries is composed by a high content of elastin laminae, which has the function of damp the surges of blood pressure from the heart, acting as a pressure reservoir. Therefore, during the systole, when the blood is forced into central arteries, their elastin stretches and stores energy. On the other way, during diastole, the fibres recoil and release energy, propelling the blood forward, generating an almost continuous blood flow to the distributing arteries during all the heart cycle. This is known as the Windkessel effect (Westerhof *et al.* 2009).

Examples of elastic arteries are the aorta and the common carotids. The aortic luminal diameter for women is approximately 29 mm and for men 32 mm (Turkbey *et al.* 2013), while the carotid artery estimated diameter varies from 6.1 mm in women to 6.5 mm in men (Krejza *et al.* 2006). Furthermore, the carotid artery distension is reported to be approximately 6.1 % (Benetos *et al.* 1993), being this value obtained in a cohort of 78 normal and hypertensive subjects. Applying the presented carotid diameters, the referred distension translates in diameter changes of 370 µm and 395 µm, for women and men, respectively.

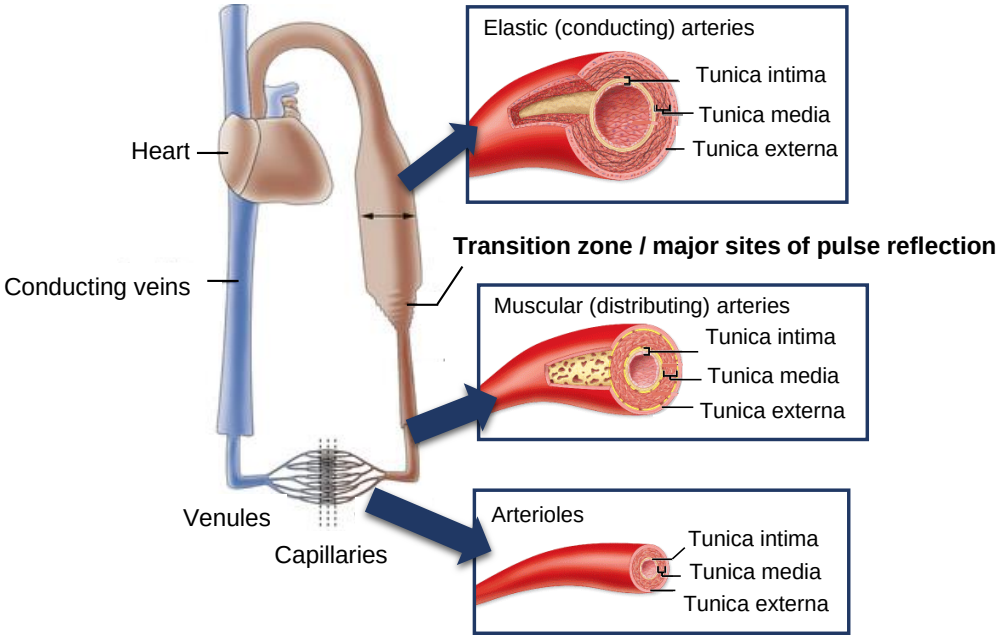

Figure 2.2. Representation of the simplified circulatory system, emphasizing the arterial wall structure (Adapted from Marieb and Hoehn 2012 and Polak *et al.* 2016).

The elastic arteries branch to the muscular arteries, also called “distributing arteries”, which deliver blood to specific organs and tissues. Brachial, radial and femoral are examples of muscular arteries, whose *tunica media* is mainly composed by smooth

muscle, being the elastin concentrated in the internal and external *tunicas*. These arteries are less distensible than the elastic ones, being more active on vasoconstriction in order to control the blood flow (Marieb and Hoehn 2012). In this work, muscular arteries are referred to as peripheral arteries. Arterioles are the smallest arteries. Even though the larger arterioles have all three *tunicas*, being their *tunica media* mainly composed by smooth muscle, smaller arterioles, which lead into the capillary beds, can be made from a single layer of smooth muscle cells spiralling around the endothelial lining. The instant blood flow into the capillary beds is determined by the arteriole diameter, which varies in response to changing neural, hormonal, and local biochemistry. When arterioles constrict, the tissues are largely bypassed, nonetheless, when arterioles dilate, blood flow into the local capillaries can dramatically increase (Marieb and Hoehn 2012).

2.2. Haemodynamics: blood flow, pressure and resistance

Three fundamental concepts have to be introduced to understand vascular circulation: blood flow (*F*), blood pressure and peripheral resistance (*R*). Blood flow corresponds to the blood volume that circulates through a vessel, organ or the entire vascular bed in a given time unit (usually expressed in ml/min or l/min). As the blood flows through an artery, with pressure *P1* at the onset and *P2* at the end, the pressure difference ($\Delta P = P2 - P1$) is imposed by the resistance of that arterial path, being the three parameters related as:

$$F = \frac{\Delta P}{R}. \qquad \text{(eq. 2.1)}$$

In the specific case of a circular tube complying a steady flow with a parabolic velocity profile, as schemed on Fig 2.3, Poiseuille's law describes the relation between pressure change with vessel inner radius (a_r), vessel length (a_l), and blood viscosity (η), accordingly with:

$$F = \frac{\Delta P \pi a_r{}^4}{8 \eta a_l}. \qquad \text{(eq. 2.2)}$$

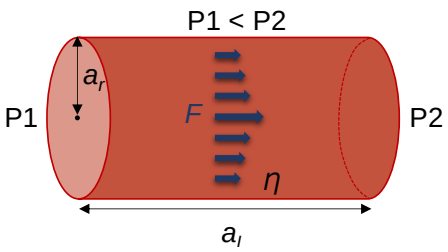

Figure 2.3. Factors influencing a steady flow in a tube.

Combining equations 2.1 with 2.2, the resistance in a uniform tube can be given by:

$$R = \frac{8\eta a_l}{\pi a_r^{\,4}}. \qquad \text{(eq. 2.3)}$$

Although this relation may not be precisely applicable in the human arterial system, it helps to understand how strongly resistance depends on arterial wall radius. Considering that blood viscosity and vessel length slowly change through the regular aging process, only the radius variation can rapidly be changed by vasoconstriction and vasodilatation, impacting dramatically resistance and flow. For this reason, the large arteries close to the heart, which do not change dramatically in diameter, contribute little to peripheral resistance. Instead, the small-diameter arterioles, which can expand or constrict accordingly with the local instantaneous metabolic needs, are the major determinants of peripheral resistance (Nichols 1990; Vosse and Stergiopulos 2011).

BP is the pressure gradient observed through the vascular system, being the driving force that keeps the blood flowing. It is defined as the exerted force per unit area of the vessel wall, being usually expressed in millimetres of mercury (mmHg). As schemed in Fig. 2.4, BP is composed by a steady element, the mean arterial pressure (MAP), and a pulsatile component, corresponding to the arterial pulse ranging between DP and SP. The pulsatile pressure is usually referred to as pulse pressure. When compared to arterioles, the resistance of the large arteries is so low that the MAP is practically the same along its path. On small arteries pulsatility drastically decreases to protect microcirculation (Muiesan *et al.* 2013).

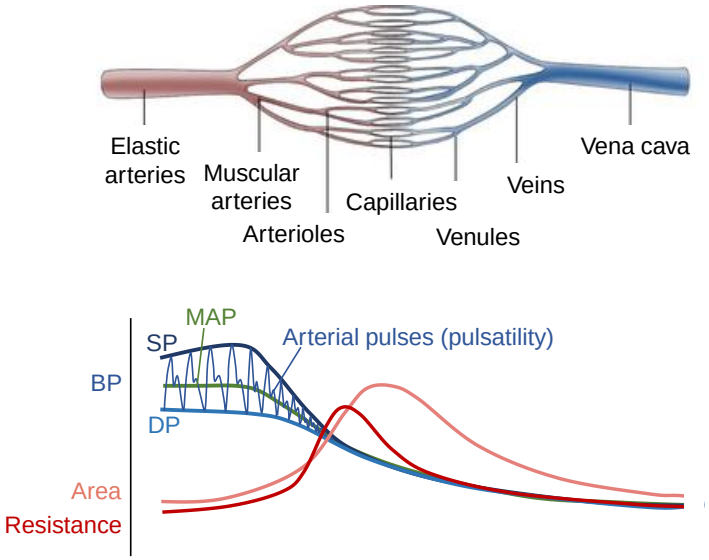

Figure 2.4. Pressure, area and resistance variation through the vascular system (adapted from Bortolotto and Safar 2006 and Polak *et al.* 2016).

The pulsatile pressure component is the consequence of intermittent ventricular blood ejection from the heart, being influenced by several cardiac and vascular factors, such as heart rate (HR) and arterial stiffness (Safar *et al.* 2003). SP and PP increase from the aorta to peripheral arteries while mean and DP show only a minor decrease of 1 to 2 mmHg toward the periphery. The average increase of PP can be as much as 10 to 14 mmHg, when moving from the aorta to the brachial artery (Safar and Jankowski 2009).

The SP and PP increase through the proximal arterial tree is known as "pressure amplification" and is associated with changes in diameter and elasticity/compliance of the involved arteries (Pauca and Wallenhaupt 1992; Weber and Segers 2015). The pressure amplification is actually a pulse wave distortion, rather than a true amplification of the pressure signal. During systole, the heart generates the pressure wave (forward wave, FW), that, as it advances through the arterial tree, suffers reflections caused by the non-uniform elasticity and viscous damping within the arterial system. As a consequence, a reflected wave component (RW) is created. So, the pulse amplitude amplification and "distortion" happens as a result of changes in the relative timings and amplitudes of the forward and reflected pressure waves (O'Rourke 1999; Kips 2011).

2.3. Arterial stiffness evaluation

The arterial elastic properties are given by elastin, which is the most inert substance in the body, with a chemical half-life measurable in decades. Elastin fracture is predicted to occur after approximately 10^9 cycles of 8% stretch, which is achieved in the proximal aorta within 40 years of life. When elastin fibres, normally bearing central pressure surges, begin to fracture, the wall stretches and the elastic arteries dilate. Consequently, with the loss of arterial elasticity, the stresses once buffered by elastin are transferred to the less extensible collagenous elements in the wall (O'Rourke and Nichols 2005).

Meinders and Hoeks explained the distension/pressure behaviour by an exponential approach, which takes in consideration the arterial cross-sectional area variation in time, $A_{cs}(t)$, with the arterial distension, according to:

$$A_{cs}(t) = \frac{\pi a_d{}^2(t)}{4}, \qquad \text{(eq. 2.4)}$$

considering that the artery is rotationally symmetrical, and $a_d(t)$ is its diameter in time. The $A_{cs}(t)$ peak corresponds to the systolic cross-section and the minimum to the diastolic

cross-sectional area, A_{diast}. The relationship between the pressure wave, p_{wave}, and the cross-sectional area variation, can be described as:

$$p_{wave}(t) = DP \exp \alpha_a \left(\frac{A_{cs}(t)}{A_{diast}} - 1 \right), \qquad \text{(eq. 2.5)}$$

where α_a is the wall rigidity coefficient. This relation can be applied over a large pressure range, allowing to calculate local arterial stiffness indexes (Meinders and Hoeks 2004; Yuan *et al.* 2013). In Fig. 2.5 the non-linear relationship between pressure and distensibility can be schematically observed as the cross-sectional area in function of pressure. The non-linear tendency is greater at higher pressures, when the vessel distends less due to the increasing recruitment of collagen fibres on the stretched vessel (Kips *et al.* 2010).

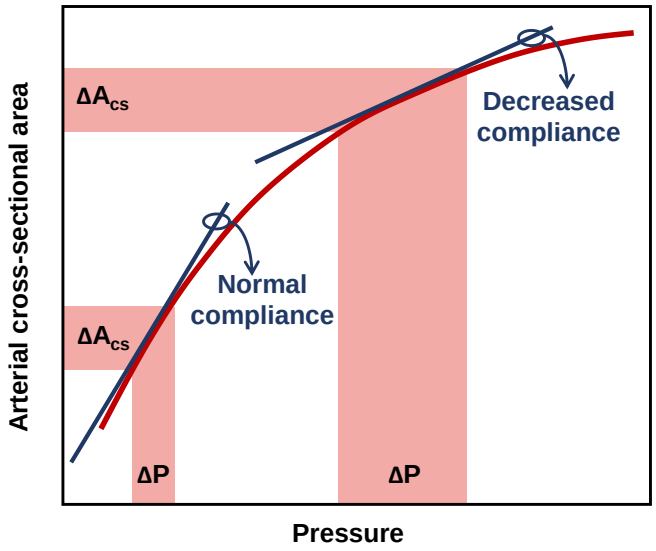

Figure 2.5. Typical area-pressure relation for an elastic artery showing the pressure/distension nonlinear behaviour.

The central arterial stiffness progression can be translated in several changes in the arterial pulse morphology, velocity and pressure values (Mitchell *et al.* 2004), which are all features that can be used as surrogates for arterial stiffness (Laurent *et al.* 2006).

In normal central elastic arteries, as previously described, the elastin expand during systole, storing energy, which is then liberated during diastole by elastin recoil. The elastic central arteries are characterized by low velocity of the arterial pulse propagation, in the order of the 6 m/s (Briet *et al.* 2012), as well as a sharp impedance mismatch in the elastic

to muscular arterial transition. A direct consequence of the arterial wall's elasticity and compliance is the phase shift of the arterial pulse, whose shape changes throughout the arterial path and its amplitude increase, as can be observed in Fig. 2.6a (Vosse and Stergiopulos 2011). The pulse suffers reflections majorly in the impedance mismatch between elastic and muscular arteries, limiting the transmission of pulsatile pressure energy to the periphery, protecting the microcirculation. At the heart, the reflected wave arrival during diastole, as schemed in Fig. 2.6b, has the physiological role of promoting an efficient coronary perfusion (London and Pannier 2010; Safar 2010; Muiesan *et al.* 2013).

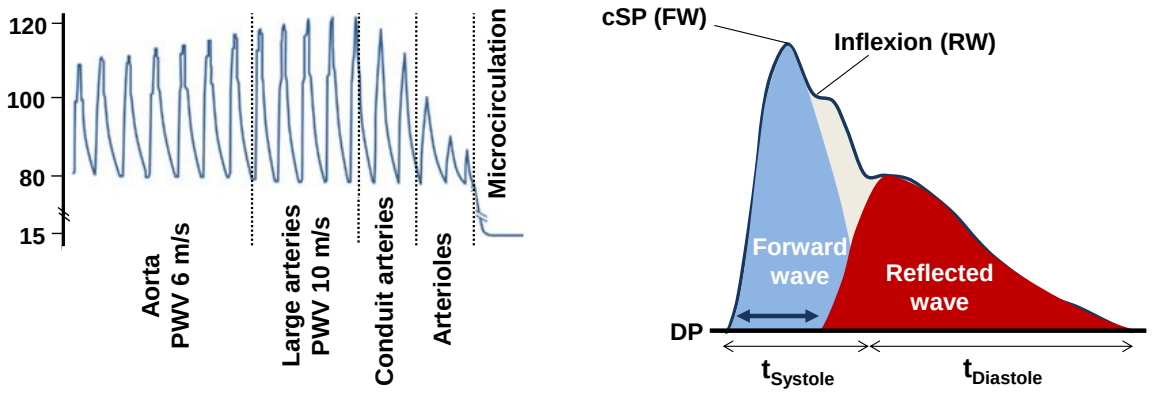

a) b)

Figure 2.6. Schematization of the physiological effects of central arterial elasticity: a) arterial pulse throughout the arterial path (adapted from Briet *et al.* 2012); b) central pulse of elastic central arteries, representing the combination of the forward with the reflected wave, ($t_{Systole}$ - systole duration; $t_{Diastole}$ - diastole duration).

With central arterial aging, the elastic walls become gradually stiffer, as the muscular arteries maintain their features. This causes the decreasing or even inversion of the impedance gradient from elastic to muscular arteries, as central PWV becomes equal or even higher than in muscular arteries. The overall aortic stiffning process features four stages, accordingly to the detailed aging cardiovascular continuum described in O'Rourke *et al.* 2010. The first stage corresponds to the normal aortic elastic fibres fatigue during life, with the gradual fracture and fraying of the elastic *lamellae*, that on the other hand cause the distension and arterial remodelling, and consequently the typical aortic stiffening. The second stage has to do with the multiplicative effect of the aortic stiffening in increasing both resistance and early wave reflections, resulting in the pulsations cannot be dampened by the elastic aorta (third stage), extending peripherally into the microvasculature, as schemed in Fig. 2.7a (O'Rourke *et al.* 2010; Muiesan *et al.* 2013), especially into the small arteries of organs with high resting blood flow, which are the

cases of the brain (Mitchell *et al.* 2011) and kidney (Briet *et al.* 2012). The fourth stage is related with the raise in aortic pulse pressure associated to arterial stiffening, which leads to an increase in cSP and a decrease of DP (Fig. 2.7b), affecting coronary perfusion and augmenting the risk of myocardial ischemia (Nichols 2005). Furthermore, once during the systole the left ventricle's pressure approach the aortic systolic pressure, the latter is a major determinant of myocardium's blood supply needs. Consequently, as cSP increases, also does the risk of left ventricle hypertrophy (O'Rourke *et al.* 2010).

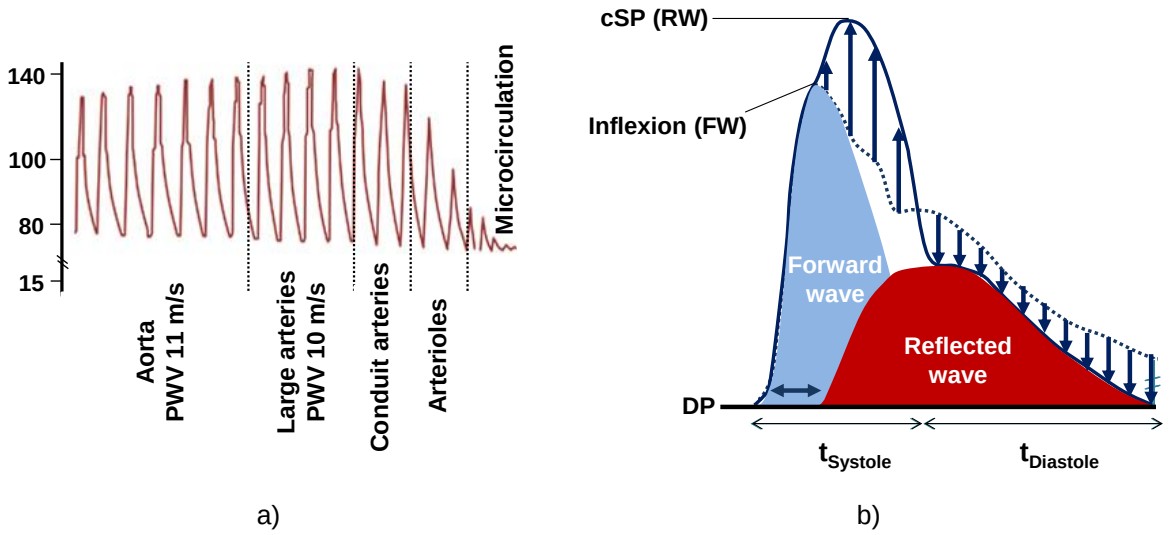

a) b)

Figure 2.7. Pathological effects of central arterial stiffness: a) arterial pulse throughout the arterial path (adapted from Briet *et al.* 2012); b) central arterial pulse of stiff central arteries, representing the combination of the forward with the reflected wave ($t_{Systole}$ - systole duration; $t_{Diastole}$ - diastole duration).

2.3.1. Pulse wave velocity

Once the pulse pressure is propagated throughout the arterial tree as a wave, it is possible to calculate the wave's velocity from the time delay (Δt) between two arterial pulses acquired at different sites of the arterial tract, knowing the distance between them (Δs):

$$PWV = \frac{\Delta s}{\Delta t}. \qquad \text{(eq. 2.6)}$$

PWV is used as a surrogate for arterial stiffness, based on the Moens-Korteweg equation:

$$PWV = \sqrt{\frac{E a_h}{2 \rho a_r}}, \qquad \text{(eq. 2.7)}$$

where E is the Young's modulus of the arterial wall tissue, a_h is the wall thickness, ρ is the blood density, and a_r is the internal radius of the artery (Bramwell and Hill 1922; Laurent *et al.* 2006). PWV is usually assessed between carotid and femoral arteries, covering the entire aorta pathway. For pulse transit time/time delay calculation, carotid and femoral pulses are obtained transcutaneous at the right common carotid and femoral arteries (Laurent *et al.* 2006) and the distance between sites should be considered as 80% of the direct external distance (Δcf), as schemed in Fig. 2.8 (Van Bortel *et al.* 2012; Mancia *et al.* 2013).

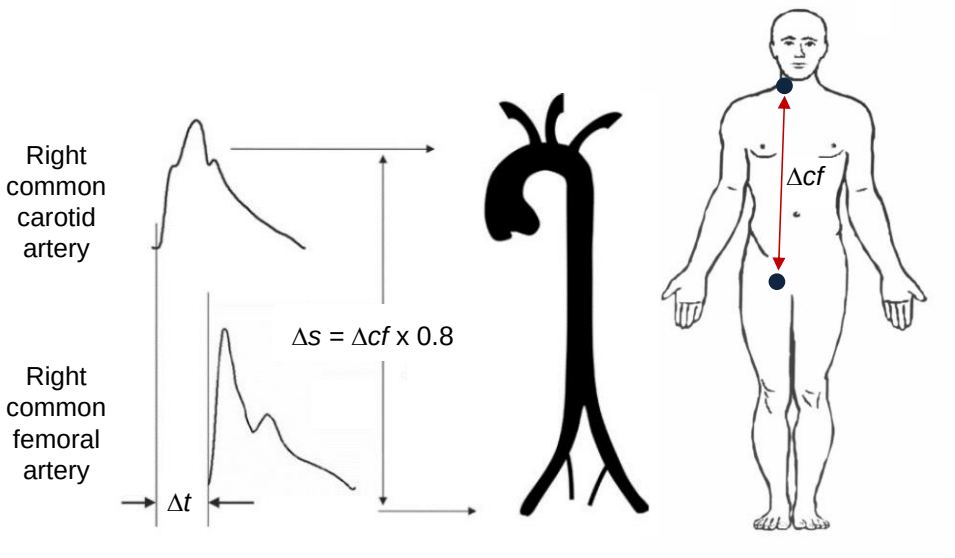

Figura 2.8. Scheme of the carotid-femoral PWV measurement (adapted from Laurent *et al.* 2006).

The carotid and femoral pulses can be either recorded simultaneously, as with the Complior device (*Alam Medical*), or sequentially using a single probe, in which the carotid-femoral pulse transit time is determined with reference to the R-wave of the electrocardiogram signal, which is the method used by in the SphygmoCor device (*AtCor Medical*) (Qasem *et al.* 2008; Van Bortel *et al.* 2012). The used arterial pulses can be from various natures, including pressure, distension, and flow (Laurent *et al.* 2006).

The carotid-femoral PWV is considered the gold-standard measurement to evaluate arterial stiffness (Laurent *et al.* 2006). The strong scientific evidence turned PWV in a recognized surrogate for arterial stiffness evaluation, being now the most recurrently used in cardiovascular risk stratification and prognosis (Laurent *et al.* 2001; Laurent *et al.* 2003; Mitchell *et al.* 2010). Accordingly to the European guidelines for the management of

arterial hypertension, a PWV value higher than 10 m/s is considered a subclinical organ damage (Mancia *et al.* 2013).

In 2010, Boutouyrie and Vermeersch, collected data from 16 867 subjects across eight European countries, in which PWV and basic clinical parameters were measured. This study established reference PWV values to different ages and BP categories, which are presented in the Table 2.1. As an example, it can be verified that for subjects with optimal to high normal BP, the mean PWV ranged from 6.1 m/s for healthy subjects with less than 30 years old, to 11.8 m/s for subjects ≥ 70 years old (Boutouyrie and Vermeersch 2010).

Table 2.1. Reference values for PWV (m/s) accordingly with age and BP category since optimal to grade II/III hypertension (data from Boutouyrie and Vermeersch 2010).

Age category	Optimal BP	Normal BP	High normal BP	Grade I HT	Grade II/III HT
<30	6.1	6.6	6.8	7.4	7.7
30-39	6.6	6.8	7.1	7.3	8.2
40-49	7.0	7.5	7.9	8.6	9.8
50-59	7.6	8.4	8.8	9.6	10.5
60-69	9.1	9.7	10.3	11.1	12.2
≥70	10.4	11.7	11.8	12.9	14.0

2.3.2. Pulse wave analysis

In the “Expert consensus document on arterial stiffness: methodological issues and clinical applications” is stated that PWA should be analysed through tree major parameters: augmentation index (AIx), cPP and cSP (Laurent *et al.* 2006). The main advantage of using PWA for arterial stiffness assessment, is that it can be performed using only one measurement site, such as the carotid artery. In this section concepts and clinical data on pulse wave analysis are presented.

Augmentation index

The pulse waveform is composed by the FW produced by the heart during systole and the RW, which is the sum of the reflections of the original wave, created in impedance mismatches in the arterial tree. Murgo *et al.* reported different types of carotid waveforms that can be assessed in humans, which can be observed on Fig 2.9 (Murgo *et al.* 1980).

In subjects with elastic central arteries it is expected to see the so-called “type-C” wave, where the cSP corresponds to the FW produced by the heart, defining the systolic pressure value, with the RW arriving in the late systole creating an inflection.

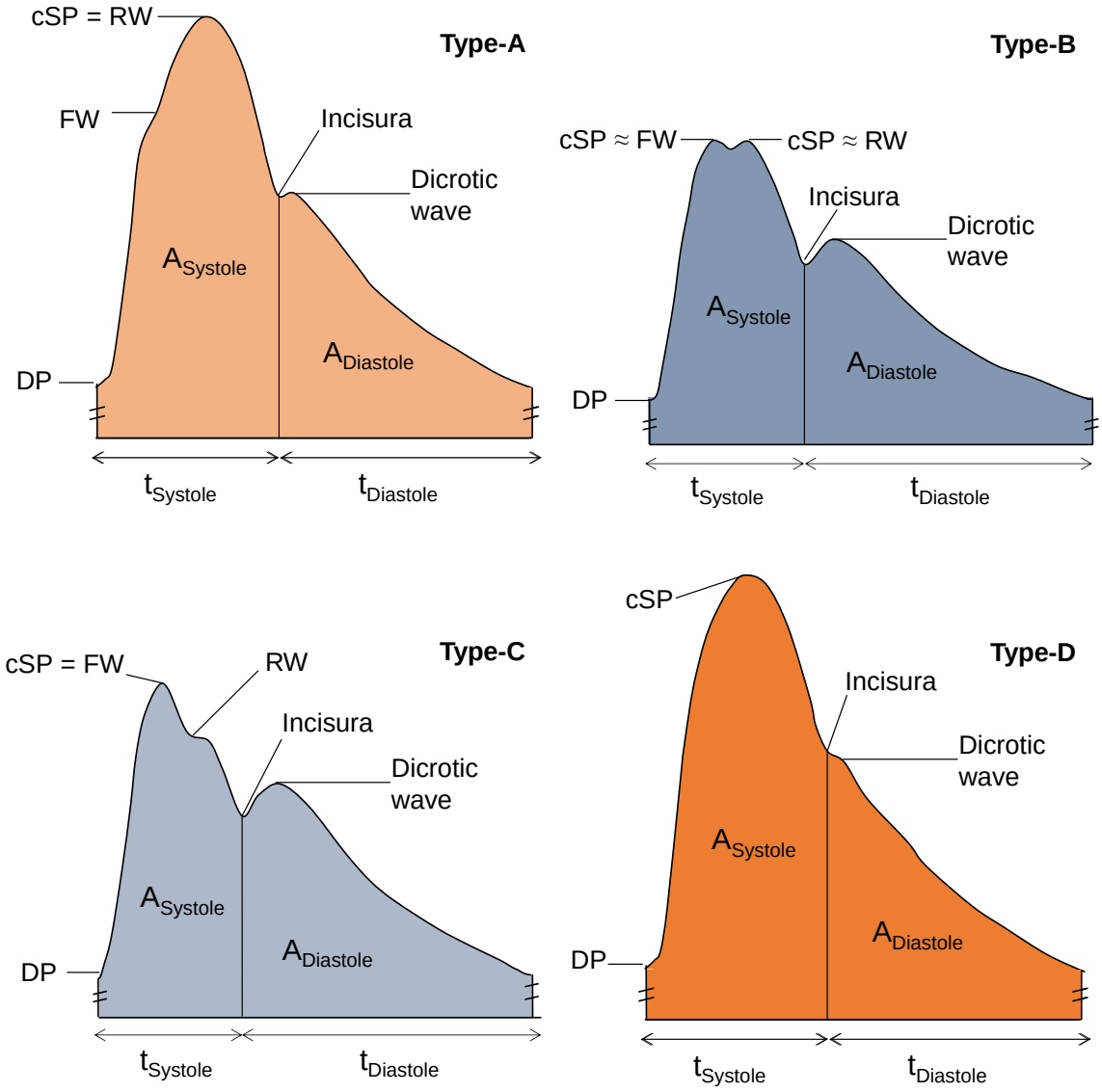

Figure 2.9. Murgo’s wave types.

With aging and central arterial stiffening, the RW tends to arrive earlier in the heart cycle, forming a second peak with approximately the same amplitude than the first (FW), being the case of the “type-B” wave. With the PWV increasing, the reflected wave arrives even earlier in the systole, being added to the FW in such way that there is an increasing of the systolic pressure, which is the case of the “type-A” wave (Murgo *et al.* 1980). Finally, in the extreme case of arterial reflections, both waves overlap in a manner that no inflexion

can be identified, being the case of the “type-D” wave. Through the aging process, an individual can present all four wave types (Kelly *et al.* 1989).

The AIx is the most well-known measure of pulse wave reflection and purposes to quantify the impact of wave reflection on the pulse wave contour, which severely changes with age (Kelly *et al.* 1989; Mitchell *et al.* 2004). AIx can be calculated applying eq. 2.8, being also frequently represented as percentage (AIx%).

$$AIx = \frac{RW\text{-}FW}{cPP} \qquad \text{(eq. 2.8)}$$

The AIx can be negative, for “type-C” waves, or positive, for “type-A” waves (Weber and Segers 2015). The augmentation index has the advantages of not depend of pressure calibration, being dimensionless, and can be derived directly from the carotid pulse wave. However, it has the disadvantages related to the influence of the magnitude and timing of wave reflection, which are sensitive to factors such as the individual’s height and heart rate (Wilkinson *et al.* 2000).

In 2006, Wojciechowska *et al.* determined AIx thresholds for age category, by analysing AIx values from 534 subjects without hypertension, diabetes, or previous nor concomitant cardiovascular disease (Table 2.2) (Wojciechowska *et al.* 2006). Latter, in Janner *et al.* 2010, were presented reference equations to calculate the expected AIx of a subject, considering their age, HR, and height for women (eq. 2.9) and men (eq. 2.10).

Table 2.2. AIx% proposed thresholds for men and women by age (years) (data from Wojciechowska *et al.* 2006).

Age	AIx% men	AIx% women
20	10	17
30	22	29
40	30	37
50	37	44
60	41	48

$$AIx = 56.28 + 0.90age - 0.005age^2 - 0.34HR - 0.24height \qquad \text{(eq. 2.9)}$$

$$AIx = 79.20 + 0.63age - 0.002age^2 - 0.28HR - 0.39height \qquad \text{(eq. 2.10)}$$

Even though AIx is being mostly reported as an arterial stiffness index, it is not only dependent on arterial stiffening and consequent acceleration of the pulse wave. London *et al.* studied a cohort of 180 patients with end-stage renal disease who underwent aortic PWV measurement and determination of arterial wave reflexions, expressed as AIx, by applanation tonometry on the common carotid artery. This study reported a persistent association of AIx with mortality of patients with normal PWV in end-stage renal failure. The intensity of the reflected wave is dependent on reflective properties on the vascular tree that can be independent from arterial stiffening (London *et al.* 2001).

Several studies have shown the predictive value of AIx. In a meta-analysis including 11 longitudinal studies, employing central haemodynamic measures from 5648 subjects in a mean follow-up of 45 months, it was concluded that AIx predicts clinical events independently of peripheral pressures (Vlachopoulos *et al.* 2010). Others works also related AIx with hypertension (Kaess *et al.* 2012) and coronary arterial disease (Weber *et al.* 2004; Ueda *et al.* 2004; Chirinos *et al.* 2005). *Matsui et al.* showed the correlation of AIx with total and low density lipoprotein cholesterol in hypertensive subjects (Matsui *et al.* 2004). The relation of arterial stiffness measured as AIx with a subtype of acute ischemic stroke (lacunar infarction) was also verified in Byun *et al.* 2014.

Central pulse and systolic pressures

As introduced before, the arteries irrigating the heart, kidneys, and brain are exposed to cSP, rather than peripheral systolic pressure (pSP). The difference between both pressures is not constant, so cSP cannot be inferred from brachial pressure as shown by McEniery *et al.* in the Anglo-Cardiff collaborative trial II, which studied the variability of cSP and the impact of cardiovascular risk factors. It was demonstrated that cardiovascular risk factors affect the pulse pressure amplification, showing data comparing cSP and pSP for 5648 healthy subjects, and concluding that cSP cannot be reliably inferred from pSP either for healthy or hypertensive subjects. Other conclusion from this study was that when stratified by pSP, 70% of the individuals considered as having high-normal blood pressure presented cSP values consistent with stage I HT (McEniery *et al.* 2008).

A recent study stablished reference values for cSP, in which Herbert *et al.* gathered cSP data from 45 436 subjects in order to stablish normal values of cSP and pressure amplification in a healthy population according to age, sex, and pSP. The authors had four

study branches: normotensives with and without cardiovascular risks and hypertension with and without others risk factors. The normotensives without risk factors were considered the “normal population”, and all the other categories were labelled as “reference population”. The results from both populations, per age category, are presented in Table 2.3. The study reported, for instance, that for the normal population, between the ages of 20 to 70 years old, the cSP ranged from 97 to 118 mmHg and 105 to 116 mmHg for female and male individuals, respectively. On the other hand, for the “reference population” the results were significantly higher, the cSP value obtained in the normal population above 70 years old, is reached in the age decade between 40 and 49 years old (Herbert *et al.* 2014).

Table 2.3. cSP (mmHg) values by age (years) for normal population (normotensives without CV risks) and reference population (normotensives with CV risks and hypertensives with or without other CV risks) (data from Herbert *et al.* 2014).

Age category	Normal population		Reference population	
	Male	Female	Male	Female
<20	105	97	109	99
20-29	103	95	110	101
30-39	103	98	114	111
40-49	106	102	118	116
50-59	110	110	123	120
60-69	114	114	128	128
≥70	116	118	135	138

Over time, a compelling body of evidence have been raised in the role of cSP as cardiovascular predictor. Boutouyrie *et al.* showed that cPP was a strong independent determinant of carotid artery enlargement and wall thickening, while MAP and peripheral PP were not (Boutouyrie *et al.* 1999). cSP and brachial/carotid PP amplification in a cohort of 180 patients with end-stage renal disease undergoing haemodialysis was studied in Safar *et al.* 2002. The patient’s follow-up had a mean duration of 52 ± 36 months, during which 70 deaths occurred, from cardiovascular and non-cardiovascular fatal events. cPP, brachial/carotid PP amplification, and aortic PWV emerged as all-cause mortality predictors in this cohort. On the other hand, brachial pressure, including PP, had no predictive value for mortality. The authors concluded that the results provided the first direct evidence that, in patients with end-stage renal disease, cPP and, mainly, the

disappearance of brachial/carotid PP amplification are strong independent predictors of all-cause mortality (Safar *et al.* 2002).

In 2007, the Strong Heart Study investigated the relation of cSP with vascular disease and cardiovascular outcome. The study evaluated the carotid artery hypertrophy, by *intima-media* thickness (IMT) and vascular mass assessment, the extent of atherosclerosis, and the incident cardiovascular events. cSP was obtained by arterial radial tonometry. The authors showed that cPP was more strongly related to vascular hypertrophy, extent of atherosclerosis, and cardiovascular events than brachial PP (Roman *et al.* 2007).

In the context of the same study, Roman *et al.* showed that cPP ≥ 50 mmHg predicts adverse CVD outcome and might serve as a target in hypertension intervention strategies (Roman *et al.* 2009). In 2010, it was also evaluated the relation between cSP and pSP in left ventricular hypertrophy by echocardiography and radial applanation tonometry, performed in 2585 subjects. Results suggested that cSP has more impact on left ventricular hypertrophy and remodelling stimulation than pSP. However, cPP was of all the addressed factors, the most important in causing vascular hypertrophy and atherosclerosis (Roman *et al.* 2010).

Several studies also report the role of central pressure monitoring in assessing the central effectiveness of antihypertensive treatments, as well as new perspectives on hypertension treatment and monitoring (Williams *et al.* 2006; Agabiti-Rosei *et al.* 2007; Boutouyrie *et al.* 2010; Masugata and Senda 2010; McEniery *et al.* 2014; Pucci *et al.* 2014). A detailed review of the effects on arterial stiffness and reflections per treatment active substance is presented in Boutouyrie *et al.* 2014.

2.4. State-of-the-art of non-invasive assessment of the arterial pulses

The gold standard technique to assess central pressure waves is aortic invasive catheterization, however as an invasive procedure, is associated with a number of potential complications (Woodrow 2000). Currently, the evaluation of the several arterial stiffness surrogates is usually performed by arterial tonometry, nevertheless there are other non-invasive techniques, based on the acquisition of pressure, flow and distension waves, which will be shortly described.

Tonometry

Central pulse waves are usually assessed by arterial applanation tonometry, which measures pressure or tension, applying the Laplace law that relates wall tension (T) with transmural pressure (P_t), vessel radius (a_r) and thickness (a_h) of a cylindrical thin wall tube, as in eq. 2.11. The transmural pressure is given by the difference between external (P_e) and internal (P_i) pressure of the artery. As can be verified in Fig. 2.10, when the pressure sensor applanates the tube wall, with P_e, the radius of the artery tends to infinite and P_t to zero. Consequently the P_e becomes equal to P_i that can then be measured (Miyashita *et al.* 2012).

$$P_t = \frac{a_h T}{a_r} \qquad \text{(eq. 2.11)}$$

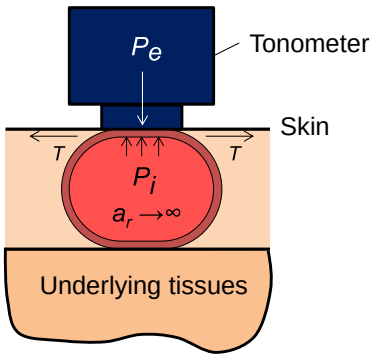

Figure 2.10. Schematic drawing of arterial tonometry principle (adapted from Miyashita *et al.* 2012).

Tonometry can be performed in several superficial arteries, since underlying hard tissues are present to enable a proper artery applanation (Drzewiecki *et al*. 1983). Tonometry data is generally accepted for radial, carotid and femoral arteries, but no consensus exists for brachial artery tonometry (Adji and O'Rourke 2012). When the arterial pulses are assessed in a peripheral artery, usually the radial, central pressure waves are synthetized using population-based generalized transfer functions (GTFs), applied in time or frequency domains. GTFs can be simplistically viewed as sophisticated low pass filters, applied to peripheral wave pulses, using the fact that the aortic pressure wave contains fewer higher harmonics than the radial wave (Williams *et al.* 2011). Even though being a worldwide applied and accepted procedure, tonometry has the limitation of may induce push-pull artefacts due to the motion of the arterial wall and/or operator, and thus might distort the shape of the curve (Boutouyrie *et al.* 2014).

Several tonometers for pulse wave acquisition are commercially available, being examples of widespread tonometers the SphygmoCor® (*AtCor medical*, Australia) and the Complior Analyse® (*Alam Medical*, France) (Avolio *et al.* 2010). The main difference between both devices is the probes' pressure sensors and shape. The SphygmoCor has a pen-like shape probe, which uses diffused semiconductor Wheatstone bridge sensors and perform acquisitions at 128 Hz, whereas, Complior uses piezoelectric sensors in a coin-like shape probe, having an acquisition frequency of 1000 Hz (Stea *et al.* 2014).

Photoplethysmography (PPG)

PPG is a low-cost optical measurement technique that can be used to detect blood volume changes in the microvascular bed of fingers, toes and ear lobes. It has been used to assess the digital beat-to-beat blood pressure and in its basic form complies only a light source to illuminate the tissue (e.g. skin), in red or a near infrared wavelength, and a photodetector (PD) to measure light intensity variations associated with changes in blood perfusion (Allen 2007). The main disadvantage of PPG is only assessing pressure waves in body extremities, being unusable on higher calibre superficial arteries, such as the common carotid. A recent example of a commercial PPG device is the pOpmètre® (*Axelife*, France) that assesses finger-toe pulse wave velocity, with the aim of provide a more comfortable and easy to routinely measure arterial stiffness (Alivon *et al.* 2015).

Oscillometry

Pulse wave acquisition devices based on oscillometry apply the usual upper arm cuffs to acquire the brachial arterial pulse. To assess the pulses, the cuff is pressurized at least 35mmHg over the actual systolic pressure creating a stop-flow condition where a small diaphragm will develop around the brachial artery at the level of the upper edge of the over-pressurized cuff. As the pressure changes, the pulse wave critical points will cause a beat on the membrane like a drumstick. Because the upper arm tissues are practically incompressible, the energy propagates and reaches the skin/over-pressurized cuff edge, causing a very small volume/pressure change in the cuff. These very small supra-systolic pressure changes are recorded by the pressure sensor in the device (Horváth *et al.* 2010; Weiss *et al.* 2012). The main disadvantage of such devices is the impossibility to assess directly the carotid pulse wave. Nonetheless, the easiness of use has been made these devices popular in general clinic, being commercial examples the Arteriograph® (*Tensiomed*, Hungary), Mobil-O-Graph® (*I.E.M. GmbH*, Germany), Vicorder® (*Skidmore Medical*, United Kingdom), and Omron® HEM-9000AI (*Omron Healthcare*, Japan).

Echotracking

Distension waves of superficial large arteries can be acquired using non-invasive vascular ultrasound wall tracking systems. When an acoustic ultrasound wave (typical frequencies between 7 and 12 MHz) propagates through the tissues it is reflected on interfaces with acoustic impedance discontinuity. Consequently, when applied to superficial arteries, the arterial interfaces *lumen-intima* and *media-externa* will reflect the acoustic signal, allowing the detection of posterior and anterior arterial wall, permitting the calculation of *intima-media* thickness (Powalowski *et al.* 2000). IMT is a commonly used surrogate marker of atherosclerosis (Bartgaile 2012), being also a powerful predictor of CVD events (Lorenz *et al.* 2007), specially stroke (Martinez-Sanchez and Alexandrov 2013; Rothwell 2000). Additionally, the use of multi-frame echotracking enables to assess the heterogeneity of the arterial wall on a segment, which is useful to the characterization of atherosclerotic plaques (Boutouyrie *et al.* 2014).

With these systems, arterial changes in diameter (distension waves) and related measures can also be obtained, with a precision of approximately 1 µm (Laurent *et al.* 2006; Kips 2011). Several studies reported the used of scaled distension waves to determine carotid artery pressure, using linear or exponential methods (Van Bortel *et al.* 2001; Vermeersch *et al.* 2008 and Kips *et al.* 2010). In the linear scaled method the distension wave is calibrated directly as a pressure wave, whereas, the exponential method uses the Meinders and Hoeks distension/pressure relation to reconstruct the pressure wave. The use of distension waves arises as an alternative to tonometry, since the arterial applanation is not required, facilitating the process of wave acquisition, for instance, in obese subjects. Examples of echo-tracking systems are NIUS02® (*Asulab*, Switzerland), Artlab® (*Esaote-Pie*, the Netherlands), and HDI500® with QLab (*Philip*s, the Netherlands).

Magnetic resonance imaging (MRI)

Recently, evolutions in imaging techniques, such as MRI, have been enabling the assessment of deep arteries, such as aorta, making possible to investigate their true arterial geometry and blood flow distribution (Prehn *et al.* 2009; Boutouyrie *et al.* 2014). MRI allows direct measurement of regional stiffness in the aortic arch (by PWV calculation), as well as to analyse distensibility in the ascending and descending aorta. The new trends are to combine MRI with arterial tonometry in order to obtain a wide-ranging analysis on central haemodynamics, non-invasively relating central pressure

with aortic and ventricular morphologies (Redheuil *et al.* 2011). The main limitations of MRI techniques are the low temporal and spatial resolutions, along with, as an imaging procedure, being impossible to access local pulse pressure (Boutouyrie *et al.* 2014).

2.5. Comparison of pulse wave data from different assessment techniques

Despite having been published guidelines on the validation of PWV devices (Wilkinson *et al.* 2010), no protocol exists yet to validate PWA and cSP devices (Stergiou *et al.* 2016). In the literature analysis it was verified that a great majority of the studies, comparing central pulse morphology and cSP assessment techniques, frequently used other studies as reference. A few others applied the standard requirements for regular brachial sphygmomanometers of the Association for the advancement of medical instrumentation (AAMI), which limit the pressure difference between the tested device and the reference in 5 mmHg, with a standard deviation (SD) up to 8 mmHg (Wassertheurer *et al.* 2010; Pucci *et al.* 2013, Stea *et al.* 2014).

The correlation between acquired data with POFpen and the non-invasive and invasive techniques was performed accordingly to similar studies found on the literature (see Table 2.4). Besides AIx and cSP, also the pulse waveforms, in time and frequency domains, can be directly compared using some of the approaches next described.

RMSD is a measure of absolute difference between signals, allowing the quantification of the variation between the data points across the entire normalized waveforms, calculated between the tested ($p_{wavetest}$) and the reference ($p_{waveref}$) pulse wave data. As showed in eq. 2.12, RMSD corresponds to the square root of the mean squared differences between the arterial pulses obtained with both techniques, where n_p is the number of compared pulse points.

$$RMSD = \sqrt{\frac{1}{n_p}\sum_{i=1}^{n_p}(p_{wavetest,i} - p_{waveref,i})^2} \qquad \text{(eq. 2.12)}$$

Other important parameter is the form factor (FF), frequently represented as percentage (FF%), relates the mean point of the pulse wave (MAP) with its amplitude, being a measure of how “peaked” the waveform is. Through the periphery, the pulse wave is distorted and becomes more peaked, consequently its FF becomes lower. It is also reported that distension waves have higher FF values than pressure waves, in approximately 6% (Kips *et al.* 2010). The same study discusses that the distension waves

are “flatter” than the tonometric waves due to the non-linear pressure-diameter relationship, as discussed in section 2.3. This fact is especially evident at higher pressures, since the arteries are stretched, the vessel distend less with the collagen fibres recruitment. At the central level, FF can be calculated as:

$$FF = \frac{MAP - DP}{cSP}. \qquad \text{(eq. 2.13)}$$

In some studies, the agreement analysis between waves is also performed in the frequency domain (Sztrymf *et al.* 2013; Agnoletti *et al.* 2014). In this procedure the pulse wave is Fourier decomposed, and the first 8 harmonics’ amplitudes are compared and submitted to correlation tests. The first harmonic corresponds to the heart frequency of the analysed pulses, being the remaining harmonics multiples of the first.

The analysed studies used different statistical approaches to investigate agreement between measurements assessed with different techniques, as can be seen on Table 2.4. Student *t*-tests are frequently used to analyse potential significant differences between results or different measuring methods. The used confidence interval is typically 95 %, reflecting a significance level (*p-value*) of $p < 0.05$. As a measure of agreement between techniques, Bland-Altman plotting is applied in the majority of the literature references.

As correlation studies, Pearson’s (PCC) and Intraclass (ICC) correlations coefficients are frequently calculated, with common confidence intervals of 95 %.

Regarding the number of participants, in the analysed literature, it ranged from 12 to 2026 subjects per study. The invasive validation studies usually include a restrict number of subjects due to the difficulties associated with the testing procedures. Therefore, being easier to perform, the non-invasive comparison can be carried out in larger cohorts.

2.6. Conclusion

In this section, cardiovascular fundamentals on arterial pressure and stiffness were introduced. The state-of-the-art of the commercial devices for cSP and AIx assessment as well as the usual procedures in their clinical evaluation, were also described. As part of the theoretical background of this work, in the next section, the fundamentals on optical fibre sensors and their advantages as biomedical monitoring systems, will be discussed.

Table 2.4. Examples of comparison and invasive validation studies of several commercial devices for central arterial pulse wave acquisition (n_{sub} - number of subjects entered the study, SCC - Spearman correlation coefficient, Δ- difference, *r* - correlation coefficient)

Studies	Compared Devices	n_{sub}	Studied parameters	Statistics	Conclusions
Van Bortel *et al*. 2001	Millar tonometer, Echo-tracking, Invasive pressure.	19 100	cSP	PCC, Bland-Altman, ($p < 0.05$)	ΔPP distension/tonometry = 3.4 ± 6.9 mmHg ($r = 0.85$, $n_{sub} = 100$) ; ΔPP distension/invasive = 1.6 ± 6.9 mmHg ($r = 0.85$, $n_{sub} = 19$).
Vermeersch *et al*. 2008	SPT-Millar tonometer, Echo-tracking.	2026	RMSD cSP AIx	Paired Wilcoxon tests, Bland-Altman analysis, ($p < 0.05$)	RMSD linear calibration = 5.2 ± 3.3 mmHg; ΔAIx linear calibration = 1.9 ± 10.1 %; ΔcSP linear calibration = 6.4 ± 4.1 mmHg.
Baulmann *et al*. 2008	Arteriograph®, SphygmoCor®, Complior ®.	51	PWV AIx	SCC, Paired t-tests, Bland-Altman analysis, ($p < 0.05$)	PWV Arteriograph/SphygmoCor ($r = 0.67$, $p < 0.001$); PWV Arteriograph/Complior ($r = 0.69$, $p < 0.001$); PWV SphygmoCor/Complior ($r = 0.87$, $p < 0.001$); AIx Arteriograph/SphygmoCor ($r = 0.92$, $p < 0.001$).
Ding *et al.* 2011	SphygmoCor®, HEM 9000AI®, Invasive data.	33	cSP	ICC, Paired t-tests, Bland-Altman analysis, ($p < 0.05$)	ΔcSP SphygmoCor/Invasive = -15 mmHg ($r = 0.91$, $p<0.001$); ΔcSP Omron/Invasive= -2 mmHg ($r = 0.90$, $p < 0.001$).
Horváth *et al*. 2010	Arteriograph®, Invasive data.	16 55 22	AIx cSP PWV	PCC, Bland-Altman analysis, ($p < 0.05$)	ΔAIx = 0.3 ± 5.7 % ($r = 0.94$, $p < 0.001$, $n_{sub} = 16$); ΔcSP = 0.56 ± 8.5 mmHg ($r = 0.95$, $p < 0.001$, $n_{sub} = 55$); ΔPWV = 0.05 ± 1.8 m/s ($r = 0.91$, $p < 0.001$, $n_{sub} = 22$).
Kips *et al*. 2010	Distension waves (ultrasound), SphygmoCor®.	148	FF%	ANOVA, ($p < 0.05$)	ΔFF% = 6.2 %.
Wassertheurer *et al*. 2010	ARCSolver®, SphygmoCor®.	302	AIx cSP	Bland-Altman analysis	ΔcSP = -0.1 ± 3.1 mmHg; ΔAIx = 1.2 ± 7.9 %.

Table 2.4 (cont.). Examples of comparison and invasive validation studies of several commercial devices for central arterial pulse wave acquisition (n_{sub} - number of subjects entered the study, SCC - Spearman correlation coefficient, Δ- difference, *r* - correlation coefficient)

Studies	Compared Devices	n_{sub}	Studied parameters	Statistics	Conclusions
Zuo *et al.* 2010	SphygmoCor®, Invasive data.	45	cSP, cPP	Paired t-tests, PCC, Bland-Altman analysis	ΔcSP = 4 ± 17 mmHg (r = 0.84, p < 0.001); ΔcPP = −20 ± 14 mmHg (r = 0.82, p < 0.001).
García-Ortiz *et al.* 2012	B-pro®, SphygmoCor®.	104	cSP, AIx	Paired t-tests, PCC, ICC, Bland-Altman (p < 0.05)	ΔcSP = 1.47 mmHg (r = 0.949, p < 0.01); ΔAIx = 5.85 % (r = 0.436, p < 0.01).
Zhang *et al.* 2013	SphygmoCor®, Pulse Pen®, A-Pulse®.	66	cSP	Paired t-tests, PCC, ICC Bland-Altman (p < 0.05)	ΔcSP SphygmoCor/PulsePen = 5.0 mmHg (r = 0.95, p < 0.01); ΔcSP A-Pulse/SphygmoCor = 3.7 mmHg (r = 0.78, p < 0.01); ΔcSP A-Pulse/PulsePen = 5.7 mmHg (r = 0.92, p < 0.001). ΔAIx Pulsepen-SphygmoCor = 5.7 % ± 10%
Pucci *et al.* 2013	Vicorder®, SphygmoCor®, Invasive pressure.	90	cSP	Paired t-tests, PCC, Bland-Altman analysis (p < 0.05)	ΔcSP Vicorder = -6.4 ± 7.4 mmHg (r = 0.92, p < 0.001); ΔcSP SphygmoCor = -2.8 ± 9.4 mmHg (r = 0.87, p < 0.001).
Sztrymf *et al*. 2013	SphygmoCor®, Invasive data.	12	FF%, Frequency	Wilcoxon tests, Bland-Altman analysis.	ΔFF% = 4.2 ± 2.8 % (p < 0.001); No significant difference between harmonics.
Agnoletti *et al*. 2014	Sphygmocor®, PulsePen®.	38	cSP, AIx, FF%, Frequency	Paired t-tests	ΔcSP = 2.7 ± 4.4 mmHg; ΔAIx = 4.2 ± 8.4 %; ΔFF% = 3.2 ± 3.5 %. The harmonics moduli were similar across the spectrum (exception of the 1st).
Pereira *et al*. 2014	Complior Analyse® Invasive data.	15	cSP, AIx, Wave morphology	Paired t-tests, Bland-Altman analysis, PCC	ΔcSP = 1.80 ± 4.20 mmHg (r = 0.98); ΔAIx = 0.24 ± 0.92% (r = 0.99).
Stea *et al*. 2014	Complior Analyse®, Complior SP®, SphygmoCor®.	112	PWV (n_{sub} = 107), cSP (n_{sub} = 98)	PCC Bland-Altman	ΔcSP SphygmoCor / Analyse = -0.7 ± 5.6 mmHg (r = 0.94, p < 0.001).

3

Fundamentals on optical fibre sensors: FBG and intensity based configurations

Optical fibres are specially known as data transmission systems for telecommunications networks. Nevertheless, optical fibres applications are not limited to information transport, and may also be used as sensors. A wide range of parameters, such as temperature, strain, refractive index, acceleration and humidity, can be monitored using OFS, with several advantages over electronic sensors (Grattan and Sun 2000). OFS are generally compact and lightweight, can be effectively multiplexed on a single fibre, are immune to electromagnetic interference, due to its dielectric nature, and they do not conduct electrical current, being safer than electromechanical devices, especially in harsh environments and medical facilities (Alberto *et al.* 2013). There are several types of OFS that use the different properties of the propagated optical signal (intensity, phase, frequency or spectral contents) to monitor different measurands. In this section, the main topics on optical fibre sensors related to the developed work are discussed.

3.1. Principles of light propagation through an optical fibre

The light propagation through an optical fibre relies on the internal reflections enabled by the refractive index transitions between the core and the cladding, accordingly to the total internal reflection principle (Ghatak and Thyagarajan 1998). The light interaction between core and cladding is governed by the Snell's law, which states that the reflection of an incident electromagnetic wave is related by:

$$n_1 sin\theta_1 = n_2 sin\theta_2 , \qquad \text{(eq. 3.1)}$$

in which θ_1 and θ_2 are, respectively, the angles of incidence and reflection, and n_1 and n_2 are the refractive indices of the interface materials. Applying the Snell's law to an optical fibre, considering n_{core} and n_{clad} as the core and cladding refraction indices, respectively, it can be defined the minimum angle of an incident ray, in the fibre cladding, to occur total internal reflection. This angle is known as the critical angle (θ_c) and is given by:

$$sin\,\theta_c = \frac{n_{clad}}{n_{core}} . \qquad \text{(eq. 3.2)}$$

As can be verified in Fig. 3.1, rays with angles lower than θ_c are refracted through the cladding. On the other hand, total internal reflection occurs for all rays with angle of incidence (θ_i) higher than θ_c. The critical angle also defines the cone of acceptance of an optical fibre.

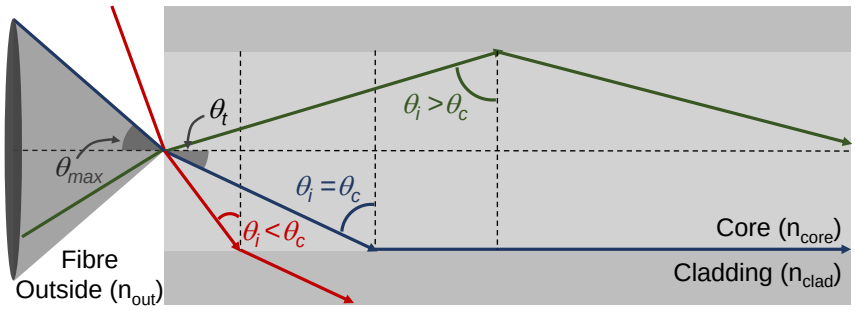

Figure 3.1. Scheme of the total internal reflection conditions and acceptance cone (n_{out} - refractive index of the fibre outside; θ_{max} - maximum angle of a ray entering the fibre and θ_t - maximum angle of a transmitted ray through the outside-fibre core interface).

The fibre numerical aperture (*NA*) is a dimensionless value that defines the range of angles of the incident light accepted by a fibre core, delineating the cone of acceptance/emission of the fibre, being defined as:

$$NA = n_{out}\,\sin\theta_{max} = \sqrt{n_{core}^2 - n_{clad}^2} . \qquad \text{(eq. 3.3)}$$

A specific optical fibre can be monomode/singlemode, as it transmits only the transversal mode with negligible mode dispersion, or multimode, which has larger diameter and NA (more than 50 µm and 0.2, respectively), allowing the transmission of several other modes of the introduced signal. The number of modes transmitted by an optical fibre is determined by the *V*-parameter (*V*), which depends on the fibre's radius (f_r), the light wavelength (λ) and *NA*, being given by:

$$V = \frac{2\pi f_r}{\lambda} NA \,. \qquad \text{(eq. 3.4)}$$

For *V* smaller than 2.405, a singlemode is propagated through the fibre, otherwise the fibre complies the transmission of multimodes. For a step-index profile, the number of modes is approximately $V^2/2$ (Ziemann *et al.* 2008). Monomode fibres, with diameters lower than 8 µm and typical NA of 0.11, are therefore better at maintaining the fidelity of the optical signals introduced over larger distances than multimode fibres (Keiser 2003). This fact is related to the different propagation length of each light ray. For the fundamental mode, the propagation length (p_{length}) is given by the fibre length (f_{length}), but for all the others rays is defined as:

$$p_{lenght} = \frac{f_{length}}{cos\theta_t} \,. \qquad \text{(eq. 3.5)}$$

However, for intensity based sensors, in which the transmitted power is related to the sensors sensitivity, higher *NA*s are more important than signal fidelity.

3.2. Silica and polymeric fibres

Regarding constituent materials, the used fibres can be of silica or polymeric/plastic materials. SOFs have their core and cladding of silica, whereas POFs are typically fabricated of poly(methyl 2-methylpropenoate), usually known as poly(methyl methacrylate) (PMMA), or other polymers such as amorphous fluorinated polymer, polystyrene and polycarbonate (Peters 2011).

The fibres used in this work were: the *PS1250/1500 (FiberCore*) for FBG engraving; the *SMF-28e+* (*Corning*) as link of the FBG fibre to the data acquisition systems; and the *GM 4001* (*Mitsubishi Rayon Co*) for the intensity based sensor. The features of the referred optical fibres are presented on Table 3.1.

Table 3.1. Features of the SOFs and POF used in this work (data from Kalachev *et al.* 2005; Mitsubishi 2010; Fibercore 2013; and Corning 2014).

Features	PS1250/1500	SMF-28e+	GM 4001
Core material	Silica	Silica	PMMA
Operating wavelength (nm)	1310 1550	1310 1550	530 570 650
Numerical aperture	0.12 - 0.14	0.14	0.5
Attenuation (dB/km)	≈ 10 (1310 nm) ≈ 120 (1550 nm)	0.03 (1310 nm) 0.02 (1550 nm)	170 (650 nm)
Core diameter (μm)	6.9	8.2	980
Cladding Diameter (μm)	125 ± 1	125 ± 0.7	1000
Coating Diameter (μm)	245 ± 15	242 ± 15	2200

PMMA and Silica, due to the differences in attenuation, have very different operating wavelength windows, as can be verified on Fig. 3.2. POF is usually operated in the visible and SOF in the infra-red (IR), around 1310 and 1550 nm.

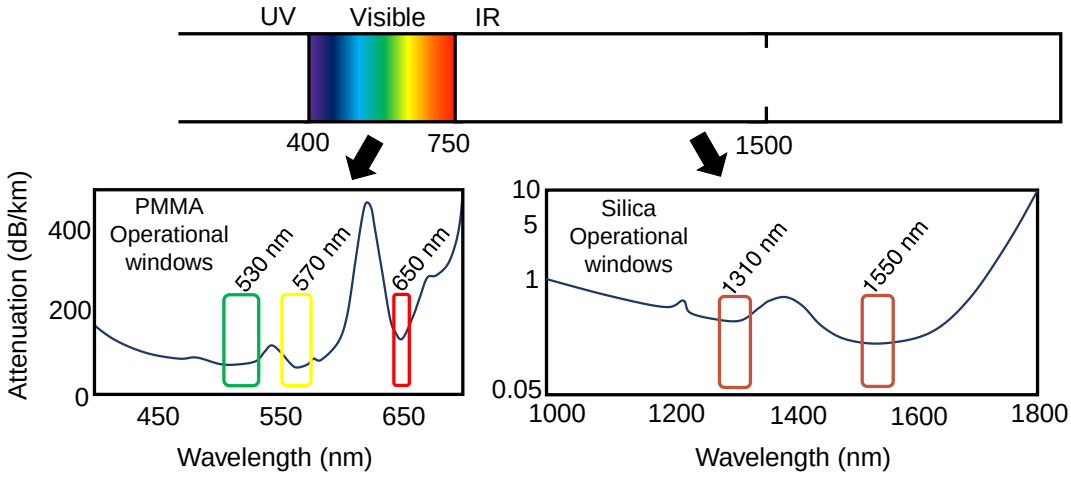

Figure 3.2. Operational windows of PMMA and silica (UV - ultraviolet) (adapted from Ziemann *et al.* 2008).

The fidelity of signal transmissions through long distances, also due to the signal residual attenuation of 1dB/km, made monomode SOF attractive for optical communications. On the other hand, in short networks, the 1 mm POF has become popular, even though a typical attenuation of 170 dB/km (650 nm) (Peters 2011). POFs great application in diverse fields are especially due to their high mechanical resilience. With a Young's module of 3.2 GPa, an elastic module of 10 %, in addition to the flexibility of the large

2.2 mm jacket, POFs allow rough handling, such as severe bending and stressing, without causing permanent damages. On the other hand SOFs have to be carefully handled since they present an elastic limit of 1 - 3 % and a Young's module of 72 GPa (Peters 2011; Bilro *et al.* 2012; Abrate *et al.* 2013).

Other advantage related with POF dimensions are the 980 μm core and the 0.5 NA, which allow a certain grade of aligning mismatch in connectorization processes between fibres, emitters and receptors. This tolerance avoids the use of the expensive precision tools for cleaving and connectorization used for the 125 μm SOFs, since their 8.2 μm core leave no margin for possible misalignments (Abrate *et al.* 2013).

3.3. FBG and Intensity sensing configurations

Optical fibre sensing systems are usually composed by four basic components, a light source, one or more optical fibres, the sensing element(s), and a photodetector or spectrometer. The light source applies the optical signal that is transmitted through the optical fibre. The fibre itself can act as a transducer (intrinsic sensor) or only as a mean to transmit the signal to and from the transducer (extrinsic sensors). The transducer is the light modulator, changing the optical signal features with the measurand, variation that can be in amplitude, intensity/optical power, phase, polarization or wavelength/frequency. Finally, the optical signal is received in the photodetector/spectrometer. In this section, the OFS techniques used in this work for micro displacement monitoring with FBG and reflection intensity based sensors, are introduced.

FBG based sensors

The first FBG inscribed in a silica fibre was reported in Hill *et al.* 1978, work developed in the Canadian Communication Research Center, Ottawa. The photosensitivity discovery was a crucial step for the FBG engraving, and, in 1989, Meltz, Morwy and Glen made FBGs writing practical by interferometric means, using UV light at 242 nm (Meltz *et al.* 1989). Since then, FBG sensors have been improved and applied as filter in telecommunications (André *et al.* 2001) and as sensors in diverse fields, with great importance in structural health monitoring from civil (Antunes *et al.* 2012) to aerospace applications (Kahandawa *et al.* 2012). In Xiong *et al.* 1999, the first FBG inscribed in POF was reported, being now used as robust and more sensitive FBG solutions for a variety of applications (Ye *et al.* 2009, Marques *et al.* 2015).

FBGs are micro periodical changes of the refractive index engraved in the fibre core. In Fig. 3.3 a basic diagram of the working scheme of a uniform FBG, is presented. When a broadband light spectrum is injected in the fibre, this optical signal will interact with the FBG, where the wavelengths that fulfil its resonation condition are reflected, while the others are transmitted. The reflected spectrum is centred at the Bragg's wavelength (λ_B) and in the transmitted signal it can be seen a suppression at the same wavelength (Othonos and Kalli 1999). FBGs act essentially as wavelength filters, bandpass in reflection and band reject in transmission (Albert 2011). The FBG are highly accurate, since wavelength is an unalterable property of the signal along the optical fibres, on contrary to, for instance, intensity. Other great advantage of FBG based sensors networks are the possibility of engraving several FBGs at the same fibre, allowing multi-point monitoring, with only one fibre and one interrogation system.

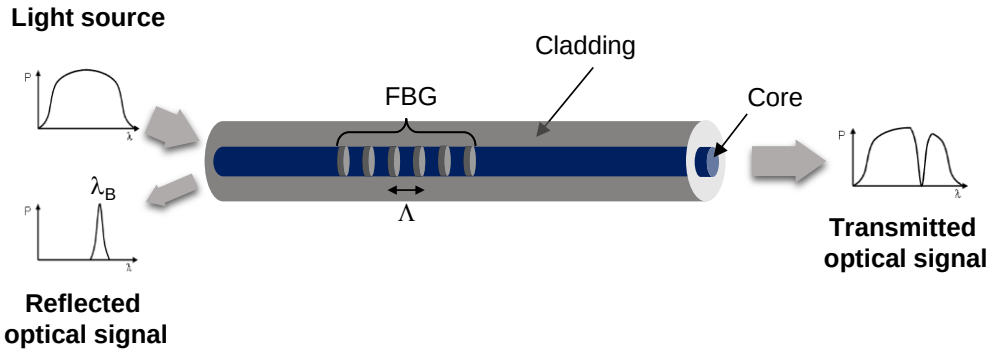

Figure 3.3. FBG working scheme.

The Bragg's wavelength is given by eq. 3.6, where Λ is the period of the grating and n_{eff} is the effective refractive index of the guided mode through the FBG.

$$\lambda_B = 2\Lambda n_{eff} \qquad \text{(eq. 3.6)}$$

The λ_B dependence on the Λ and n_{eff}, turn the FBG sensitive to mechanical (Δl) and temperature (ΔT) variations, accordingly to (Othonos 1997):

$$\Delta\lambda_B = 2\left(\Lambda\frac{\partial n_{eff}}{\partial l} + n_{eff}\frac{\partial\Lambda}{\partial l}\right)\Delta l + \left(\Lambda\frac{\partial n_{eff}}{\partial T} + n_{eff}\frac{\partial\Lambda}{\partial T}\right)\Delta T\ . \qquad \text{(eq. 3.7)}$$

The first term of eq. 3.7 right side represents the strain effect on an FBG, which corresponds to a change in the grating spacing and the strain-optic induced change in the refractive index. The strain effect (ε_z) may be expressed as:

$$\Delta\lambda_B = \lambda_B(1-p_e)\varepsilon_z\,, \qquad \text{(eq. 3.8)}$$

where p_e is the effective strain-optic constant defined by eq. 3.9, where p_{11} and p_{12} are components of the strain-optic tensor, and ν is the Poisson's ratio.

$$p_e = \frac{n_{core}^{\ 2}}{2}\left[p_{12} - \nu(p_{11}+p_{12})\right]. \qquad \text{(eq. 3.9)}$$

For a typical silica optical fibre p_{11} = 0.113, p_{12} = 0.252, ν = 0.16, and n_{core} = 1.482, which when applied in the above equations, results in an expected FBG (λ_B = 1550 nm) sensitivity of 1.2 pm/με.

The second term of eq. 3.7 right side represents the temperature effect on the FBG. A shift in the Bragg wavelength due to thermal expansion changes the grating spacing and the refraction index. This wavelength shift, for a temperature change ΔT, can be expressed as in eq. 3.10, where α is the thermal expansion coefficient of the fibre ($\approx 0.55\text{x}10^{-6}$ for silica), being given by $\partial\Lambda/\Lambda\partial T$. Whereas ζ, which is equal to $\partial n/n\partial T$, represents the thermo-optic coefficient, being approximately $8.6\text{x}10^{-6}$ for Germanium doped silica fibres. From the referred equation, for an FBG (λ_B = 1550 nm) it is expected a temperature sensitivity of 13.7 pm/^{o}C.

$$\Delta\lambda_B = \lambda_B(\alpha+\zeta)\Delta T \qquad \text{(eq. 3.10)}$$

The dual sensitivity of the FBGs can represent a problem in knowing if the detect $\Delta\lambda_B$ is due to temperature or mechanical variations. To static strain measures, usually an FBG sensing approach has to have a second sensor, isolated from mechanical effects, to detect temperature variations. For dynamic measures, in which the different strains applied to the fibre have much higher frequencies than the temperature changes, the latter can be removed by applying high pass filters. Consequently, in this case is not necessary the supplementary FBG (Leitão *et al.* 2013).

In this work, the used FBGs were inscribed by the phase mask method, as reported by Marques 2013, using an UV KrF pulsed excimer laser (*BraggStar Industrial-LN*, *Coherent*) operating at 248 nm, applying pulses with energy of 5 mJ and repetition rate of 500 Hz. The FBGs were used as the sensing element for displacement. In the Fig. 3.4 it can be seen a schematic diagram of the FBG reflected spectrum changes due to its compression and distension.

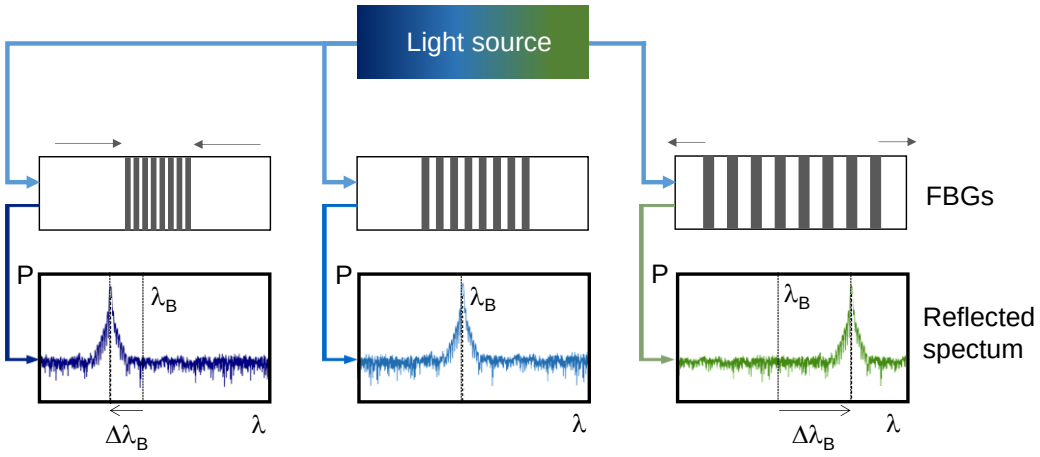

Figure 3.4. Schematization of the FBG compression and distension effects in the reflected spectra.

Intensity based sensors

The working principle of intensity fibre sensors (IFSs) rely on the variation of the light intensity with a measurand. Such solutions have been reported in several applications, such as to detect acceleration (Antunes *et al.* 2014), turbidity (Keizer *et al.* 2015) and displacement (Orłowska *et al.* 2015).

IFSs can be used in intrinsic and extrinsic configurations. The intrinsic intensity sensors have several configurations, for instance using interaction with the measurand by micro (Rothmaier *et al.* 2008) and macrobending (Silva *et al.* 2013), side-polished macrobending (Bilro *et al.* 2011; Jing *et al.* 2015), or v-shaped insertions on the fibre (Mesquita *et al.* 2016).

As extrinsic approaches, the most known configurations are based on fibre coupling, where the applied optical signal leaves the fibre to be modulated by the measurand, re-entering the same fibre (reflection configurations) or entering a second fibre(s) (transmission configurations). Examples of the referred configurations schemes can be seen in Fig. 3.5.

In the reflection configuration, which is applied in this work, the fibre acts as the emitter of the applied signal in the surface to monitor, and receptor of the reflected component. For this approach, a 2x1 optical coupler is needed, where the double part ensures the transmission of the emitted signal by the optical source, for instance an LED, to the second part of the coupler in order to be applied in the reflector. In this approach, the

reflected component enter in the same fibre, being then collected to the double part of the coupler, and finally captured by the photodetector. In front of the single fibre it should be a reflector element, acting as a mirror to the optical signal emitted by the fibre. As the measurand moves the reflector, its distance to the fibre tip changes along with the intensity of signal collected by the optical fibre, as is schemed in more detail in Fig. 3.6.

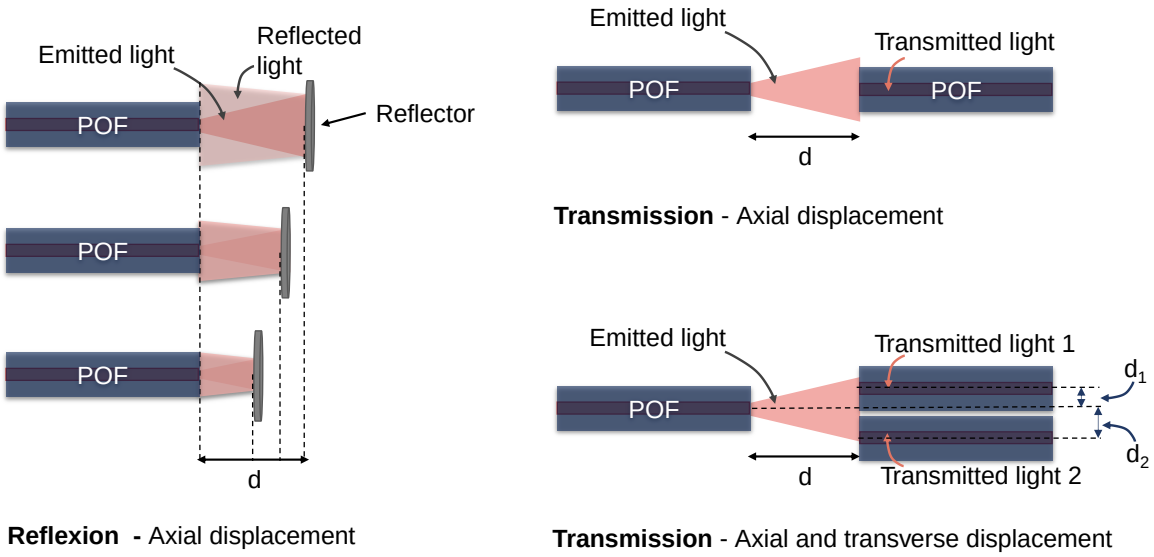

Figure 3.5. Schematic examples of IFSs configurations (d, d_1 and d_2 – different distances).

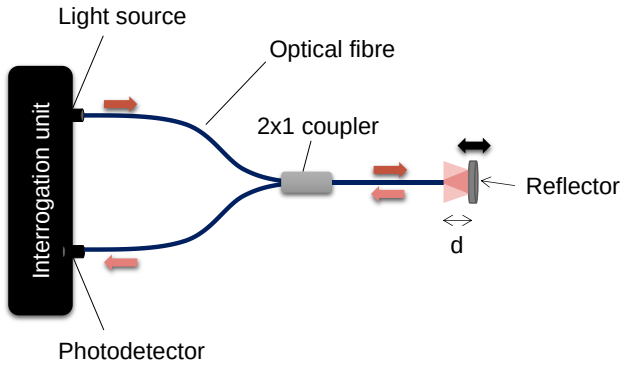

Figure 3.6. Schematic setup of a reflection configuration using a single fibre as emitter and receptor.

The expected signal intensity variation with the distance between fibre and reflector (*d*) can be calculated. In Fig. 3.7a it can be seen that the distance between the emission cone extremities and the fibre centre (*h*) can be calculated as:

$$h = 2d\tan(\arcsin NA), \qquad \text{(eq. 3.11)}$$

therefore,

$$h = 2d\frac{NA}{\sqrt{1-NA^2}}. \qquad \text{(eq. 3.12)}$$

The light cone at the fibre entrance, after travelling 2d in the fibre outside, and considering the reflector a 100 % reflective surface, have the same power that the emitted (P_E), changing only the beam spreading area, and consequently, the collected intensity (I_C), which, can be given by:

$$I_c = \frac{P_E}{\pi\left(f_r + \frac{2d.NA}{\sqrt{1-NA^2}}\right)^2} \qquad \text{(eq. 3.13)}$$

In the Fig. 3.7b it can be seen that for small distances the behaviour is linear, and is within this range that the sensitivity is maximized.

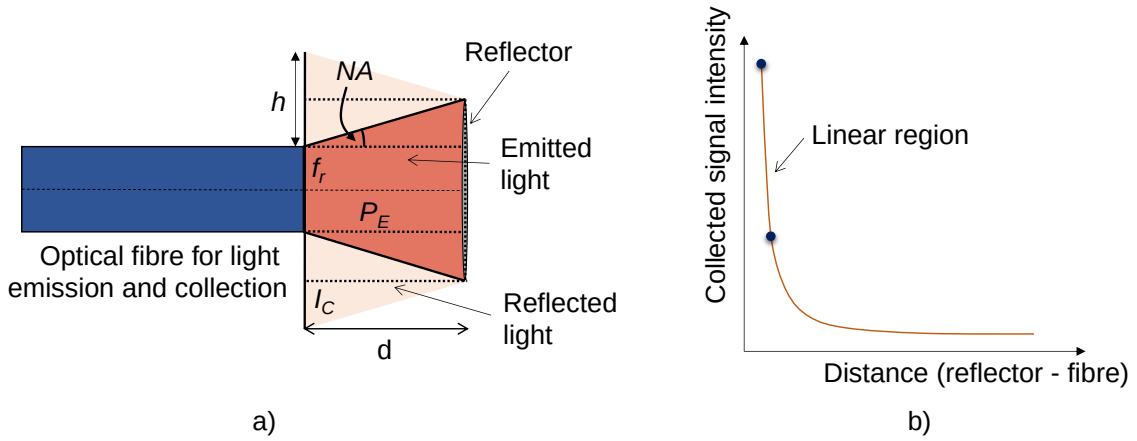

Figure 3.7. Schematization of the collected signal intensity: a) by the fibre, considering the reflector as a 100% reflective surface; b) variation with the distance between the reflector and fibre.

In IFSs, is fundamental to potentiate the intensity transmitted through the fibre, and an easy way to get high power in these configurations is to use multimode fibres, due to their larger cores and cones of acceptance (NAs) than singlemode fibres. The use of such fibres, also decrease the cost of IFS solutions for the reasons described earlier. The simplicity of this technique in terms of design and interrogation equipment has stimulated its application in different fields over the years. The great advantage of such systems is obtaining sensitive, robust and low-cost sensors interrogated with simple equipments based on LEDs as power sources and PDs to detect the intensity variations. These and

other OFS approaches are presently applied in the broad biomedical field, as is discussed in the following section.

3.4. Optical fibre sensors in biomedical applications

The first great application of optical fibres to medicine had the purpose of illuminate internal organs. Together with cameras miniaturization, the introduction of the optical fibres was revolutionary for endoscopy (Nezhat 2011). During the past decades, the same technology has been adopted to create several biomedical devices for medical treatments deliver and as transducers for monitoring parameters of interest for both therapeutic and diagnostic purposes (Taffoni *et al.* 2013).

OFS are now widely studied and applied in the medical field, for both chemical and physical measurands, allying their great features as sensors with the fact of being electrically isolated from the patients, which easies the equipments certification process for being commercialized as medical devices (ISO 2003). Currently, OFS are used as biomedical monitoring solutions in a wide range of applications, whose examples are following presented.

Non-invasive monitoring of vital signals

In the hospital routine, four vital signals are important to be frequently measured: body temperature, respiratory rate, heart frequency and blood pressure. Solutions to monitor the respiratory and heart rate have been explored (Silva *et al.* 2011; Petrovic *et al.* 2014; Chethana *et al.* 2016), and also as a current trend on OFS, using embedded sensors on smart textiles (Grillet *et al.* 2008, Quandt *et al.* 2015). Optical fibre solutions are attractive for smart medical textiles because they allow both sensing and signal transmission. On the other hand, the use of intensity POF sensors allows the development of cheap, lightweight, flexible and robust sensors, as they are able to measure high strain values without damage. The sensors configurations more reported in smart textiles are with FBGs and POF intensity based sensors (Massaroni *et al.* 2015).

In the cardiovascular field, some pressure radial waveform monitors had been presented using FBGs. In 2005, Van Brakel described a radial bracelet with an optical fibre containing two FBGs, forming a Fabry-Perot interferometer, which allowed the registering of the arterial pressure wave (Van Brakel *et al.* 2005). More recently, Sharath *et al.* presented a watch like structure with an FBG to detect the distension movements of the

radial artery (Sharath *et al.* 2014). A FBG method, based on the last device presented, was also used to detect the pulse propagation time between carotid and radial arteries (Sharath *et al.* 2015), but the quality of the carotid waves seemed not to be sufficient to use it to calculate cSP. The sensors ahead described in this dissertation are a part of this research field, allowing to register quality arterial pulses in the carotid artery with the purpose of to performing PWA and cSP calculation.

Minimally invasive monitoring

OFS have several attractive features to invasive monitoring, such as high flexibility and small size of both sensors and cables, allowing their insertion within deep-seated tissues. Their accuracy, sensitivity and frequency response (bandwidth of hundreds of kHz) are adequate for dynamic temperature, pressure and displacement monitoring applications. On the other hand, once more, their immunity to electromagnetic interference allows the use of OFS during MRI or computerized tomography guided procedures (Schena *et al.* 2016). As examples, fibre optic catheters with tip pressure sensors are currently used in intravascular, muscle compartment, intracranial, and intraocular pressure measurements (Clausen and Glott 2014).

OFS have been also applied in minimally invasive thermal treatments for tumour removal, for instance by radiofrequency ablation (Yokoyama *et al.* 2008), high intensity focused ultrasound (Wang *et al.* 2014) and laser ablation (Tosi *et al.* 2016). Research also have been made in the use of optical fibres as *in vivo* dosimeters used during radiotherapy. The small dimensions of OFS based dosimeters, allied with being lightweight and flexible, shown that they are minimally invasive and therefore particularly suited to *in vivo* dosimetry. A fibre dosimeter can then be placed directly inside the patient, for example, during brachytherapy treatments, as the optical fibres can be placed in the tumour itself, or into nearby critical tissues requiring monitoring, through the same applicators or needles used for the treatment delivery, providing real-time and *in-situ* dosimetry information (O'Keeffe *et al.* 2015).

Another great application of OFS is as force sensors, in minimally invasive surgery, to improve tactility by medical operators (Song *et al.* 2011, Abushagur *et al.* 2014), in procedures, such as vitreoretinal microsurgery (Balicki *et al.* 2011) and biopsies (Henken *et al.* 2012), as needles shaping sensors.

MRI monitoring

The immunity to electromagnetic interferences turned OFS widely studied solutions to be implemented in medical environments with high electromagnetic fields, especially in MRI (Alberto *et al.* 2013). OFS technology is particularly suitable to develop MRI compatible sensors, since its immunity to electromagnetic fields contribute to its safety and functionalities unalteration. Additionally, the materials of the optical fibres do not perturb magnetic fields inside the MRI scanner, which is crucial for the preservation of the imaging quality (Taffoni *et al.* 2013).

Examples of OFS applications in MRI range from the assessment of needles' shape, deflection and submitted force during imaging guided procedures (Park *et al.* 2010) to the estimation of physiological parameters, such heart and respiratory rates (Narbonneau *et al.* 2008, Jonckheere *et al.* 2009).

Biochemical sensing

Regarding biochemical measurands, OFS sensors are used to detect the presence of specific chemical and biological species or monitoring their concentrations (Pospíšilová *et al.* 2015). Several chemical sensors were described to monitor diverse measurands, including gases (Grassini *et al.* 2014) as CO_2 (Bao *et al.* 2013), H_2S (Tabassum *et al.* 2013), and NH_4^+ (Rodríguez *et al.* 2014), and dissolved ions, as Cu_2^+ (Chu and Chuang 2015) and Zn_2^+ (Heng *et al.* 2016).

OFS have been also reported in a large number of biosensing applications to monitor complex compounds. Recently, a POF surface plasmon resonance sensor for the detection of vascular endothelial growth factor (a cancer biomarker) was reported by Cennamo *et al.* 2015. Other compounds were also able to be detected in diverse optical fibre techniques, being examples: DNA using optical fibre nano tips coated with molecular beacons (Giannetti *et al.* 2015); estrogen-like molecules and proteins (Wittliff *et al.* 2008; Guo *et al.* 2016), pathogenic agents recurring to immunosensors (Tawil *et al.* 2014; Srinivasan *et al.* 2016), and even illicit drugs (Li *et al.* 2012) and pollutants (Zhong *et al.* 2011; Yildirim *et al.* 2014). The research in detection of biochemical species with OFS have been developing a new trending concept, the lab-on-fibre technology, which foresees highly functionalized devices integrated into a single optical fibre (Consales *et al.* 2012; Cusano *et al.* 2015; Ricciardi *et al.* 2015).

3.5. Conclusion

Within the present chapter, the base fundaments of the developed work on OFS were exposed. The FBG and intensity sensors configurations were presented, as well as several examples of OFS applications in different biomedical areas.

From the literature research, regarding the optical fibre applications for arterial pulse acquisition, no solution was found to enable performing PWA and cSP calculation from pulses obtained in the carotid artery. The advantages of the optical fibre sensors in biomedical applications, as well as the few developed works studying their application in the carotid pulse acquisition, made them a suitable solution to explore. Therefore, the present work arises as a new contribution to this field.

Since this dissertation is organized by the published and submitted papers, whose introductions are very similar, in order to not repeat information, this chapter together with Chapter 2 embody the introductory concepts of the following chapters.

4

The developed optical fibre sensors

4.1.

Feasibility study using fibre Bragg gratings

The implementation and feasibility studies of an FBG based probe, for non-invasive monitoring of the carotid pulse, are described in this section. Assessment tests were carried out in different volunteers and it was possible to acquire the carotid pulse waveform in all subjects. In one of them, the sensor was also tested in terms of repeatability. Although further developments will be required for clinical implementation, the first studies suggested that the FBG technology can be a valid alternative to the commonly used electromechanical tonometers.

4.1.1. Sensor assembly and signal detection

The applied FBG, was engraved through the phase mask technique, in a photosensitive singlemode optical fibre (*PS1250/1500, FiberCore*). It presented a Bragg wavelength of 1550.20 nm, at room temperature (23 ^{o}C), having a 4 mm length.

The proposed probe, identified as FBGbox, consists in a small outer plastic box (35 × 35 × 20 mm) crossed by an optical fibre with the FBG positioned in the middle. The fibre was pre-tensioned, becoming the Bragg grating sensitive to elongation and compression. As presented in Fig. 4.1, a latex membrane was placed between the box and a stainless steel sphere (with a diameter of 9 mm), which works as the interface between the FBG and the common carotid.

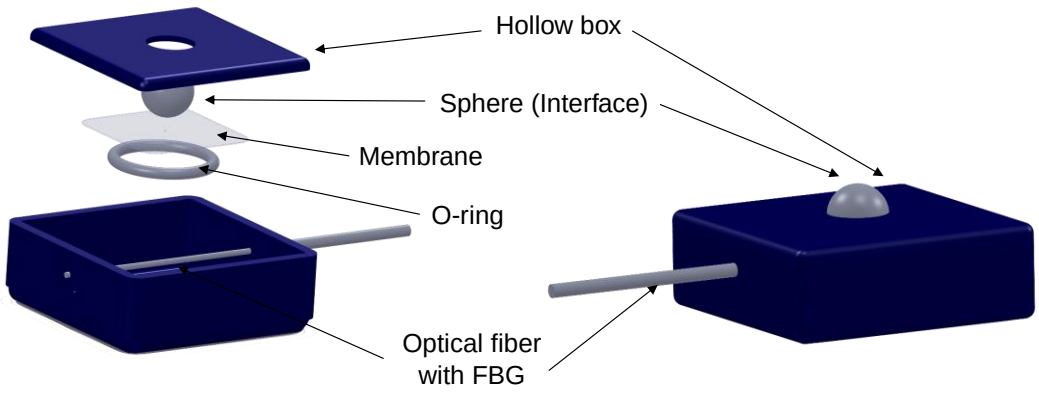

Figure 4.1. FBGbox - components drawing.

During the data acquisition process, the sensor was placed over the carotid artery and the obtained signal was monitored in real time. For the sensor interrogation, the signal from a C + L broadband optical source (*ALS-CL-17-B-FA, Amonics*) was launched into the optical fibre, being a small spectral band (centred at λ_B) reflected in the FBG, which is directed by an optical circulator to the spectrometer (*I-MON 512E-USB, Ibsen*), as can be schematically observed in Fig. 4.2a. The system presented a maximum acquisition rate of 970 Hz. The photograph and the probe application in a subject can be seen in Fig. 4.2b and c, respectively.

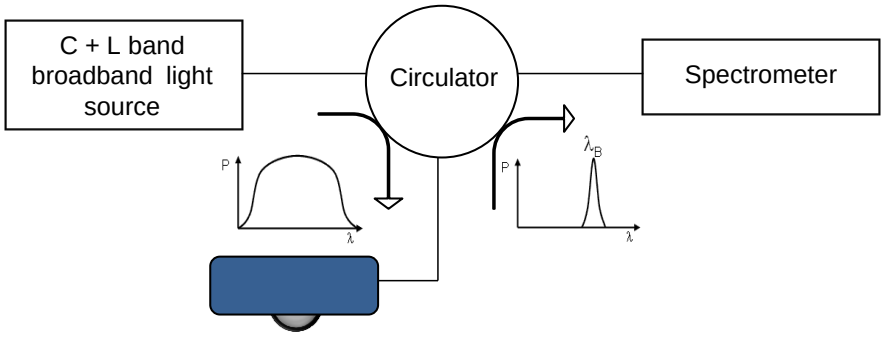

a)

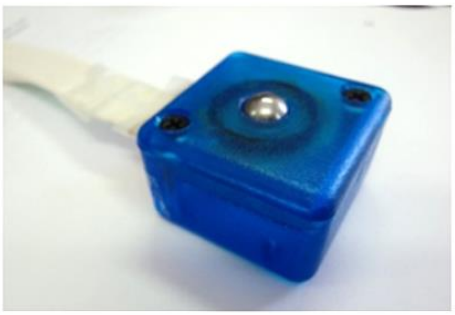

b) c)

Figure 4.2. FBGbox: a) interrogation system scheme, b) photograph, and c) application in a subject.

4.1.2. Sensor calibration

The FBGbox was characterized to displacement and its accuracy in pulse wave acquisition was also evaluated by applying mechanical synthetized waveforms. The system displacement calibration was performed with the controlled vertical movement imposed on the sphere. For this task it was used a micrometric translation stage to displace the metallic sphere and consequently the Bragg grating. As can be seen on Fig. 4.3, the Bragg wavelength dependence with the sphere displacement is described by a linear function, with an $r^2 > 0.99$. Considering this result, the pulse waveform assessed with the sensor is directly proportional to the Bragg wavelength. The probe showed a displacement sensitivity of 2.04 pm/µm.

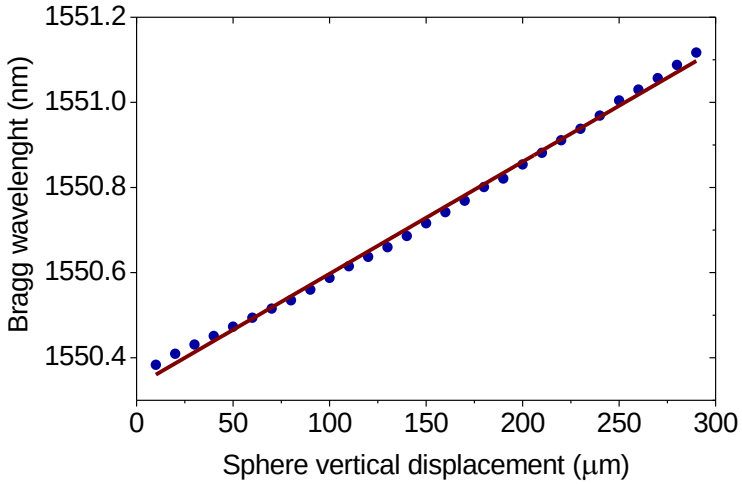

Figure 4.3. Bragg wavelength variation with the vertical sphere movement with linear fitting (r^2 > 0.99; slope = 2.0 × 10^{-3} nm/µm).

The experimental setup to analyse the sensors response to mechanical waveforms, schemed in Fig. 4.4, was composed by a waveform generator (*33220A, Agilent Technologies*), whose produced signals were amplified by a high-voltage piezoelectric amplifier (HVPZT) (*E-508.00*, *Physic Instrumente*) and applied to an Z/Tilt Piezoelectric (PZT) Flexure Stage (*P287.70, Physic Instrumente*). This specific PZT actuator was chosen due to its movement range being close to the carotid distension values, with a maximum displacement of 700 µm. For the characterization studies, the sensor was placed with the top of the sphere in contact with the moving part of the flexure stage. The generated signals were simultaneously monitored with an oscilloscope (*TK-220, Tektronix*).

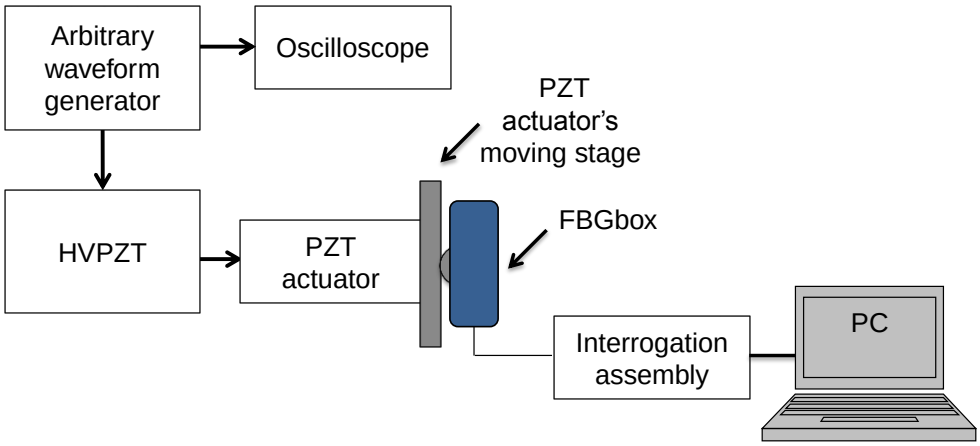

Figure 4.4. Sensor characterization setup.

For this test, several waveforms were considered, namely the “type-B” and “type-C” Murgo’s waveforms. As it can be seen in Fig. 4.5, the FBG sensor detects and follows the PZT actuator path, allowing the identification of all characteristic points of the waves, even the ones with relatively low amplitude differences.

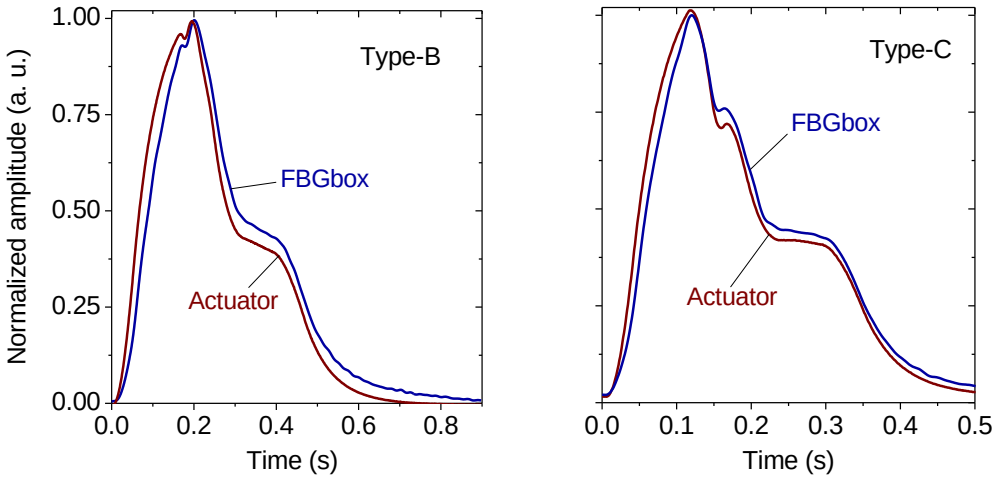

Figure 4.5. Sensor response to synthetized “type-B” and “type-C” Murgo’s waveforms.

To measure the accuracy of the sensor response, it was considered the RMSD between the PZT applied and FBGbox acquired waves. The obtained results were 7.23×10^{-3} and 45.14×10^{-3}, for the “type-B” and “type-C”, respectively. Although a lower RMSD to “type-B” wave was obtained, both values are close to zero, showing an accurate response of the sensor in following the actuator motion. These results supported the application of this sensor to assess the pulse wave in human carotids.

4.1.3. Tests in subjects

The FBGbox was tested in four human carotids of healthy subjects with an average age of 25 years old (± 2 years), being the subjects identified as I, II, III, IV. For the data acquisition, the tonometry standard protocol was used, which consists in detecting the carotid pulse by hand and placing the sensor in that location, using the recommendations presented in Table 4.1. The recording process started when a steady pulse sequence was observed. This acquisition process requires some training for the correct detection of the carotid pulse, as does the common process with the state-of-the-art tonometric devices. The acquired data, corresponding to the sensor’s Bragg wavelength over time, was filtered and normalized in amplitude between 0 and 1. Repeatability tests were carried out in one subject (IV) during five days, being the pulse wave assessed in the same day

period. In each of these times, at least eight consecutive pulses were recorded and analysed. The acquired data were also filtered and normalized between 0 and 1.

Table 4.1. Recommendations for carotid tonometry (adapted from Van Bortel *et al.* 2012)

a)	Measurements should be performed in a quiet room with stable room temperature;
b)	Perform measurements in supine position after at least 10 minutes of rest;
c)	Measurements should preferentially be done at the right common carotid;
d)	Because of diurnal variations repeated measurements should be done at the same time of the day;
e)	No meal, caffeine or smoking is allowed within 3 hours before measurement;
f)	Speaking and sleeping are not allowed during measurements;
g)	Data should be the mean of registrations during at least one respiratory cycle (about 5 - 6 s).

The FBG sensors are sensitive to strain and temperature. In the present application, temperature effects resulted in the drifting of the measured signal baseline at very low frequencies, whereas the optical noise usually occurs at much higher frequencies. In the data processing, it was used a digital filter to minimize both effects, allowing the assessment of the arterial pulse wave critical points. For this purpose, it was used a FFT bandpass filter (between 0.7 and 50 Hz), and all the results here presented were filtered with this method. In Fig. 4.6, raw and filtered data acquired in subject I can be seen. These data demonstrate that the applied filter substantially reduces the increasing tendency of the signal, which was due to temperature changes in the sensor when placed in contact with the skin. At the same type the high frequency optical noise is reduced.

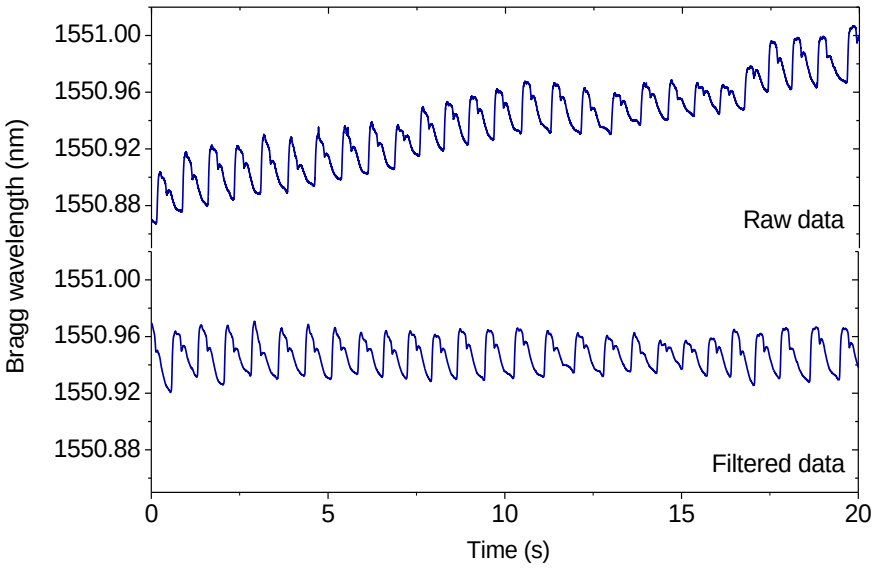

Figure 4.6. Raw and filtered data acquired in the subject I.

From the filtered data, the pulses sequences were selected in order to calculate the average pulse, for posterior temporal and amplitude analysis. In Fig. 4.7**,** the pulses sequences of the processed data, acquired in the four subjects, are presented. It can be seen that for the same subject the wave pattern is similar over time.

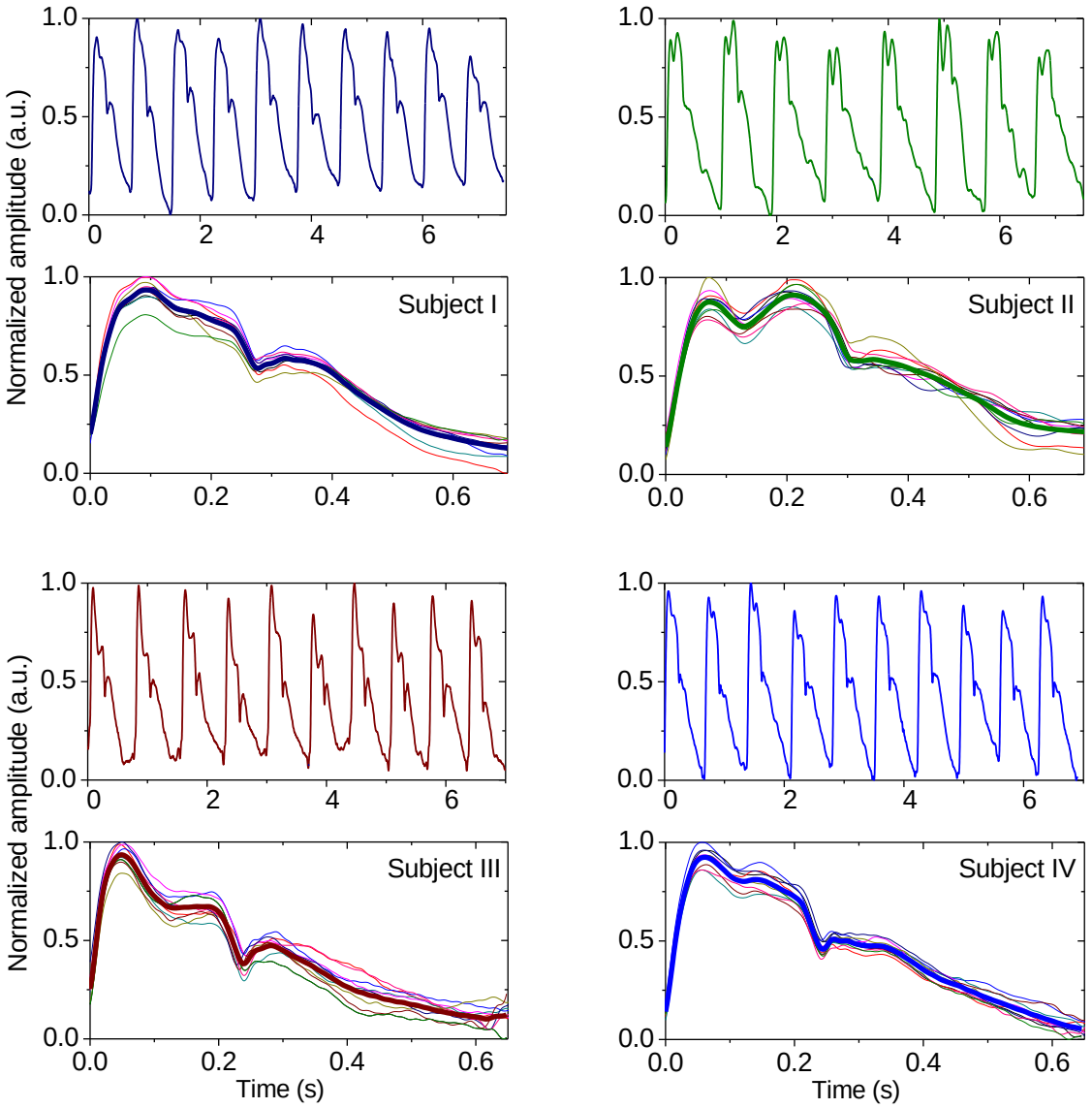

Figure 4.7. Acquired pulse waveforms in the carotid artery of the four human subjects. The top graphs represent the acquired sequences, whereas the bottom charts show the overlapping of the pulses and the respective mean pulse (bold).

All participants had a unique identification curve, presenting different AIx values, calculated before the mean pulses normalization between 0 and 1. The subjects I, III, and IV presented type-C waves, with values of AIx_{I} = -0.10 ± 0.04, AIx_{III} = -0.28 ± 0.05, and AIx_{IV} = -0.13 ± 0.03. The subject II presented a slightly positive AIx_{II} = 0.04 ± 0.04, having

been considered a type-B wave due to the amplitude of the FW and RW peaks being very similar. In the Fig. 4.8, the RMSD between each pulse on the sequence and the mean pulse can be seen for each subject. Small deviations between pulses of the same sequence can be observed with values never reaching a 10 % deviation.

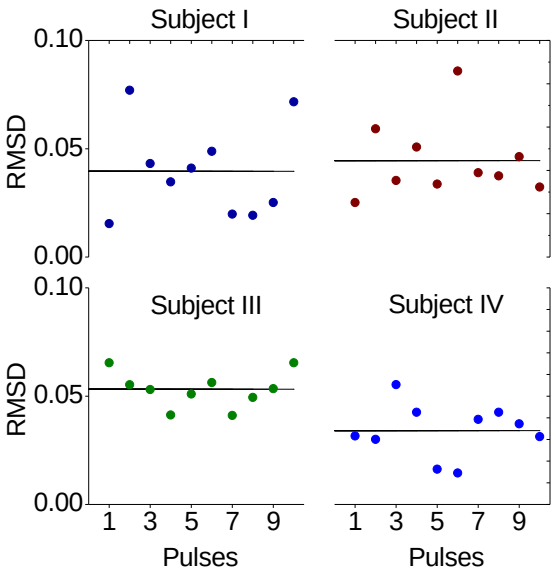

Figure 4.8. RMSD between each sequence pulse and the mean calculated arterial wave, with the mean RMSD value represented as the solid line.

Regarding to the repeatability tests, the analysed pulse wave sequences are presented in Fig. 4.9, where each graph represents eight pulses of the acquired signal in each day.

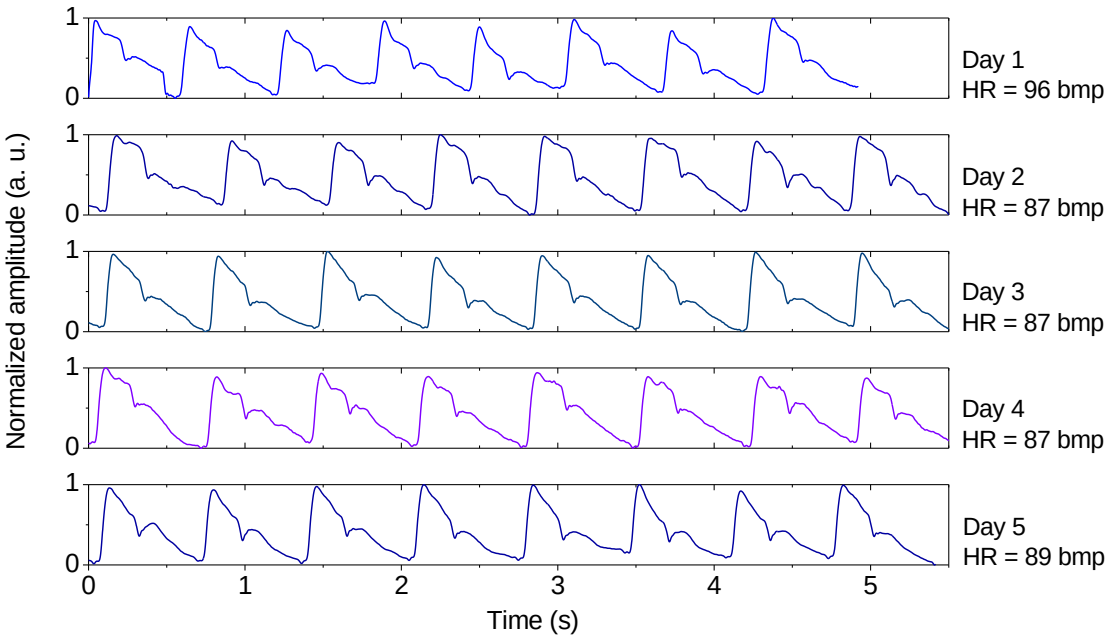

Figure 4.9. Acquired data in 5 consecutive days for the subject IV.

It can be understood that a low noise pulse wave was detected with a clear distinction of the identification points of the carotid pulse wave. The cSP, inflexion and incisura can be detailed seen on Fig 4.10a for the mean pulse of the subject IV. The mean AIx for the week was -0.19 ± 0.05, value that, as expected, is close to the value earlier assessed for the same subject (AIx_{IV} = -0.13 ± 0.05), showing a good repeatability with a maximum RMSD of 7 % (Fig. 4.10b).

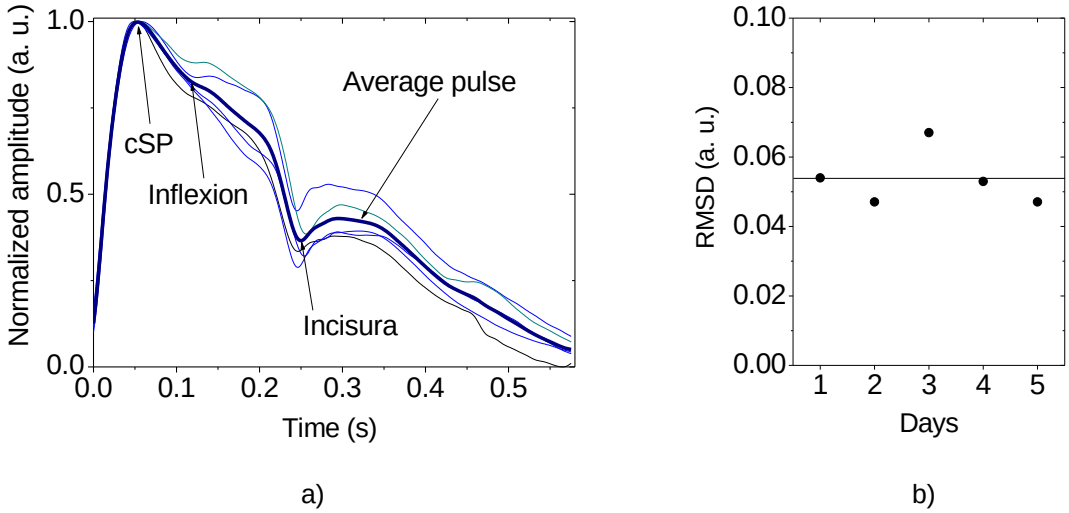

Figure 4.10. Average pulse of five consecutive days: a) pulse wave critical points and b) RMSD values of the arterial pulse of each day (dots) to the average pulse of the week, with the mean RMSD represented as the solid line.

4.1.4. Discussion

This work started with the development of an assembly capable of transferring the carotid distending movements to a pre-tensioned optical fibre with a FBG, using a sphere which was in contact with the FBG and the carotid artery, transcutaneously.

The developed probe was characterized to displacement, showing a linear behaviour with a displacement sensitivity of 2.04 pm/µm, and an operating range of 280 µm. Concerning the response to arterial synthesized waves, applied by the PZT actuator, the sensor presented a good agreement with the applied waves, presenting a mean RMSD of 2.6 %.

Four subjects were studied, and for all of them steady and regular pulse sequences were obtained, with a deviation between pulses always lower than 10 %. The quality of the acquired pulses allowed PWA, with the identification of the cSP, inflexion and incisura points. The obtained AIx values were between -0.28 and 0.04, which was expected for young healthy subjects.

The repeatability studies were performed in five consecutive days, whose pulse waves were acquired in the same period of the day. The mean deviation between the average pulses from each day and the weak mean pulse was approximately 5.7 %, which is below the maximum deviation allowed by the initial requirements.

4.1.5. Conclusion

The high sensitivity of FBGs can impose them as a valuable technology, with the advantages offered by the optical fibre technology over the traditional sensors. In this section, it was reported the initial study performed with a FBG based OFS to acquire the carotid pulse wave.

This work delivered promising results in the application of the FBG technology in the pulse wave acquisition, and the developed sensor seems to be a valid alternative to electromechanical tonometer. Besides the good results, the FBGbox testing showed that its user friendliness could be improved, and therefore a second FBG based approach was developed with a pen-like shape (FBGpen). Details of this probe design, characterization and performance, are presented in the following section.

4.2.

Portable pen-like probe based on fibre Bragg gratings

In this section, a second version of the FBG based probe is presented. This probe has a pen-like shape, facilitating its application on the carotid artery. The sensor was characterized and its response to controlled waveforms was studied. Finally, tests were performed on human subjects. The developed sensor has a displacement sensitivity of 21.20 pm/μm, and showed its ability to detect the carotid pulse wave transcutaneously in the neck surface.

4.2.1. Sensor assembly and signal detection

The proposed sensor uses a FBG, engraved in a photosensitive optical fibre (*PS1250/1500, FiberCore*) by the same method reported in section 4.1.1, with a Bragg wavelength of 1547.10 nm at room temperature (23 ^{o}C). The probe's body consists of an aluminium tube (diameter = 1 cm) crossed by the optical fibre with the FBG, as schemed and photographed in Fig. 4.11. The fibre is fixed in points A and B, with the FBG positioned in the middle of these points. Point A is located at the probe movable interface, which is maintained in extension by a metallic spring. To improve the sensor stability when monitoring the carotid pulse, it was implemented a stabilization cover, as showed in the referred figure. In this work, this probe is identified as FBGpen.

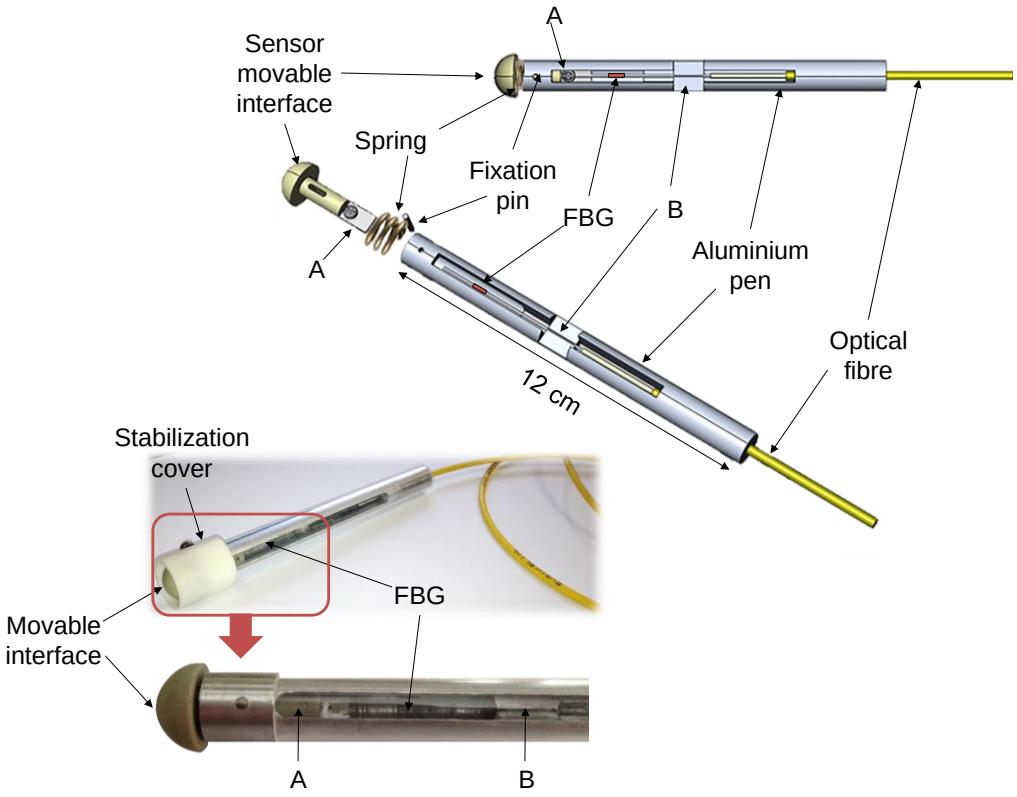

Figure 4.11. FBGpen technical drawing and photographs.

The assembly process begins with the insertion of the fibre through the tube extremity, after what the bare fibre is glued with epoxy to point B, which is left curing for 1 day. At the top of the tube is inserted the polymeric interface that is pushed from the exterior in, with the spring at its minimum longitudinal position, as the extremity of the fibre is glued to it. After curing during another day the interface is left free and the spring pullet out, stretching the optical fibre. When the sensor's movable interface is placed in contact with

the carotid artery, its distension movements cause the interface movement and consequent FBG deformation.

Changes were made in the data acquisition setup, concerning the one presented in the subsection 4.1.2., in order to improve portability and autonomy. The new FBG data acquisition system is composed by a C band light source module (*AS4500, B&A Technology*), a circulator (*6015-3, Thorlabs*), the spectrometer (*I-MON 512E-USB, Ibsen*), and a rechargeable battery (*8000mAH*, *LC-Power*), as can be schematically observed on Fig. 4.12a. The data can be acquired using a computer, or in the present case, a tablet (see Fig. 4.12b). The use of the tablet and the rechargeable battery highly improved the portability and autonomy of the system, as the acquisition system has now around eight to ten hours of autonomy.

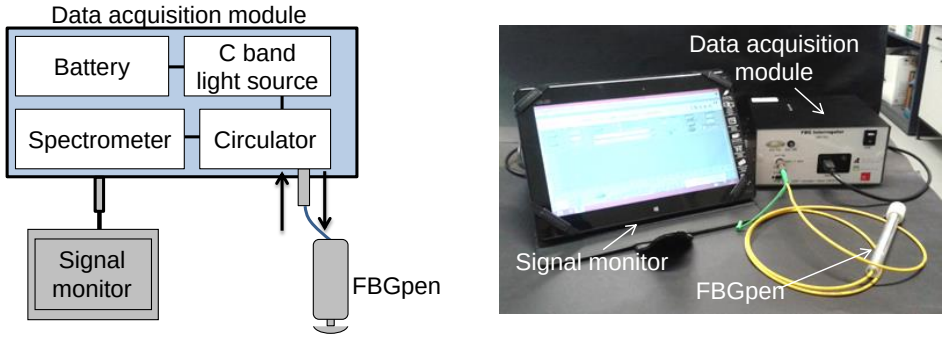

Figure 4.12. FBGpen data acquisition system a) scheme and b) photograph.

4.2.2. Sensor calibration

The sensor calibration to displacement was performed in the same experimental setup of FBGbox in order to attain Bragg wavelength dynamic range and sensitivity. In furtherance of assessing the probe's accuracy, the response to synthetized Murgo's mechanical waveforms was also studied.

The probe presented a linear behaviour between 1546.60 and 1547.02 nm, for a total Bragg wavelength variation of 420 pm. From the linear fit between the measured Bragg wavelength and the interface movement, a sensitivity of 21.20 ± 0.04 pm/μm was reached, as can be seen on Fig 4.13. The stabilization cover, showed in Fig. 4.11, has also the function of to limit the interface movement within the region with linear behaviour and higher sensitivity.

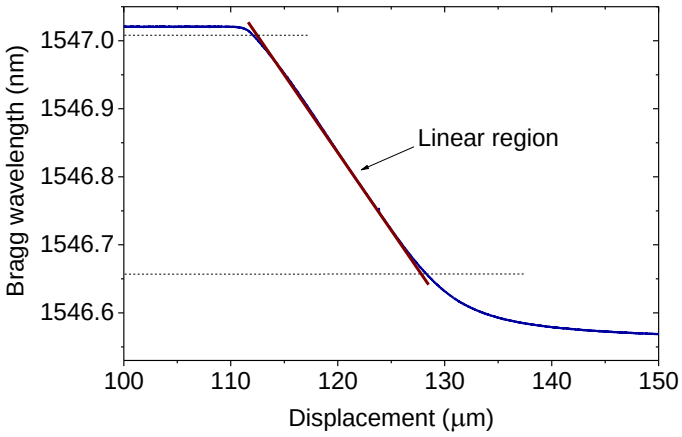

Figure 4.13. Bragg wavelength variation with the interface displacement with linear fitting (r^2 = 0.99, slope = 21.20 ± 0.04 pm/μm).

As presented in Fig. 4.14, the sensor showed the capacity to resolve two similar waveforms. In this test, the sensor accuracy was once more assessed by calculation of the RMSD, wherein the obtained mean values was 0.06.

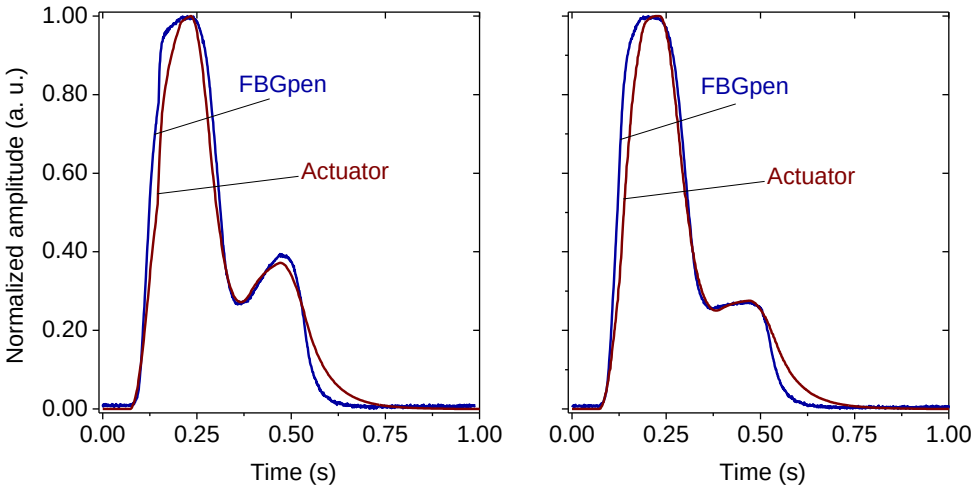

Figure. 4.14. Sensor response to synthetized pulse waveforms.

4.2.3. Tests in subjects

Human testing was carried out following the standard tonometry protocol. In Fig. 4.15, the sensor application in one of the subjects can be seen. The raw data assessed with the sensor usually shows oscillations due to respiratory movements, temperature effects on FBG and some artefacts due to operator movements, which were removed from the original signal by digital filtering, as presented in section 4.1.3.

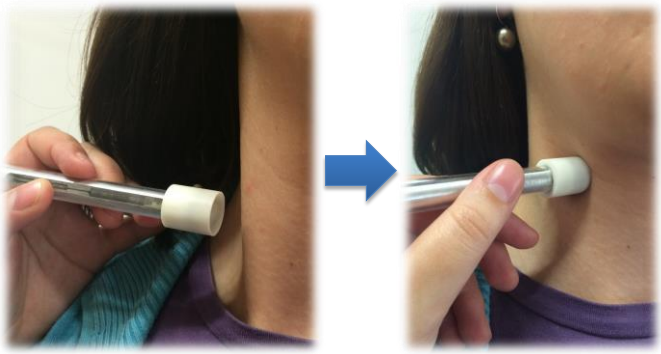

Figure 4.15. Arterial pulse wave acquisition in the carotid artery.

The central pulse pressure waves from four healthy subjects, with ages between 16 and 35 years, are showed in Fig. 4.16, where it can be seen that all subjects presented their unique wave pattern.

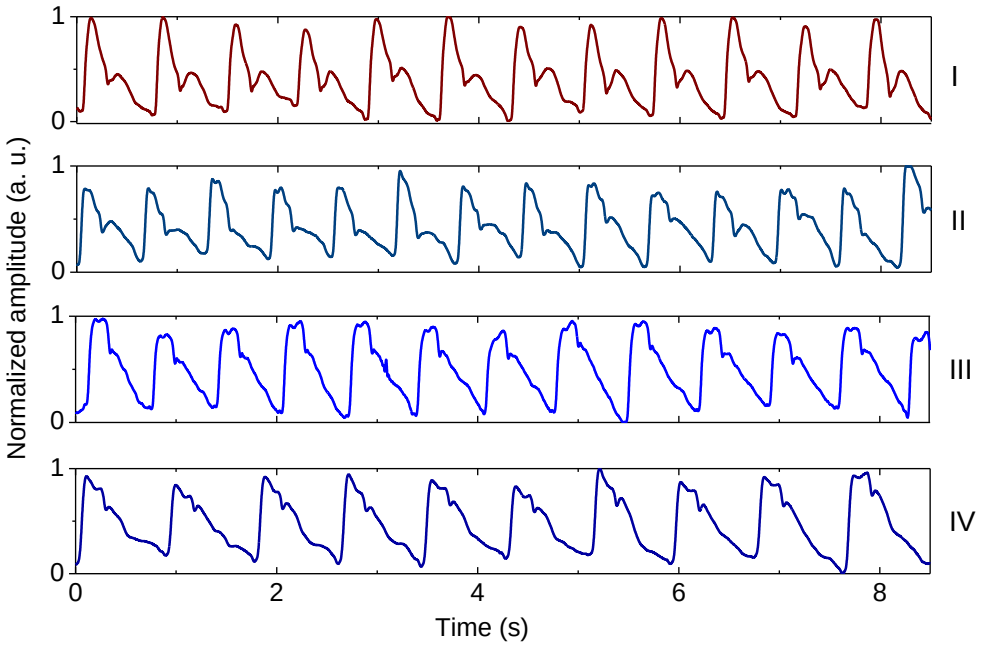

Figure 4.16. Arterial pulse waves detected in four human subjects.

In Fig. 4.17 are presented the detailed pressure waves acquired in a 16 year-old male (Subject I) and a 28 year-old female (Subject IV), as well as the respective frequency components, which are almost null after 15 Hz. This result is expected, since the physiological pressure in humans has its largest components below 14 Hz (Nichols 1990). It can also be verified the arterial pulse critical points components: cSP, inflection and incisura. The Subject I presented an AIx of -0.472 and the Subject IV -0.172.

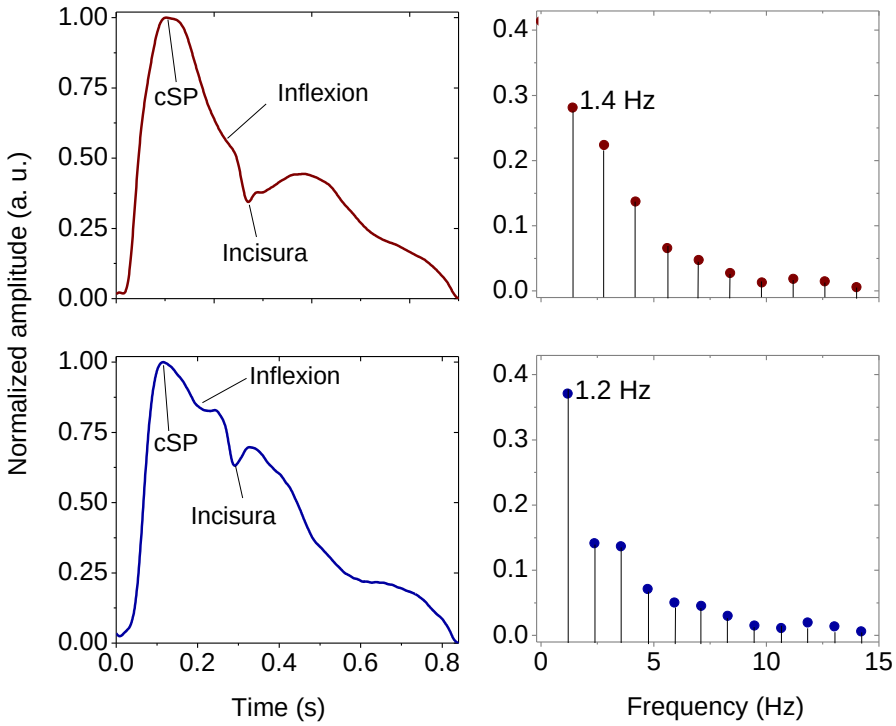

Figure 4.17. Arterial pulse waves, of subjects I and IV, in time and frequency domains.

The AIx values are negative, and therefore accordingly to Murgo's classification both waves are type-C waves. Once more, expected for two healthy young subjects.

4.2.4. Discussion

In this work a new pen-like probe using an FBG to monitor the arterial pulse was proposed. A new interrogation approach was also developed in order to improve portability and autonomy of the data acquisition system. FBGpen presented a sensitivity of 21.20 ± 0.04 pm/μm, corresponding to ten times the value obtained with FBGbox, sacrificing however the sensor dynamic range, which become around 16 μm. The accuracy tests showed a RMSD of approximately 6% and the tests in subjects demonstrated its capability of successfully detect the central arterial pulse.

Detailed pulse wave analysis was performed for two subjects, one male with 16 years-old and a female with 28 years-old. It can be seen an accentuated difference in the amplitude of the first two harmonics, due to difference in the reflection wave arrival time and amplitude. As can be noted in the Fig. 4.18, with the natural arterial stiffening effect, the major reflection components began to arrive earlier in systole, increasing the AIx and the pressure load in the left ventricle. Since the individuals are both young and healthy, they

have negative AIx, presenting “type-C” waves, but the normal effects of aging are well denoted in the pulse wave morphologies of these subjects with 12 years of age difference.

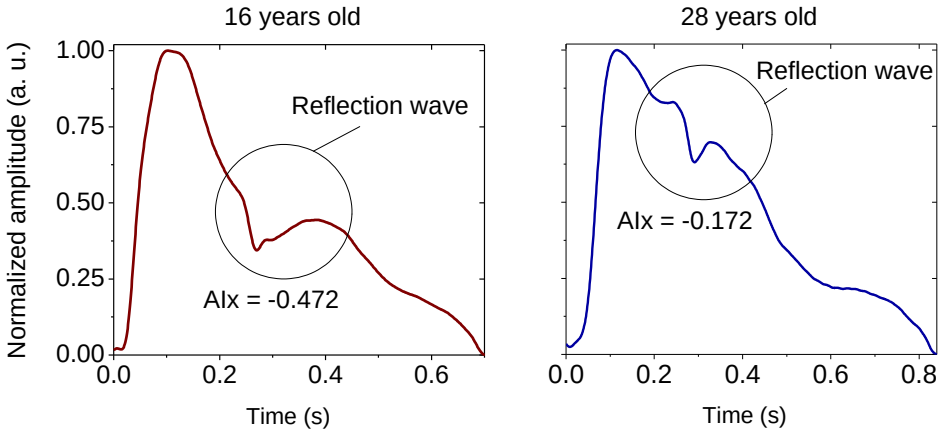

Figure 4.18. Arterial pulse wave morphologies of Subject I (16 years old) and Subject IV (28 years old).

4.2.5. Conclusion

A high sensitivity was achieved with this new approach. The sensor response was in good agreement with the controlled imposed waveforms. It was also possible to obtain the pulse waveforms in the studied four volunteers, each one having their own pulse wave morphology. Two subject’s waveforms were studied in time and frequency domain, which clearly showed the effects of normal arterial stiffness effects with aging.

This work delivered more promising results for the application of FBG technology in the pulse wave acquisition. However, besides the development of new reliable sensors to arterial pulse assessment, a second goal of this dissertation was to produce low cost solutions. Even though the systems for FBG interrogation have been decreasing in price, they are still a relatively expensive technology, which could delay its introduction in the general clinic market, which need reliable and low cost solutions. To surpass this FBG limitation, an intensity based pen-like POF approach was also explored, and the results are presented in the next section.

4.3.

Cost-effective intensity based sensor

In this section, an intensity based plastic OFS for non-invasive monitoring of the carotid pulse waveform is presented. The advantages of this sensing method are the low implementation cost, high robustness, and signal processing simplicity. At this work stage, it was also developed an automated interface for data processing. As preliminary proof of concept, the sensor was used to detect the arterial pulse waveform in some human subjects, allowing the assessment of central pressure.

4.3.1. Sensor assembly

The first version of the intensity based probe, named POFpen, comprised a cylindrical support, holding a PMMA POF (*GM 4001, Mitsubishi Rayon Co*) at the centred position, 3 mm spaced out from the sensor end surface, as schemed in Fig. 4.19.

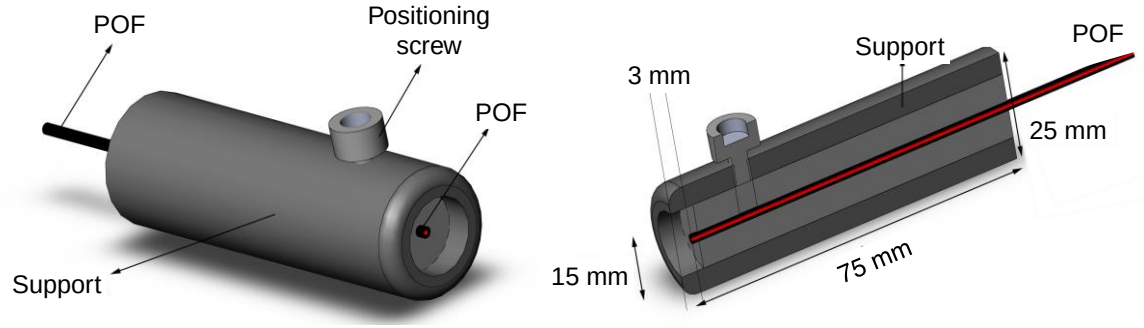

Figure 4.19. Schematic drawings and photography of the first version of POFpen.

After some preliminary testing, the support of the POF was improved to a 3D printed polylactide pen, schematically presented in Fig. 4.20a. Along this section, both versions appear, regarding different work stages.

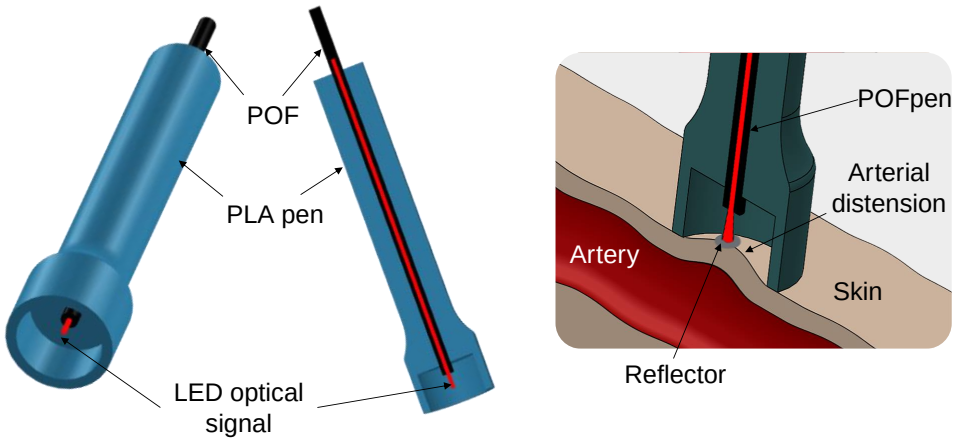

Figure 4.20. Schematic drawing of: a) the *POFpen*'s latest version and b) application on the carotid's reflector.

The sensor operates in reflection, using a 2x1 coupler (*P/N IF-562*, *Industrial fiber optics*), a red LED source (*IF-E96, Industrial fiber optics*) and a photodiode *(IF-D91, Industrial fiber optics*), being its system schemed in Fig. 4.21. For the pulse acquisition, it is launched an optical signal in the fibre from the LED source. Once out of the fibre, the

signal is reflected in the adhesive taped on the neck (above the carotid artery), returning to the fibre, reaching the photodetector. The micro distension movements of the carotid change the distance between the reflector and the fibre, modulating the reflected light. This sensing approach can allow to assess the pulse waveform without pressing the artery in the way needed for arterial tonometry.

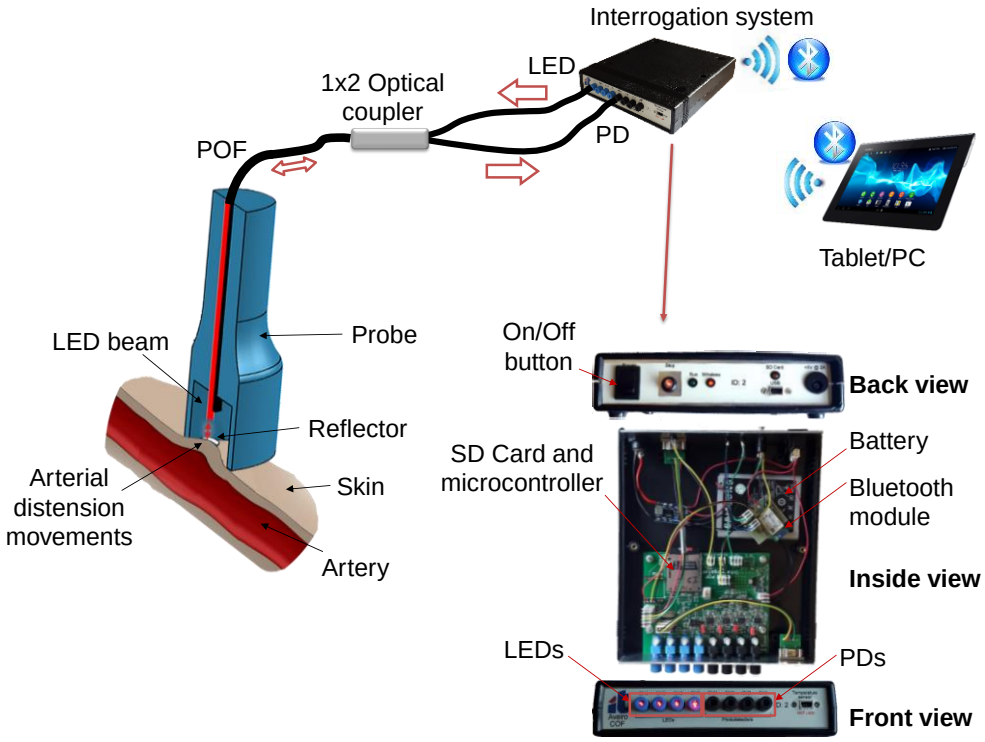

Figure 4.21. POFpen acquisition system scheme and interrogator photograph.

The interrogator uses a microcontroller (*PIC24FJ256DA206*, *Microchip Technologies*), with a 16-bit ADC, which operates in a full-scale voltage of 2.5 V, resulting in a resolution of 38.15 µV. The interrogation module is remotely controlled in the computer by a *LabVIEW*® customized application using *Bluetooth*®, allowing the real-time monitoring and saving of the assessed data. The system is powered by a battery that provides an autonomy higher than 24 hours.

4.3.2. Calibration

The calibration to displacement was performed using the same experimental approach earlier presented. The sensor exhibited a linear behaviour, with a dynamic range of 295 µm, being the measured signal amplitude, as function of the reflector displacement,

presented in Fig. 4.22. From the linear data fitting, a sensitivity of 727 ± 10 μV/μm was attained, with a determination coefficient of $r^2 = 0.99$.

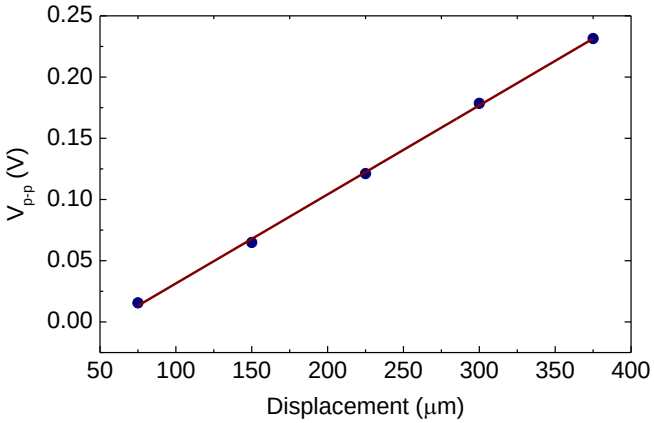

Figure 4.22. Sensor response to displacement with linear fitting (r^2 = 0.99; slope = 727 ± 10 μV/μm).

4.3.3. Data processing interface

In this section the developed algorithm for fast and easy processing of the pulse wave data is presented. The *Labview*® application, used to control the data acquisition system, creates "*.txt" files after each acquisition, which can be loaded in the developed Matlab® graphical user interface (GUI), presented in Fig. 4.23.

The pulse wave is a periodic signal with a steady component, corresponding to the diastolic pressure. It also usually complies very low frequency noise related with intrinsic factors to the patient and operator, such as respiratory and small involuntary movements. In the GUI, any pulse sequence ".txt" file can be loaded in order to proceed to its filtering, calculation of the average pulse, PWA and cSP calculation.

After the file loading, the data is graphed for the operator to select the data sequence to be segmented into individual pulses for subsequent overlapping and calculation of the average pulse. For an accurate segmentation, precise calculation of the "cutting" point of the pulses is essential. In this work, the pulses segmentation is performed by the points of the data sequence where the 2nd derivative is maximum, as showed in Fig. 4.24, a recognized method by the field's experts (Laurent *et al.* 2006).

After segmentation, the pulses are normalized between 0 and 1, and finally superimposed to determine the average pulse, from which are calculated: systolic peak, inflexion,

incisura, $t_{systole}$, $t_{diastole}$, *FF* (MAP point of the central arterial wave). After introduction of the brachial pressure levels, the cSP is calculated.

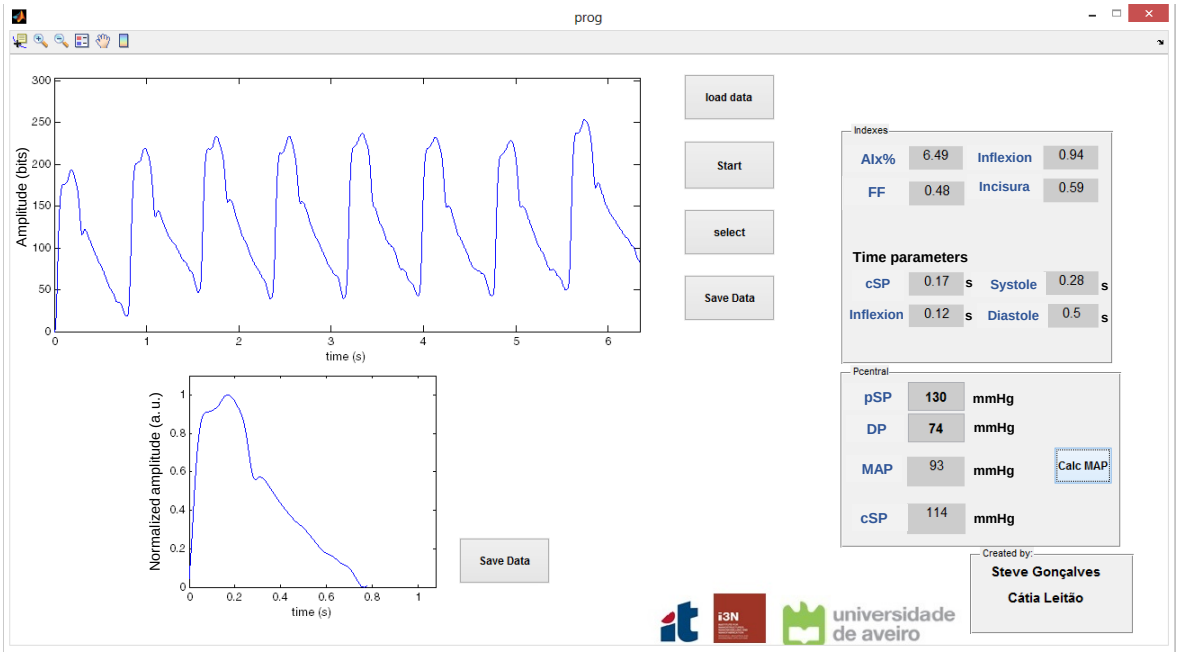

Figure 4.23. GUI developed in Matlab® - steps to the calculation of the average pulse, critical points, AIx and cSP.

The determination of the pulse wave critical points starts with the identification of the cSP peak, which corresponds to the absolute maximum of the average pulse. The other critical points are determined by analysing the 2nd derivative, whose peaks allow the determination of the inflexion point and incisura, as can be observed in Fig. 4.24.

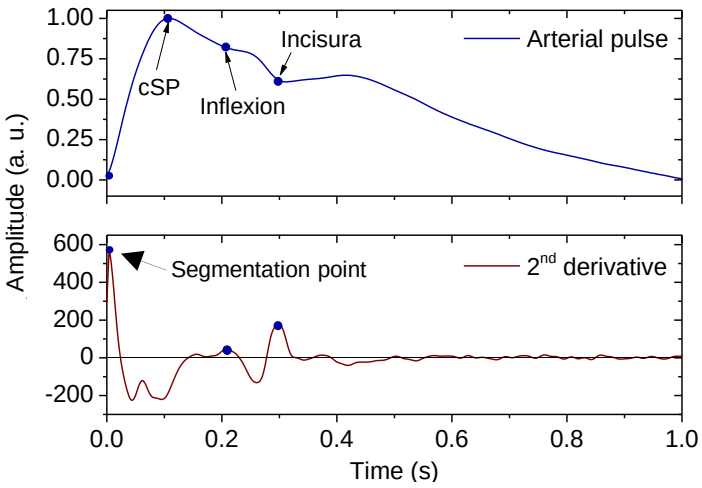

Figure 4.24. Use of the 2nd derivative to identify the inflexion and incisura (subject's heart rate - 60 bpm).

First the incisura is determined, corresponding to the 2nd derivative maximum between 20 and 50% of the wave. After that, the maximum of the 2nd derivative between the wave foot and incisura is found, matching the inflexion.

To ascertain if the cSP corresponds to FW or RW, it is determined whether the inflection point occurs before or after the cSP point. The FF corresponds to the arithmetical average of all pulse wave points. Concerning the time parameters, $t_{systole}$ matches to the incisura index and $t_{diastole}$ corresponds to the subtraction of $t_{systole}$ to the total pulse duration.

4.3.4. Tests in subjects

As preliminary proof of concept, similarly to the past sections, the sensor was used to detect the arterial pulse waveform in human subjects. Once more the data acquisition followed the tonometry protocol and clinical recommendations. The carotid artery was found by palpation, and where the heart beat was more strongly felt, it was placed the reflective adhesive, as can be observed in Fig. 4.25.

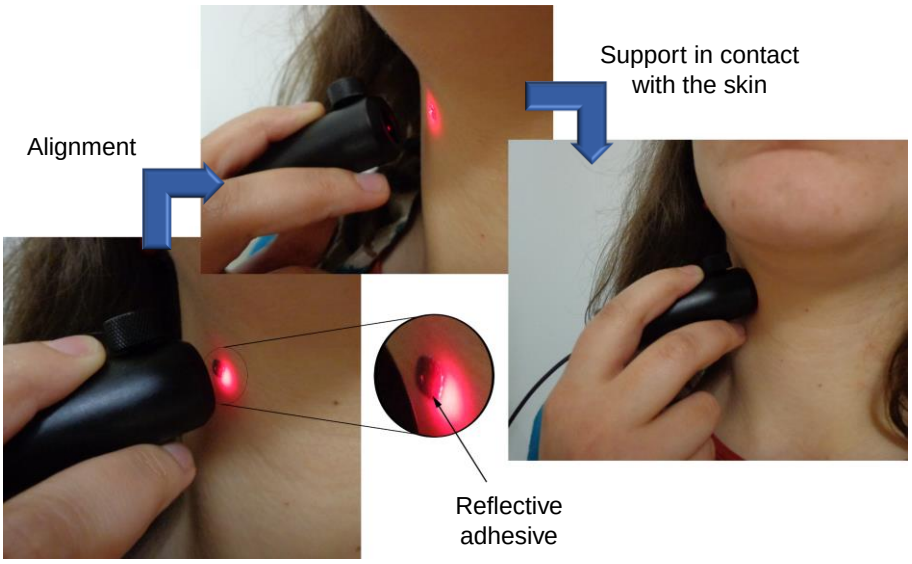

Figure 4.25. Sensor placement in the measuring location (with the reflective adhesive attached above the carotid artery).

The acquisitions were performed in four healthy subjects, denominated MN29 (male, 25 years old), SN21 (female, 28 years old), MS02 (female, 31 years old) and CL13 (female, 30 years old). Segments and overlapping of the pulses can be observed in Fig. 4.26, for the four subjects. It can be perceived that the superimposed pulses are very similar to each other, showing that the sensor has good stability, repeatability and ability to assess

the pulse wave. Subject MS02 presents the most unstable pulse segment due to a more profound respiration, which modulated the pulse wave signal. However, after normalization and overlapping this modulation is negligible.

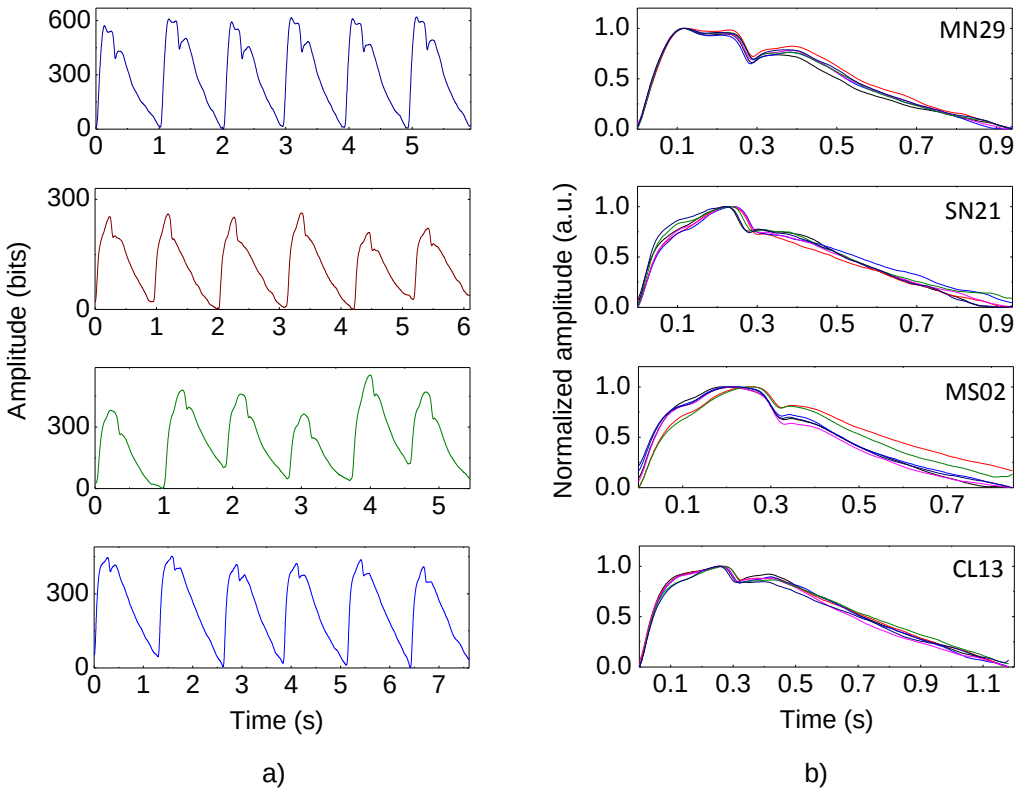

Figure 4.26. Pulses a) sequence of acquired in each subject and b) overlapping for average pulse calculation.

As the pulses are normalized, the FF is a point between 1 and 0. Matching MAP to FF and DP to the wave foot, is performed the pressure calibration. The pressure values and FF of each subject are represented in Table 4.2. After calibration, the assessed central pressure profiles can be seen on Fig. 4.27.

Table 4.2. Brachial pressures, MAP, FF and cSP values.

Subject	pSP (mmHg)	DP (mmHg)	MAP (mmHg)	FF (a. u.)	cSP (mmHg)
MN29	110	67	81.3	0.53	94
SN21	112	79	90.0	0.49	101
MS02	95	58	70.3	0.50	83
CL13	89	61	70.3	0.55	76

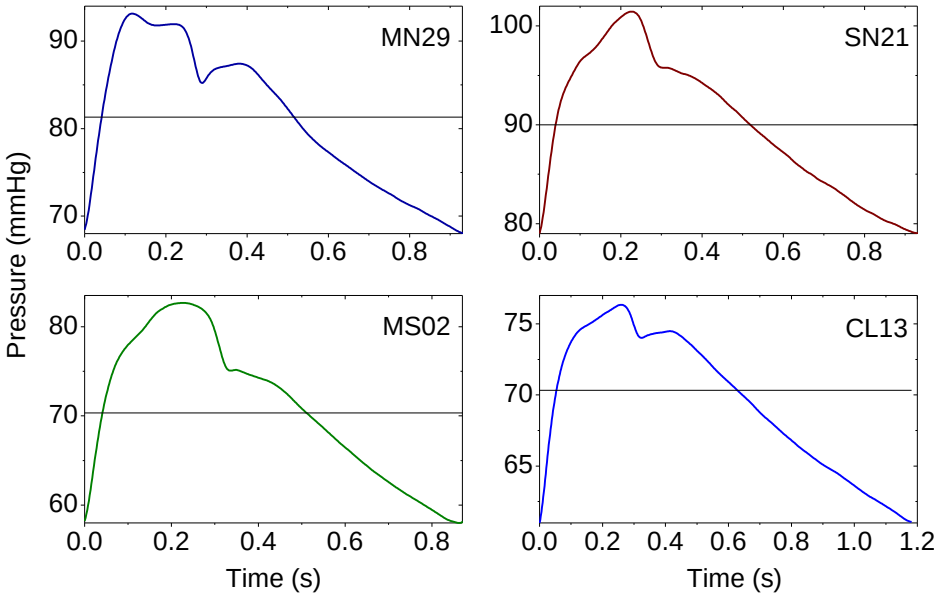

Figure 4.27. Calibrated pressure waves for the four studied subjects (the horizontal line represents MAP).

It can be verified that the cSP values do not correspond to a direct inference of the brachial blood pressure, and subjects with very similar brachial pSP, such as MN29 (110 mmHg) and SN21 (112 mmHg), can have very different cSP, 94 mmHg and 101 mmHg, respectively.

Repeatability study

Acquisitions were performed in 5 healthy subjects whose anthropometric data are presented on Table 4.3. These measures had the goal of testing the same subject at the same conditions, in different days and periods. Two measurements per day, one at the morning period and the other in the afternoon, were performed during a week using the exam procedure reported before.

Table 4.3. Anthropometric and family history data of the analysed subjects.

Subject	Gender	Age (years)	Weight (Kg)	Height (m)	Cardiovascular problems in the family
1	Male	25	65	1.73	No
2	Female	28	58	1.60	No
3	Female	32	58	1.60	No
4	Female	31	64	1.66	Yes
5	Female	30	63	1.64	Yes

From the acquired data sequences, for each morning and afternoon periods, an average pulse was calculated. For each subject, it was also calculated the average pulse for the mornings and afternoons of the all week. The RMSD was assessed by comparing each pulse with the week average pulse for each period, being the results presented in Tables 4.4 and 4.5, for morning (M) and afternoon (A), respectively. As can be seen on both tables, RMSD values are very low and in accordance with the application requirements, showing that the sensor is reliable, maintaining a constant response throughout the days.

Table 4.4. RMSD values between the morning pulses and the week average morning pulse (Mn – 'n' stands for the day of the week, starting on Monday, and AM represents average morning pulse of all week).

Subject	M1/AM	M2/AM	M3/AM	M4/AM	M5/AM	Average RMSD
1	0.057	0.034	0.055	0.070	0.070	0.057
2	0.029	0.072	0.038	0.018	0.031	0.038
3	0.026	0.038	0.020	0.021	0.056	0.032
4	0.031	0.060	0.030	0.131	0.023	0.056
5	0.063	0.033	0.074	0.029	0.040	0.048

Table 4.5. RMSD values between the afternoon pulses and the week average afternoon pulse (An –'n' stands for the day of the week, starting on Monday, and AA represents average afternoon pulse of all week).

Subject	A1/AA	A2/AA	A3/AA	A4/AA	A5/AA	Average RMSD
1	0.032	0.026	0.032	0.067	0.087	0.049
2	0.032	0.047	0.015	0.047	0.032	0.035
3	0.030	0.021	0.022	0.031	0.013	0.023
4	0.137	0.023	0.070	0.035	0.054	0.064
5	0.031	0.066	0.034	0.044	0.020	0.039

In Fig. 4.28, the superimposition of the mean morning and afternoon pulses of each subject is represented. It can be seen that the wave morphologies change little from morning to afternoon, being the main differences in HR, with some subjects having higher HR (low pulse duration) at the morning and others at the afternoon. It can be also verified that the small differences in HR had more impact in the diastolic than the systolic duration.

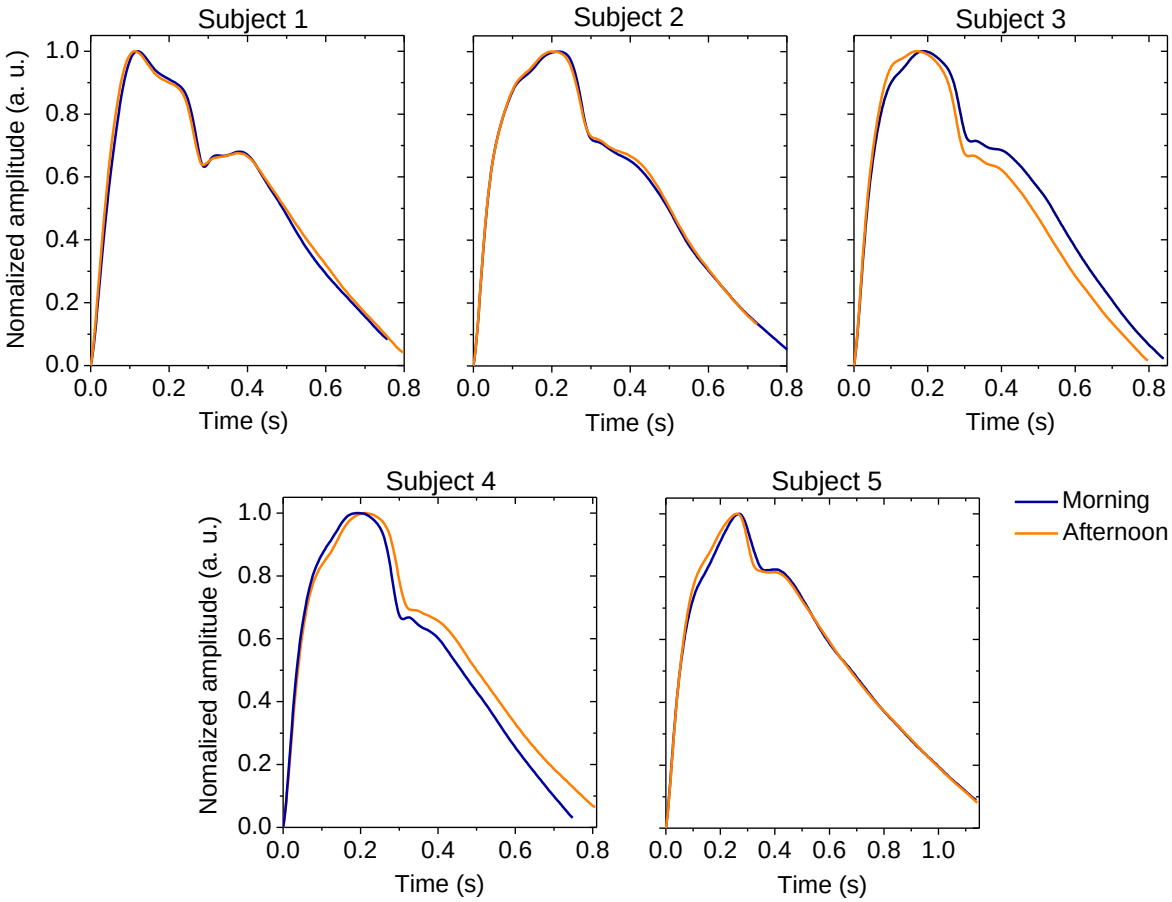

Figure 4.28. Comparison of the average pulses of morning and afternoon for each subject.

Study of the central arterial pressure before and after exercise

In order to test the sensor for the same subject at different HR conditions, a volunteer was subjected to a test to evaluate central pressure in the resting position, followed by 5 minutes of running, after stopping for 2 minutes and 4 minutes. The Fig. 4.29 shows the central pulse shape and respective pressure values, being possible to see the changes from the resting (R) position, to immediately (AE), 2 (AE2) and 4 (AE4) minutes after exercising.

It can be seen that the central pulse wave changes in morphology and pressure between the different conditions. A notable change is the almost disappearance of the dicrotic wave, which is the slight pressure increasing usually seen after the incisura. Nevertheless in the situation AE4, it can be denoted the start of the dicrotic wave resurging.

With regards to SP values, as presented on Table 4.5, both peripheral and central pressures rise after the running, to which follows pressure recover to the basal values. It

can also be verified that 4 minutes after exercise, despite the pSP being lower than the resting values, the cSP still not recovered to its basal value.

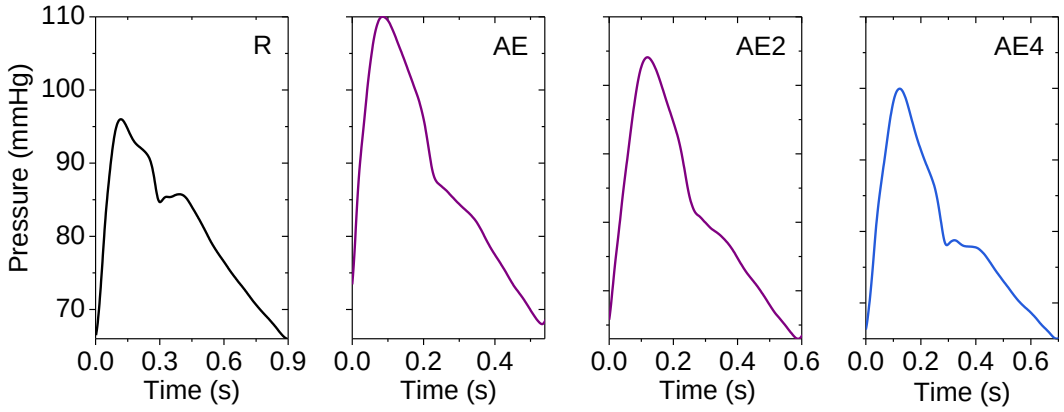

Figure 4.29. Mean arterial central pressure profiles of subject 1 in the different situations, after and before running.

Table 4.5. pSP, DP and resulting cSP, for four different HRs.

State	HR (bpm)	pSP (mmHg)	DP (mmHg)	cSP (mmHg)
R	67	111	66	96
AE	112	126	68	110
AE2	101	116	63	105
AE4	86	108	65	99

4.3.5. Discussion

In this section it was presented a simple and low cost intensity based POF sensor for pulse waveform monitoring. The probe presented a sensitivity of 727 ± 10 µV/µm, for a dynamic range of 295 µm. The device was tested in four volunteers to assess cSP. To accomplish this goal, the pulses were segmented and overlapped to calculate the average pulse, which was calibrated to pressure using brachial DP and MAP values. In the data analysis, it was verified two subjects, with very similar pSP values, presenting significantly different cSP.

The second step was testing the probe's repeatability, for which 5 subjects were recruited to preform measures during 5 consecutive days. The RMSD values between the day periods, morning and afternoon, were calculated for all the subjects, in which the

maximum values were around 6 % for both periods, below the maximum accepted deviation for pulses assessed in the same subject (10 %).

Finally, the probe was tested in a subject before and after physical exercise. Right after running, both pSP and cSP increased. After 4 minutes, the pSP had been re-established to its resting value, which not happened to the cSP that was still higher than in the beginning. This test stressed once again that the pSP lowering is not necessarily translated into the exactly same behaviour of cSP.

4.3.6. Conclusion

The preliminary proof of concept showed that the sensor can be used to monitor pulse waveform and the cardiac rhythm. With the proposed arrangement, the POFpen and interrogation unit reached a sensitivity suitable for arterial pulse wave assessment. The preliminary testing presented promising results in the use of POFpen for cSP assessment. Its low fabrication costs allied to the good stability and accuracy in detecting the arterial pulses, turned POFpen the chosen sensor to perform pre-clinical analysis, which is presented in the next chapter.

5

Pre-clinical evaluation

Distension waves have already been used, and may be preferable to pressure, to perform PWA and cSP monitoring, due to the non-necessity of artery applanation (Hirata *et al*. 2006). In this chapter results are presented in the evaluation of the accuracy of cSP estimation with POFpen, having as reference regular arterial tonometry. This study had as main goal to ascertain the viability of presenting POFpen for clinical evaluation procedures in broader cohorts, being for that reason referred to as pre-clinical study. For that purpose, carotid distension and pressure waveforms were acquired in 15 young subjects. FF%, RMSD, harmonic decomposition and central systolic pressures obtained with both techniques were analysed. The strong PCC, found between techniques in cSP assessment, supported future clinical evaluation studies in larger cohorts.

5.1. Materials and methods

Within this pre-clinical study, 15 subjects with ages between 22 and 34 years old, were recruited. After giving their informed consent, in each one, the carotid pulses were acquired with the two probes, POFpen and Complior Analyse®.

POFpen and Complior have the same clinical exam procedure, following the tonometry recommendations. The acquisition process began with the subject in supine position followed by a short cardiovascular risk questionnaire. The patient rested for about 10 minutes before the data acquisition, which usually took no more than 2 minutes. The brachial blood pressure was assessed before and after each measure to confirm haemodynamic stability, using a commercial pressure cuff (*M6 Comfort*, *OMRON*). POFpen and Complior cannot be used simultaneously, as in each patient there is usually only one optimal location for pulse waveform acquisition, so the measurements were performed consecutively. The pulses acquired with both techniques were calibrated with the same brachial MAP and DP values, assessed between both acquisitions.

Curves from the two devices were superimposed in time domain, as carried out in similar studies (Sztrymf *et al.* 2013; Agnoletti *et al.* 2014), for FF% and RMSD calculation. To analyse the frequency components of the waves assessed with both techniques, Fourier decomposition was performed, after which the amplitudes of each harmonic (until the 8^{th}) were compared. The difference between techniques was statistically analysed by paired student's *t*-tests, Pearson correlation and Bland-Atman analysis. Two-tailed values of $p < 0.05$ were considered statistically significant. The statistical calculations were performed with IBM SPSS Statistics 23.

5.2. Results

The characteristics of the 15 volunteers of the study as well as the brachial arterial pressures used to calibrate the arterial pulses, are represented in Table 5.1. All the patients were healthy and only one had recent hypertension diagnosis, which was treated and under control, with normal pressure values.

After data processing, and pulses normalization between 0 and 1, the acquired pulses with both techniques were superimposed for comparison, as the examples showed in Fig. 5.1. A first assertion is that POFpen waves, even though presenting similar morphology, tend to have a higher curve integral than pressure waves.

Table 5.1 Characteristics of the volunteers and brachial pressure values assessed through the acquisition process.

Variables	Quantity
Male gender, n_{sub} (%)	5 (33.3)
Age, y ± SD	29.2 ± 3.6
Weight, kg ± SD	63.9 ± 13.1
Height, m ± SD	1.66 ± 0.10
BMI, kg/m^2 ± SD	22.99 ± 2.43
Hypertensives, n_{sub} (%)	1 (6.7)
Anti-hypertensive treatment, n_{sub} (%)	1 (6.7)
Cardiovascular family history:	
None, n_{sub} (%)	3 (20)
Hypertension without events, n_{sub} (%)	5 (33)
Hypertension with events, n_{sub} (%)	7 (47)
Cholesterol:	
Normal, n_{sub} (%)	11 (73)
Borderline, n_{sub} (%)	4 (27)
Smoking habits:	
Never smoked, n_{sub} (%)	13 (81)
Ex-smoker (> 1 y), n_{sub} (%)	2 (19)
Arterial blood pressure:	
Systolic pressure (mmHg ± SD)	106 ± 11
Diastolic pressure (mmHg ± SD)	62 ± 7
Mean arterial pressure (mmHg ± SD)	77 ± 7

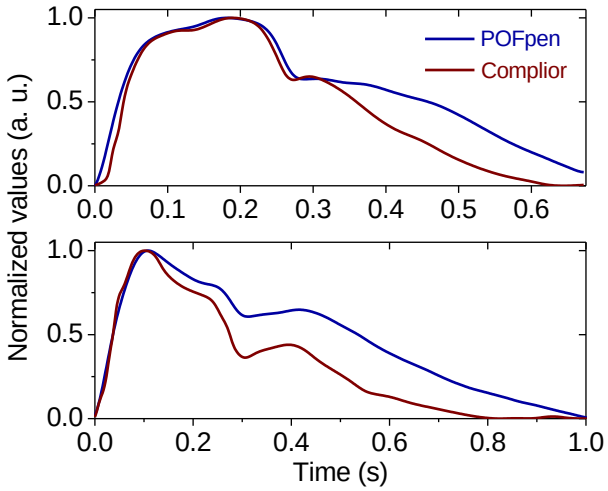

Figure 5.1. Superimposed waves acquired by POFpen and Complior in two subjects.

As can be seen in Table 5.2, the difference between curves is more pronounced during diastole (RMSD = 0.15 ± 0.03 a. u.) than during systole (RMSD = 0.09 ± 0.03 a. u.), resulting in a mean RMSD of 0.14 ± 0.02 a. u..

Table 5.2. Form factor, RMSD, harmonics amplitudes and cSP results for both techniques.

Variables	POFpen	Complior
RMSD (a. u. ± SD)	0.14 ± 0.02	
Systolic RMSD (a. u. ± SD)	0.09 ± 0.03	
Diastolic RMSD (a. u. ± SD)	0.15 ± 0.03	
Form Factor (%)	51.1 ± 5.2	41.5 ± 5.7
Harmonics amplitude (a. u. ± SD)		
1st Harmonic	0.360 ± 0.031	0.373 ± 0.061
2nd Harmonic	0.182 ± 0.027	0.183 ± 0.035
3rd Harmonic	0.089 ± 0.028	0.095 ± 0.026
4th Harmonic	0.049 ± 0.014	0.060 ± 0.017
5th Harmonic	0.049 ± 0.012	0.054 ± 0.014
6th Harmonic	0.029 ± 0.012	0.034 ± 0.015
7th Harmonic	0.020 ± 0.007	0.025 ± 0.013
8th Harmonic	0.015 ± 0.004	0.022 ± 0.006
cSP (mmHg ± SD)	96.6 ± 13.0*	96.0 ± 11.9

*values after FF% correction

Even though the assessed distension waves presented higher FF% values, a linear relation between both sensors results, with a slope of 1.01 ± 0.13 a. u., was verified, as presented in Fig. 5.2a. The corresponding Bland-Altman plot, in Fig. 5.2b, shows a mean FF% difference of approximately 10 ± 2 %. This value is used to correct POFpen FF% before cSP calculation.

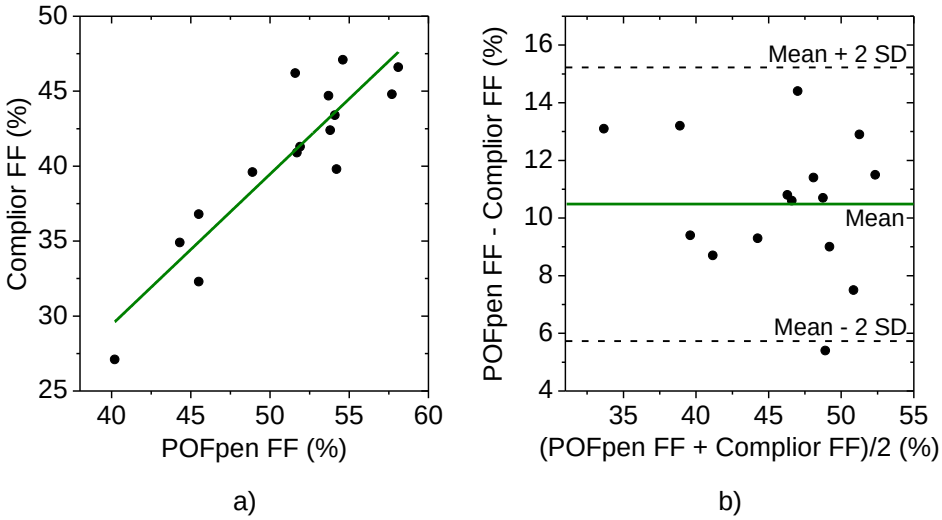

Figure 5.2. Relation between the FF% of distension and pressure waves: a) dispersion plot with linear fit (PCC= 0.91 (p < 0.001), slope = 1.01 ± 0.13 a. u.) and b) Bland-Altman plot.

Concerning the frequency components, in Table 5.2 it can be seen that the highest difference between both probes is 0.013 a. u., verified for the 1st harmonic, being all the

other variations below this value. The mean harmonics amplitudes for each device are graphically represented in Fig. 5.3. Paired *t*-tests had shown that the first four harmonics are not significant different between them ($p < 0.05$), and Pearson correlation studies revealed that the 2nd - 7th harmonics are correlated ($p < 0.05$).

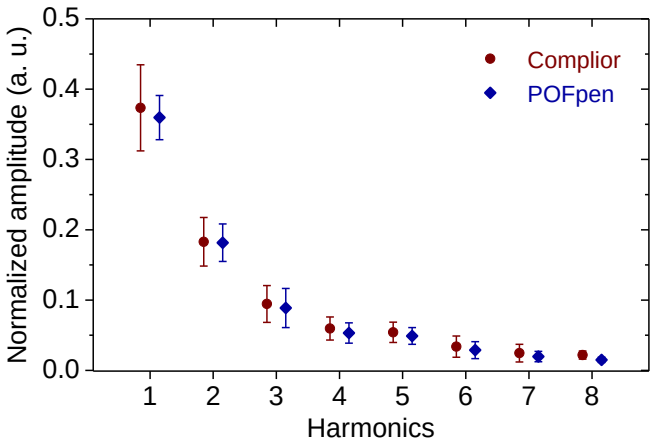

Figure 5.3. Fourier decomposition of the waveforms for POFpen and Complior - average amplitude of each harmonic with respective SD.

To calculate cSP with POFpen, the pulses FF% was corrected using the 10 % mean difference reported earlier. The results, presented in Table 5.2, are very similar between techniques and, as can be seen in Fig. 5.4a, both assessed pressures have a linear proportionality between them, with a PCC of 0.99 ($p < 0.001$).

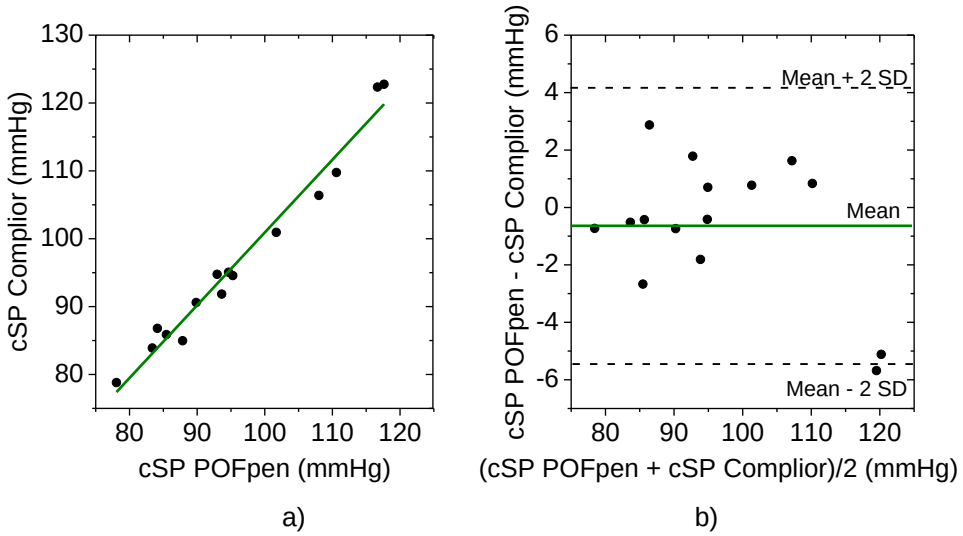

Figure 5.4. Adjusted cSP obtained by POFpen and Complior: a) dispersion plot with linear fit (PCC = 0.99 ($p < 0.001$), slope = 1.07 ± 0.05 a. u.) and b) Bland-Altman plot.

The Bland-Altman analysis of Fig. 5.4b shows that almost all the results are within the confidence interval as well as a POFpen slight underestimation of cSP in 0.6 ± 2.4 mmHg.

5.3. Discussion

The present study had the aim of to assess the POFpen accuracy before its introduction in broader clinical trials, using as reference the most recent version of Complior, the Complior Analyse®.

Some studies on Complior Analyse validation were found in the literature. In 2013, Sztrymf *et al.* reported a small study with 12 patients, comparing Complior's signals with invasive aortic pressure data, showing that there was no statistical difference in the amplitude of the harmonics between both signals and the form factor differences between techniques were 4.2 ± 2.8 %. Pereira *et al.* reported another invasive study, with 15 patients, comparing pulses obtained by Complior and invasive aortic pressure assessment, resulting in a Complior underestimation of cSP of 1.80 ± 4.20 mmHg (Pereira *et al.* 2014). Finally, Stea *et al.* performed the comparison of Complior Analyse with SphygmoCor, which is the most used arterial tonometer worldwide. In this study, involving 120 patients, a cSP difference of -0.7 ± 5.6 mmHg between both techniques was detected, concluding that Complior Analyse can be interchanged with SphygmoCor (Stea *et al.* 2014). The presented data supported the use of Complior to preliminarily validate POFpen.

In this work, results from a 15 subjects' cohort were analysed, starting with the study of RMSD between POFpen and Complior acquired waves, considering the latter as the reference device. A mean RMSD of 0.14 was achieved, deviation that was considered admissible, due to the expected differences related to their unalike nature (distension and pressure). FF% was also evaluated, had been verified a difference of 10 %, very close to the results achieved by Kips *et al.*, which reported the comparison of pressure waves acquired with SphygmoCor® with distension waves assessed by Echotracking, obtaining a FF% difference of around 6 %. These identified variations between distension and pressure waves derive from the viscoelastic properties of the arterial walls.

The pulse waves were also analysed in the frequency domain by performing Fourier decomposition of the signal, similarly to other studies (Sztrymf *et al.* 2013; Agnoletti *et al.* 2014), were the amplitudes of the first 8 harmonics were compared. All the harmonics presented similar amplitude, never differ more than 0.013 a.u..

Finally cSP was compared for both techniques. Given the FF% reported mean difference of 10 ± 2 %, from all the POFpen assessed waves, FF% were subtracted 10 % to calculate cSP. After that correction, the cSP difference between techniques was 0.6 ± 2.4 mmHg, in the range of the difference between Complior and SphygmoCor reported by Stea *et al.* 2014.

5.4. Study limitations

Nevertheless the consistency of the presented results, some limitations should be addressed and taken in consideration when interpreting the data, especially the small cohort, with subjects within the same age range and low BMI. Other limitation was the non-random order of the acquisitions, the POFpen was always used after the Complior device. Since it was a preliminary test, in a small cohort, it was chosen to standardize the procedure in all the acquisitions. Nevertheless the study limitations, the results were praiseworthy in to fundament the POFpen final evaluation through clinical studies.

5.5. Conclusions

In this work, POFpen and Complior acquired carotid waves were compared to analyse the ability of obtain the central pressure from the distension waves. It was observed that POFpen assessed pulses had a higher FF% than the reference. Regarding cSP, a strong linear correlation between central pressures calculated with both curves was found, showing the possibility of to obtain central pressure from distension waves. These results support the application of POFpen in future clinical studies.

6

Non-invasive clinical evaluation

In this section, it is presented data from the non-invasive clinical evaluation of POFpen, using a commercial piezoelectric device, Complior Analyse®, as reference technique. 76 patients with ages between 20 and 80 years old entered the study. The pulses from all the subjects were superimposed to calculate the deviation of the pulse wave morphology between techniques. AIx% and cSP values were compared using intraclass correlation and Bland-Altman plots. Strong correlations were found between techniques, showing that the POFpen can measure pulse waves accurately, allowing to assess the AIx% and cSP.

6.1. Materials and methods

A total of 81 patients, with prescribed PWV and cSP with Complior Analyse®, were recruited from the HT consultation of the CHBV (Aveiro, Portugal). The exclusion criteria were arrhythmia, premature ventricular beats, respiratory problems, movement artefacts and severe mental problems. After the criteria application, 76 patients were suitable candidates for the study, which was approved by the local ethics committee.

The exams were carried out by two experienced technicians, in 10 different random days during a period of 5 months. POFpen testing was always performed after the prescribed cSP and PWV exams, in order to not influence the regular exam routine. The brachial BP values were evaluated before, in between and after both devices acquisitions to assess haemodynamic stability, using the sphygmomanometer *M6 Comfort* from *OMRON*. Nevertheless, the used BP values to calibrate the pulses acquired with both techniques were the ones taken between the two measurements.

The pulses assessed with both devices were superimposed for all subjects, and were analysed by RMSD, FF%, 8 first harmonics amplitude, AIx% and cSP, being all values expressed as mean ± SD. AIx% was calculated only for the patients whose inflexion was distinguishable in the waves assessed with both technologies, which happened for 53 subjects. Furthermore, cSP comparison was performed in 71 subjects, since the pressure of the remaining 5 was miscalculated by the software of one or both devices.

Differences between techniques were tested by sample student t-test. ICC, usually applied to evaluate different techniques outputs to acquire the same variable in the same subject, and Bland-Altman plots were used in the analysis of the POFpen measurements accuracy. An ICC between 0.7 and 0.8 was considered to represent a strong agreement between techniques and a correlation higher than 0.8 a very strong agreement. A $p < 0.05$ was taken as significant. The statistical calculations were performed with IBM SPSS Statistics 23.

6.2. Results

The demographic and clinical characteristics of the patients that entered the study are presented on Table 6.1. It can be verified that the population, with an average age of 53 years old, was overweight, 40 % had dyslipidaemia, 16 % diabetes and 93 % hypertension, whereas 34 % were smokers or ex-smokers. Not all the subjects were

actuality hypertensives because in the consultation patients with suspected hypertension are also seen, diagnosis that was not always confirmed. 7 % of the patients who entered the study had a previous acute myocardial infarction and 12 % a previous cerebrovascular event, considering transient ischemic attack, hemorrhagic or ischemic stroke. The PWV, assessed with Complior, presented a mean value of 9.02 ± 2.67 m/s.

Table 6.1. Demographic and clinical characteristics of the study subjects.

Variables	Quantity
Male gender, n_{sub} (%)	42 (55)
Age, years ± SD	53 ± 16
BMI, kg/m^2 ± SD	28 ± 5
Dyslipidemia, n_{sub} (%)	30 (40)
Diabetes, n_{sub} (%)	12 (16)
Hypertension, n_{sub} (%)	71 (93)
Smoking habits:	
Never smoked, n_{sub} (%)	50 (66)
Ex-smoker (> 1 year), n_{sub} (%)	15 (20)
Current smoker, n_{sub} (%)	11 (14)
PWV (m.s^{-1})	9.02 ± 2.67
Acute myocardial infarction, n_{sub} (%)	5 (7)
Cerebrovascular accident, n_{sub} (%)	9 (12)
Brachial BP	
Systolic pressure (mmHg ± SD)	136 ± 20
Diastolic pressure (mmHg ± SD)	81 ± 11
Mean arterial pressure (mmHg ± SD)	100 ± 12

In Fig. 6.1 three examples of superimposed waves detected with Complior and POFpen can be seen, showing the morphology similarity in type-A, B and C waves.

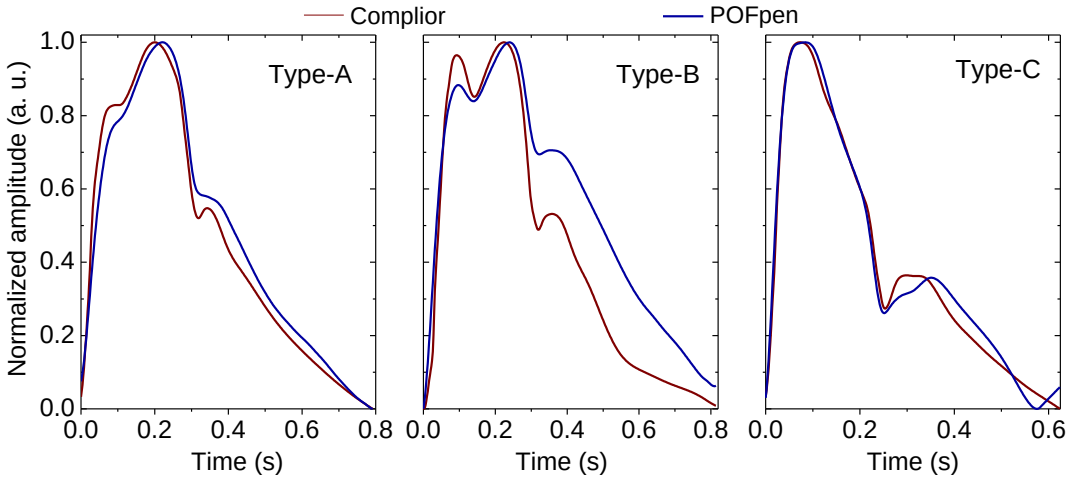

Figure 6.1. Examples of type-A, B and C waves acquired with Complior and POFpen.

The superimposition of the pulses showed an average RMSD of 0.13 ± 0.05 a. u., and a mean ICC of 0.96 ± 0.03. Similarly to the pre-clinical tests, the FF% from distension and pressure waves differed from each other in approximately 10 ± 4 %, Complior presented a mean FF% of 39 ± 4 % and POFpen 49 ± 4 %.

Regarding the frequency components, the maximum verified difference was in the 1st harmonic (0.02 a. u.). Nevertheless, all the harmonics were significantly correlated accordingly to intraclass correlation analysis.

As concerns to AIx%, the results scatter plotting, presented in Fig. 6.2a, shows a slope of 0.80, with an ICC of 0.91 ($p < 0.001$). As can be verified in Bland-Altman graph (Fig. 6.2b), a mean difference of 1.89 ± 12.22 % was found, and almost all the values were within the confidence interval, showing a good accuracy profile.

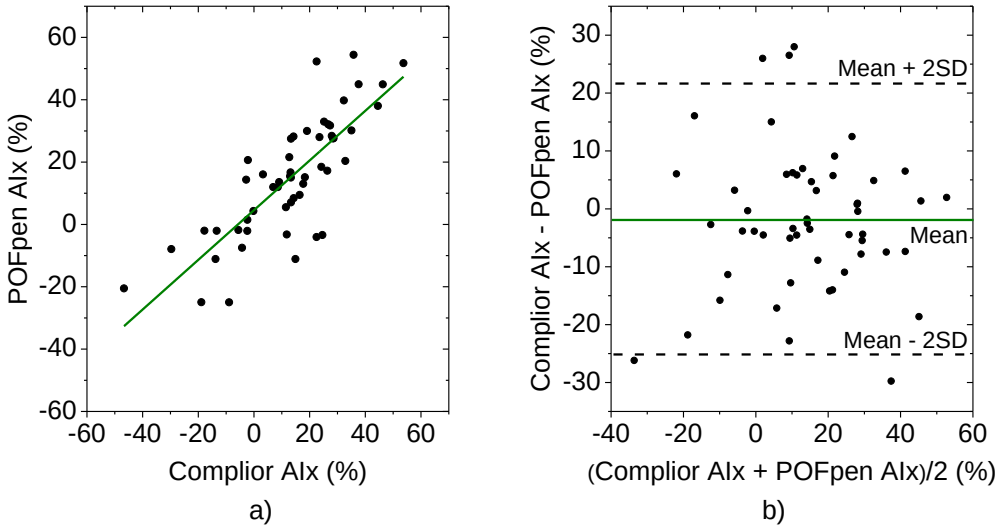

Figure 6.2. AIx estimated with POFpen and Complior as: a) scatter plot with linear regression (ICC = 0.91 ($p < 0.001$), slope = 0.80 ± 0.08) and b) Bland-Altman plot (n_{sub} = 53).

As performed in the pre-clinical study, for cSP calculation the POFpen FF% were corrected subtracting 10 % of the original value for each subject.

After the correction, the resulting mean cSP pressure difference was -1.2 ± 5.2 mmHg. The dispersion profile was analysed (see Fig. 6.3a), having presented a slope of 1.00 ± 0.03 and an ICC of 0.98 ($p < 0.001$). Bland-Altman analysis showed once again a good accuracy profile, as can be observed in Fig. 6.3b.

In this work it was also performed correlation tests between arterial stiffness, evaluated by means of PWV with Complior, and AIx% and cSP assessed with both techniques. As can

be verified in Table 6.2, cSP data from both techniques was highly correlated with arterial stiffness. On the other hand, only AIx% calculated from the POFpen waves was significantly correlated with PWV.

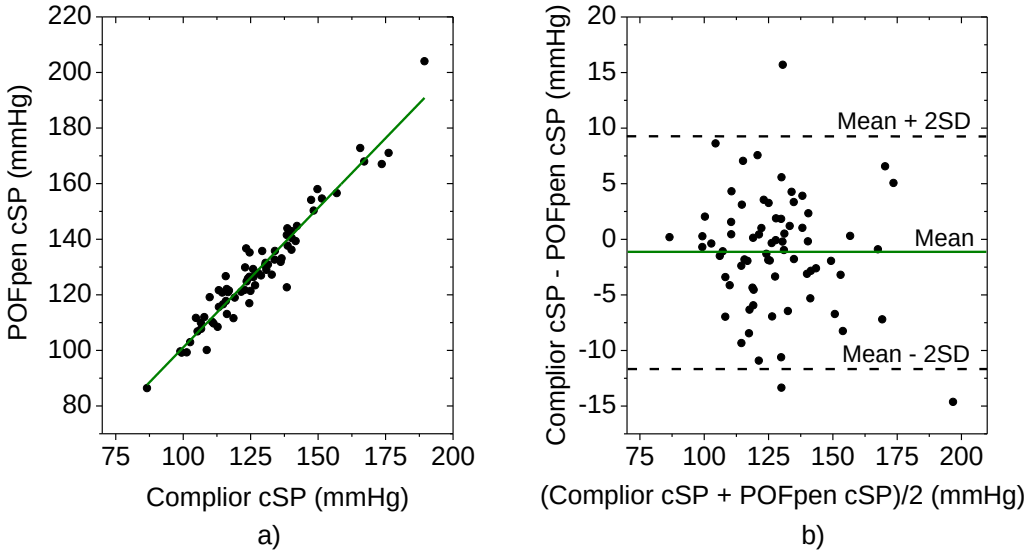

Figure 6.3. cSP estimated with POFpen and Complior as: a) scatter plot and linear regression (ICC= 0.98, slope = 1.00 ± 0.03) and b) Bland-Altman plot (n_{sub} = 71).

Table 6.2. ICC and significance grade between PWV and AIX% and cSP for both techniques (very significant, ^{ns}non-significant) for a confidence level of 95%.**

	AIx% POFpen	AIx% Complior	cSP POFpen	cSP Complior
ICC PWV	0.389	0.155	0.672	0.644
p	0.004**	0.184^{ns}	< 0.001**	< 0.001**

6.3. Discussion

With this study it was intended to clinically evaluate the carotid pulse acquisition with the POFpen using as reference the Complior analyse. This commercial device has been extensively used for PWV, cSP and AIx% assessment. Literature reports recent data on Complior invasive and non-invasive validation, evaluating its performance with reference to intra-aortic and SphygmoCor® pulses, respectively. Complior cSP and AIx% comparison with invasive pressure waves presented the mean difference in pressure of 1.80 ± 4.20 mmHg and AIx% of 0.24 ± 0.84 % (Pereira *et al.* 2014). Regarding the non-invasive validation with SphygmoCor, it was reported a cSP difference between techniques of -0.7 ± 5.6 mmHg (Stea *et al.* 2014). This study stated that Complior and

SphygmoCor are interchangeable, and being the devices more used in epidemiologic studies, it was considered that any of the two devices could be used as reference in this validation study.

Measurements were performed in 76 patients, a similar number of subjects of other clinical evaluation studies, such as the comparison of arterial tonometers reported by Zhang *et al*. in 2013, in which 66 subjects were enrolled.

Regarding the present study, results showed that waves acquired with POFpen and Complior are superimposable, having a mean deviation between techniques of about 13 ± 5 %, and an average correlation coefficient of 0.96 ± 0.03. It was also verified that the 8 harmonics amplitudes were significantly correlated.

Concerning the AIx% values, a very strong correlation, with an ICC coefficient of 0.91 ($p < 0.001$), was found between techniques as well as a residual mean difference of -1.89 ± 12.22 %. Bland-Altman analysis showed that the majority of the values were within the confidence interval, showing a good accuracy profile without visible bias. The AIx% is usually associated with a greater standard deviation between techniques, however the results are within the range presented in the validation of commercial devices (Zhang *et al.* 2013).

FF% was calculated for all the curves, and similarly to the pre-clinical study, the distension waves presented higher values than pressure waveforms in approximately 10 %. After FF% correction, the cSP difference was -1.2 ± 5.2 mmHg, with the POFpen slightly overestimating cSP, presenting a strong ICC of 0.98 ($p < 0.001$) between techniques. The Bland-Altman analysis showed a good accuracy profile for the device as well as absence of bias. These results are once more in the range of other studies evaluating commercial devices (García-Ortiz *et al.* 2012; Agnoletti *et al.* 2014).

Lastly, correlation studies between cSP and AIx% values, assessed with both techniques, and arterial stiffness, measured as PWV, were carried out. cSP data from both devices were highly correlated with arterial stiffness, with ICCs of 0.672 and 0.644 ($p < 0.001$) for POFpen and Complior, respectively. On the other hand, for AIx%, only the values calculated from the POFpen waves were significantly correlated with PWV (ICC = 0.389, $p < 0.005$). A possible explanation for this finding is that AIx% assessed with POFpen, being calculated from distension waves, seems to be more related with arterial

viscoelastic properties, and consequently with arterial stiffness, than AIx% usually inferred from pressure waves.

6.4. Study limitations and future perspectives

A limitation of the current study was the fact that the acquisitions could not be made in a random order, due to logistic issues. As future work, it is proposed to assess the inter-operator repeatability with pulse wave acquisitions performed in a random order. The other identified limitation, which is transversal to the non-invasive validations methods, was the non-simultaneity of the pulses acquisition.

6.5. Conclusions

This work had the goal to clinically evaluate POFpen in the assessment of the central arterial pulse for AIx% and cSP calculation, using a commercial piezoelectric probe as reference. For both parameters, strong correlations were found. Additionally, AIx% data estimated with POFpen were significantly correlated with PWV, which do not happed with the AIx% values assessed with the piezoelectric device. The results validate POFpen as a promising low cost and simple solution for arterial pulse acquisition. Nevertheless, in order to support these findings, invasive evaluation was also performed and the results are presented in the next chapter.

7

Invasive clinical evaluation

The aim of the work presented in this chapter was to evaluate the accuracy of carotid pulse waveform assessment with POFpen, using as reference intra-aortic pressure readings. This cross-sectional study included 29 subjects referenced for cardiac catheterization. Pulse waves were obtained simultaneously in the root of the aorta, and in the right common carotid with POFpen. The pulse waves were compared by RMSD%, FF% first 8th harmonic's amplitude, AIx% and cSP. The PWA indexes assessed with the POFpen demonstrated similar accuracy to non-invasive commercial devices. The results indicate that the POFpen performance is suitable to acquire carotid pulse wave.

7.1. Materials and methods

This cross-sectional study, performed at the CHUC-HG (Coimbra, Portugal), aimed to evaluate the similarity between carotid distension waves acquired with POFpen and intra-aortic pulse waves. The data was collected in 7 random days, in a period of approximately 4 months. 37 patients with suspected coronary artery disease and/or valvulopathies, who underwent cardiac catheterization, were recruited.

For the patients entering the study, they could not present arrhythmia, premature ventricular beats, respiratory problems, movement artefacts and/or severe mental problems, which happened for 29 patients. Clinical information was obtained from the patients and respective clinical files, including age, sex, weight, height, personal clinical history, smoking habits, and pharmacological treatment. The study was approved by the local ethics committee.

The intra-aortic pulse waves and pressure values were assessed during catheterization, which was performed using a 6-Fr Judkins right catheter connected to a pressure transducer, with a saline infusion system. The equipment used was the *Siemens* Artis Zee with AXIOM Sensis hemodynamic recording system. The acquisition of the aortic and the carotid waves was made simultaneously. After each acquisition, that took no longer than 2 minutes, brachial BP was measured using a commercial pressure cuff (*M6 Comfort*, *OMRON*).

The pulses similarity analysis was performed by evaluating their RMSD, FF% and amplitude of the first 8 harmonics. The point-to-point correlation between the curves, obtained with both techniques, was also carried out for all patients.

The AIx% evaluated by both techniques was calculated for the patients whose pulse waves presented a clear incisura, in both intra-aortic and POFpen waves, which happened for 21 individuals. Respecting to the cSP appraisal with POFpen device, it was only performed in the subjects that presented pSP equal or higher than invasive cSP, since aortic-brachial pressure amplification cannot be negative, which was achieved for 15 individuals.

Data was compared by paired student t-tests and expressed as mean ± SD. Similarly to the work presented in the last chapter, the correlation between procedures was analysed by ICC. An ICC between 0.7 and 0.8 was considered to represent a strong correlation between techniques, and an ICC higher than 0.8, very strong. Finally, Bland-Altman plots

were used to evaluate agreement between cSP estimated with both invasive and non-invasive techniques. Two-tailed values of $p < 0.05$ were considered statistically significant.

7.2. Results

The baseline characteristics of the cohort enrolled in the study are showed in Table 7.1. The group was majorly composed by male subjects (69 %), with ages between 47 and 88 years old. Regarding to CV risk factors, the subjects were slightly overweight, with a BMI of 26 ± 4 kg/m^2, 69 % presented dyslipidemia, 24 % diabetes, 59 % had reported HT and 24 % were or had been smokers. 24 % had past coronary artery bypass grafting, and 59 % were submitted to coronary angioplasty. 28 and 21 % had suffered acute myocardial infarction and/or stroke, respectively. The subjects mean pSP was 145 ± 28 mmHg.

Table 7.1. Demographic and clinical characteristics of the 29 subjects enrolled in the study.

Variables	Quantity
Male gender, n_{sub} (%)	20 (69)
Age, years ± SD	69 ± 11
Weight, kg ± SD	72 ± 13
Height, m ± SD	1.66 ± 0.09
BMI, kg/m^2 ± SD	26 ± 4
Dyslipidemia, n_{sub} (%)	20 (69)
Diabetes, n_{sub} (%)	7 (24)
Reported Hypertension, n_{sub} (%)	17 (59)
Smoking habits:	
Never smoked, n_{sub} (%)	22 (76)
Ex-smoker (>1year), n_{sub} (%)	4 (14)
Current smoker, n_{sub} (%)	3 (10)
Coronary Artery Bypass Grafting, n_{sub} (%)	7 (24)
Coronary Angioplasty, n_{sub} (%)	17 (59)
Acute Myocardial Infarction, n_{sub} (%)	8 (28)
Stroke, n_{sub} (%)	6 (21)

In Fig 7.1, examples of superimposed invasive and POFpen waveforms recorded in 4 patients are presented, showing that both curves have similar morphology. Potential differences in the pulse wave morphologies, were studied in the time and frequency domains. The RMSD% obtained was 11 ± 3 % and the difference in FF% was 7 ± 3 %. The pulses point-by-point ICC evaluation showed a very strong mean correlation of 0.97 ± 0.02.

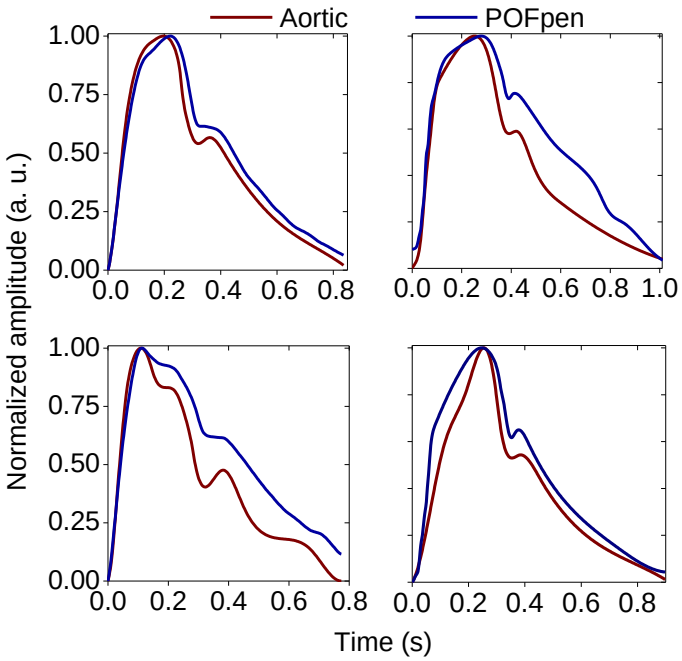

Figure 7.1. Superimposed intra-aortic and POFpen waves for 4 patients.

Results from the frequency study, presented on Fig. 7.2 and Table 7.2, show that the average harmonics amplitude differences are below 1 %. Paired t-tests demonstrated that there are not significant differences between the first 7 harmonics ($p < 0.05$) and ICC demonstrated that all the harmonics are correlated, except for the 7th.

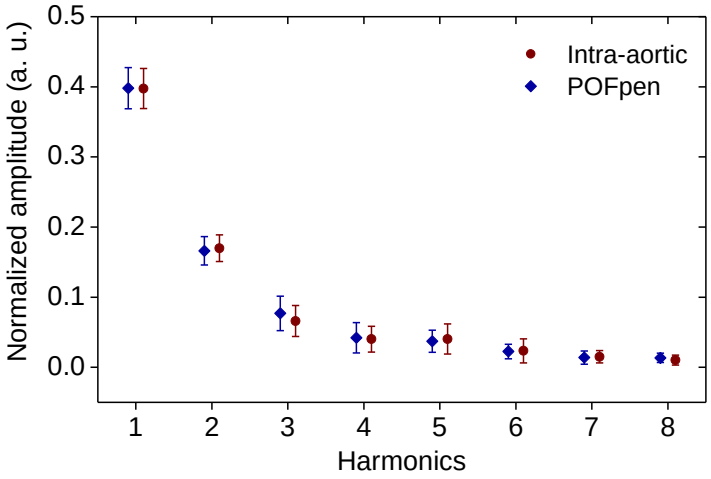

Figure 7.2. Fourier decomposition of the intra-aortic and POFpen acquired waveforms, data represented as average amplitude with respective standard deviation.

Table 7.2. Frequency domain analysis – harmonics' amplitude (values as mean ± SD, ND - non-significantly different, D – significantly different).

Harmonics	Invasive signal	POFpen signal	Paired t-tests	*p*	ICC	*p*
1	0.398 ± 0.029	0.398 ± 0.029	ND	0.949	0.50	0.040
2	0.170 ± 0.019	0.166 ± 0.020	ND	0.443	0.60	0.011
3	0.066 ± 0.024	0.059 ± 0.022	ND	0.561	0.73	0.000
4	0.040 ± 0.018	0.042 ± 0.022	ND	0.585	0.71	0.001
5	0.040 ± 0.021	0.037 ± 0.016	ND	0.317	0.74	0.000
6	0.024 ± 0.017	0.023 ± 0.010	ND	0.720	0.63	0.006
7	0.015 ± 0.009	0.014 ± 0.010	ND	0.539	0.46	0.055
8	0.010 ± 0.007	0.014 ± 0.007	D	0.019	0.61	0.044

In relation to AIx% values, linear regression was performed to compare both techniques, as can be seen on Fig. 7.3a. The results presented a strong ICC of 0.79 ($p < 0.001$), even though the values assessed with POFpen presented a smaller coefficient of variance (1.04) than the invasive signals (1.36). Fig. 7.3b shows that the great majority of the data are within the confidence interval, with POFpen underestimating AIx% by 3.7 ± 12.5 %.

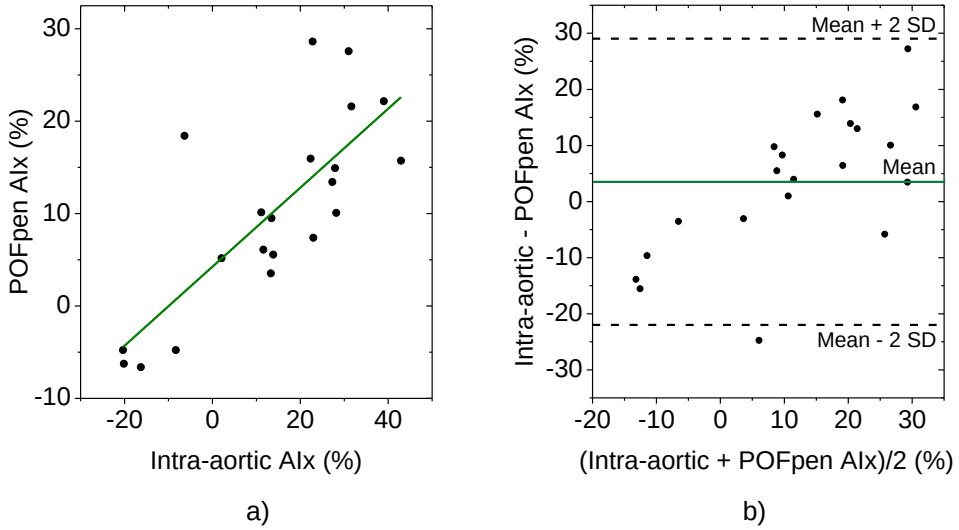

Figure 7.3. AIx estimated with POFpen and intra-aortic pressure probe as: a) scatter plot with linear regression (ICC = 0.79 ($p < 0.001$), slope = 0.43 ± 0.08) and b) Bland-Altman plot.

The cSP results can be seen on Fig. 7.4. The scatter plot (see Fig. 7.4a) showed a linear tendency, with a very strong ICC of 0.94 ($p < 0.001$). In the Bland-Altman plot (Fig 7.4b), despite a cSP underestimation by POFpen of 4.2 ± 11.1 mmHg, it can be seen that all data points are within the confidence interval, without visible bias.

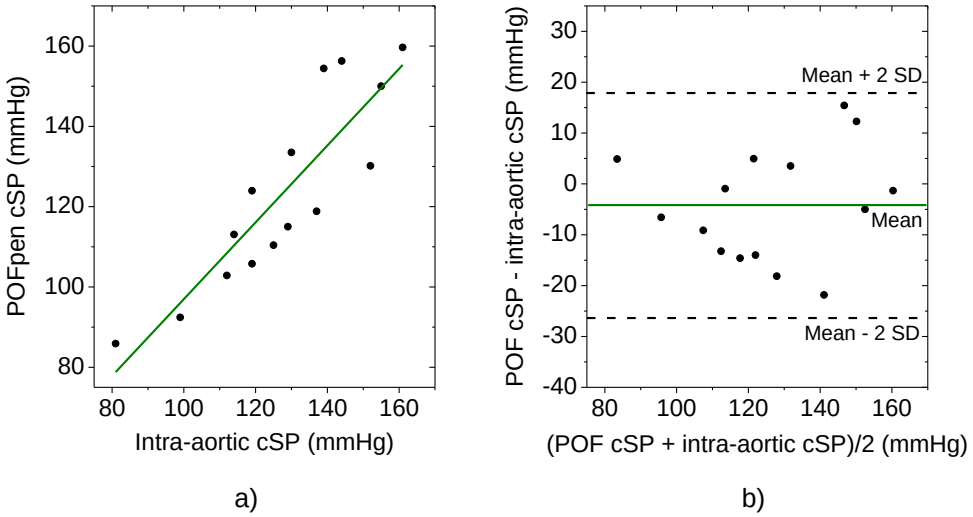

Figure 7.4. cSP estimated with POFpen and intra-aortic pressure probe as: a) scatter plot and linear regression (ICC = 0.94 (p < 0.001); slope = 0.96 ± 0.14) and b) Bland-Altman plot.

7.3. Discussion

This work had the main goal to ascertain the accuracy of POFpen device in acquiring central pulse waves, performing simultaneous invasive pressure measurements, in the aortic root of 29 patients.

Invasive comparison is considered the gold-standard process to validate non-invasive devices for central pulse waveform acquisition. Studies employing commercial devices, as Complior Analyse® and SphygmoCor®, had performed this kind of evaluation. In Ding *et al.* 2011 the invasive validation of SphygmoCor® and Omron HEM9000-AI® is presented, by estimating cSP in 33 subjects. The results were significantly associated with the invasive measurement in the ascending aorta, with a Pearson's correlation coefficient of 0.91 (p < 0.001) and 0.90 (p < 0.001), for SphygmoCor and Omron, respectively. It was also reported that both devices underestimated cSP with a difference of −15 mmHg for SphygmoCor and −2 mmHg for Omron.

In 2013, Sztrymf *et al.* reported a validation study complying 12 patients, in which radial pulses obtained with Complior and invasive acquisitions were compared, showing that there was no statistical difference in the amplitude of the harmonics calculated from both signals and the form factor differences between techniques were 4.2 ± 2.8 %. Pereira *et al.* 2004 reported another invasive study, in 15 patients, comparing carotid pulses assessed by Complior and aortic invasive catheter, achieving an underestimation of cSP calculation of 0.80 ± 4.20 mmHg.

In the present study the acquired signals with both techniques were overlapped, being verified an overall deviation of 11 ± 4 %, with a FF% difference of 7 ± 3 %, which is in agreement with the results found in Kips *et al.* 2010 (6 %), and close to the value reported in Sztrymf *et al.* 2013 (4 %). It should be noticed that in this case, besides the viscoelasticity of the arteries, the different acquisition locations also contribute to dissimilarities in the pulses morphology. However, a very strong mean ICC of 0.97 ± 0.02 was obtained in the point-by-point correlation analysis between pulse waves.

In the frequency domain, the differences in the harmonic amplitudes never reached 0.01 a.u., with overall differences meaningfully inferior to the presented in Sztrymf *et al.* 2013. Statistically, the first 7^{th} harmonics were not significantly different and all the harmonics, excepting the 7^{th}, were correlated.

Regarding AIx%, an ICC of 0.79 ($p < 0.001$) was obtained, for a mean difference between techniques of less than 4%. However, a positive bias was noticed, appearing to be related to the lower coefficient of variance of POFpen results, 1.04 vs 1.36 for invasive waves, which is probably caused by the different nature of the pulses as well as different arterial locations.

Finally, cSP values were compared for 15 subjects. A high pressure variability was verified between the pulses acquisition and the brachial pressure measurement moments. Therefore, several times the pSP assessed after the pulses acquisition presented a lower value than cSP and, consequently, for these patients were only compared the waveforms and not cSP. Even though this occurrence, this study achieved the minimum number of subjects usually entering in invasive validations of commercial tonometers (Sztrymf *et al.* 2013 and Pereira *et al.* 2014).

The cSP statistical analysis showed an ICC of 0.94 ($p < 0.001$) and the Bland-Altman plot a mean pressure difference of -4.2 ± 11.1 mmHg, with all values between the confidence interval and without observed bias. POFpen seems to underestimate cSP, similarly to other commercial techniques (Ding *et al.* 2011; Pucci *et al.* 2013).

7.4. Study limitations

As study limitations, it should be referred the age and health conditions of the subjects, who were in its great majority doing catheterization in an urgent context. This constraint is transversal to all invasive validations, since it would be unethical to appeal a healthy person to a catheterization without a clinical justification. Another limitation was the

impossibility to perform intra-carotid readings, due to the fact that it would also be unethical to submit the patients to carotid exploring, once the catheter navigation on the carotid artery presents a much higher risk to the patient than in aorta, which is in the path of the regular exam.

An additional important limitation was the impossibility to take in consideration all the patients data to calculate cSP. In the present study, a great quantity of subjects presented pSP, measured right after the acquisitions, lower than cSP measured invasively. This could be owed to inaccuracies on the brachial pressure estimation, natural pressure variability of the subjects, or rapid nitrites effects on vasodilatation, which are commonly applied. Due to this registered negative pressure amplification throughout the aortic-brachial arterial path, which is not supposed to happen physiologically (Laurent *et al.* 2006), it was made the decision of not comparing the cSP values assessed by the two techniques in those situations.

7.5. Conclusions

In the presented cross-sectional study, it was showed that the waves estimated by both techniques presented a very strong mean correlation and harmonic's amplitude differences not higher that 0.01 a. u.. AIx% obtained with the two techniques presented a strong ICC. Concerning the cSP results, a very strong correlation of 0.94 ($p < 0.001$) was found, with an estimated difference between techniques within the range verified in commercial devices. It was concluded that POFpen is accurate in the acquisition of carotid pulse waveforms, being a simple and low cost alternative to tonometry in the appraisal of PWA and cSP.

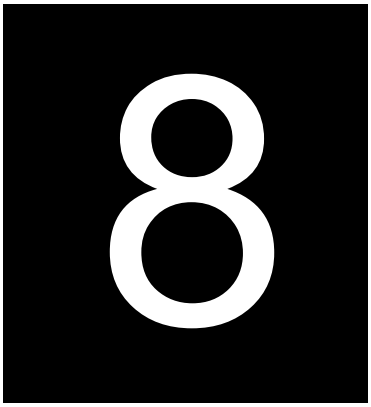

Final remarks

8.1. Conclusions

This thesis, structured in 8 chapters, started by revising the importance of blood pressure monitoring, at peripheral and central locations, in hypertension assessment and CVD prevention. Reviewing the literature, it was verified that central pressure and other arterial stiffness indexes are yet no regularly used in the clinical context, even though several research groups have been studied and demonstrating their prognostic values. Several reasons were pointed out as explanation of the underuse of these techniques, such as training need for its execution and the high cost of the devices to perform carotid pulse acquisition.

The application of OFS emerged as a suitable technology to acquire carotid pulses, as they present several application advantages over conventional electromechanical solutions. In the biomedical field, they are highlighted by the high sensitivity, stability, immunity to electromagnetic radiation, safety and possibility of low cost designs. In the development of the present work, three optical fibre systems were developed to assess the carotid arterial pulse, one of them having been clinically evaluated.

Before the presentation of the developed work and obtained results, two chapters (2 and 3) introduced the general concepts on arterial stiffness, central haemodynamics and optical fibre sensors. Since this thesis is organized as the sequence of the published papers, the two referred chapters embody the theoretical background for all the following.

In Chapter 4, the three developed probes, FBGbox, FBGpen and POFpen were presented. In the table 8.1, the main features regarding sensitivity and resolution, as well as robustness, user-friendliness and cost of the three probes, are compared. The first probe was developed to analyse the feasibility of detecting the carotid pulse with optical fibre sensors. The human testing delivered promising results, even though the sensor shape and robustness needed improvements to be a ready to use prototype for the clinical environment.

The constraints of FBGbox, were overtaken by the development of FBGpen. From the one version to the other, sensitivity was greatly improved (≈ 10 times). However, this upgrading happed with the sacrifice of the dynamic range, which drastically decreased. In spite of that, in the individuals testing, the sensor allowed to acquire the pulse wave in all the enrolled subjects, presenting its robustness and user-friendliness greatly improved.

The recent low cost devices for central pressure estimation based on oscillometry, derive central pressure directly from the brachial arterial pulse, which is not necessarily accurate (Kips 2011). On the other hand, the remaining devices are expensive, which can be an obstacle to the central arterial appraisal in primary care as well as in research purposes. Therefore a second goal of the work was to develop a low cost solution. To achieve this aim, an approach based on intensity modulation was implemented with the development of POFpen. For its attainment, an all-plastic pen, design to support a POF, was fabricated recurring to a 3-D printer. The basic material needed for its assembly is a 2x1 POF coupler, a photodetector, a LED, a Bluetooth® module and the controlling electronics. The probe works in reflection, therefore to assess carotid pulse, a small round adhesive reflector should be placed in the neck area, where the highest pulsatility was felt, to acquire the pulse wave. As can be analysed from Table 8.1, POFpen allied the advantages of FBGbox and FBGpen to low cost and robustness.

Table 8.1. Features of the three developed probes

	FBGbox	**FBGpen**	**POFpen**
Sensitivity	2.0 pm/µm	21.2 pm/µm	727.2 µV/µm
Interrogation systems resolution	0.5 pm	0.5 pm	38.15 µV
Displacement resolution	0.25 µm	0.02 µm	0.05 µm
Displacement range	280 µm	16 µm	295 µm
Robustness*	++	+++	+++++
User-friendliness*	++	++++	++++
Cost*	++++	++++	+

*Qualitative variable (minimum +, maximum +++++)

No clear guidelines exist to the validation and certification of the new devices for central arterial pressure assessment. Additionally, the literature review presented on Chapter 2 showed that commercial devices demonstrate considerable differences in cSP calculation in relation to the invasive gold-standard. These differences support the need for better regulation for the devices validation, as well as their calibration methods. The Artery Society have been working on creating guidelines and standards to the validation of new devices, as happened already for the PWV devices, whose certification and calibration methods are well stablished (Wilkinson *et al.* 2010). The task has been more difficult to

accomplish for PWA and cSP devices, for which an agreement on the best calibration algorithm and validation technique was not reached yet.

The clinical evaluation of POFpen was then performed according to the studies found in the literature including commercial devices, in which the new technologies are usually compared with the most ancients and widely applied devices worldwide, such as SphygmoCor® and Complior®, and with the invasive pressure assessment gold-standard. Some commercial devices have theirs calibration algorithms protected, therefore is not accurate to use a device with a different calibration method as a reference in a validation study. For this dissertation, it was chosen to non-invasively evaluate POFpen comparing it with Complior® Analyse, since both devices use the same method for the arterial pulses calibration. Lastly, the invasively evaluation was performed comparing POFpen results with pressure waves acquired at the aortic lumen, in a catheterization context.

The pre-clinical study had as main goal to ascertain and gather evidence of POFpen performance, before its proposal for clinical evaluation. In that study, POFpen pulse waves, assessed in healthy young subjects, were compared with the Complior Analyse carotid pulses. The POFpen waves presented FF% higher than Complior's, agreeing with Kips *et al.* 2010 study, in which is reported a difference between distension and pressure waves from about 6 %. Even though the FF% difference, a very strong correlation was attained for the cSP values obtained with the two techniques ($r = 0.99$, $p < 0.001$) as well as a very small cSP difference, which after FF% correction, was of 0.6 ± 2.4 mmHg. The encouraging results from this pre-clinical testing reinforced that the POFpen presented the performance needed to meet the application requirements, having been the basis for its clinical evaluation proposal.

The clinical evaluation begin with the non-invasive study, using as reference the Complior Analyse, performed in 76 subjects from the hypertension consultation of the cardiology service of CHBV. It was found a main difference in FF% of approximately 10%, in agreement with the value obtained in the pre-clinical study, nevertheless a very strong correlation was found between the pulse waves ($r = 0.96 \pm 0.03$). In this study the assessed AIx% was compared for 53 subjects, having been obtained a deviation of $-1.89 \pm 12.22\%$ ($r = 0.91$, $p < 0.001$). The cSP difference, after FF% correction, was -1.2 ± 5.2 mmHg, with an $r = 0.98$ ($p < 0.001$). The reported values are very close to the ones presented in similar studies (Vermeersch *et al.* 2008; García-Ortiz *et al.* 2012; Agnotelli *et al.* 2014, Stea *et al.* 2014).

Concerning the invasive study, the waves measured with both techniques presented a mean correlation of 0.97 ± 0.02 and harmonics amplitude differences not higher that 0.01. The appraised AIx% and cSP values demonstrated a strong (0.79, $p < 0.001$) and a very strong (0.94, $p < 0.001$) ICC, respectively. Once more, the difference between techniques was within the range verified for commercial devices (Zuo *et al.* 2010; Pucci *et al.* 2013). It was concluded that POFpen is accurate, being a simple and low cost solution for acquisition of carotid pulse waves for PWA and cSP estimation.

The resume of the results obtained in both invasive and non-invasive evaluation are presented on Table 8.2. Analysing all the studies, it can be seen that for RMSD and FF%, better results were achieved when comparing POFpen to the pressure intra-arterial readings, allowing to calculate cSP and obtaining results in the order of the commercially available devices, without the need of FF% correction. When analysing the point-by-point correlation performed between the pulses, both studies presented very strong ICC and similar results.

Comparing the harmonics amplitude differences, it was verified that its differences between amplitudes were residual, and for the non-invasive and invasive studies, all the harmonics were correlated, except for the 7th harmonic of the invasive data. It was not attributed importance to this result, since the main pulse energy is in the first 5 harmonics, having the 7th and 8th, residual amplitudes, as can be verified in table 7.2 (Chapter 7).

Table 8.2. Comparison of the results obtained in the invasive and non-invasive studies.

Variable	Study	Pre-clinical Non-invasive	Non-invasive	Invasive
RMSD (%)		14 ± 2	13 ± 5	11 ± 3
ΔFF (%)		10 ± 2	10 ± 2	7 ± 3
Harmonic's maximum amplitude difference (a. u.)		0.01	0.02	0.01
Point-by-point waves correlation		-	0.96 ± 0.03	0.97 ± 0.02
ΔAIx (%)		-	1.9 ± 12.2 %	3.7 ± 12.5 %
AIx Correlation		-	0.91 (p < 0.001)	0.79 (p < 0.001)
ΔcSP (mmHg)		0.6 ± 2.4*	-1.2 ± 5.2*	-4.2 ± 11.1
cSP correlation		0.99 ($p < 0.001$)	0.98 ($p < 0.001$)	0.94 ($p < 0.001$)

*cSP obtained after FF% correction

Regarding AIx values, the non-invasive comparison achieved better results. In the case of AIx, no assumptions are made, since its calculation is not pressure dependent, and

consequently, comparisons in the same arterial location should retrieve better results. Nevertheless, both studies results are within the values of correlation and difference found for commercial devices (Vermeersch *et al.* 2008; Wassertheurer *et al.* 2010; García-Ortiz *et al.* 2012).

Lastly, with reference to cSP values, important differences were verified in the invasive and non-invasive studies. In the first, being aware of the FF% difference detected between both the non-invasive techniques, the performed calibration procedure complied the subtraction of 10 % to the FF% POFpen values before calculate cSP. Procedure that results in a minimal cSP difference between devices. For the non-invasive study, no FF% correction was performed, proceeding to the direct calibration of the waves. Even though presenting a higher difference than in the non-invasive studies, the reported value is within the range found in the literature.

In resume, the main goals of the work were achieved by the development of the three optical fibre prototypes and the evaluation of POFpen in a total of 120 subjects, ranging from young and healthy to hypertensive, with past cardiovascular events and elderly people. Since the results were in agreement with the accuracy of the commercial devices, it is concluded that the POFpen is a valid new technology in cSP assessment.

8.2. Future work perspectives

In the future, some clinical and technologic studies are planned to be carried out. The first is the cSP variation assessment before and after exercise, in order to continue the preliminary test described in section 4.3.4. With this work, the recovery time of the central and the brachial pressures to the basal levels, after exercise, is intended to be analysed. Other work is already scheduled, in which is envisioned the study of the cSP and central arterial wave morphology in the myocardial infarction, with the main goal of evaluating the prognostic value of PWA and cSP in the infarction recover.

In the technologic field, it has already started the development of a new approach to fix the intensity sensor in the neck, in order to measure cSP during longer periods of time, without the need of medical help (Leitão *et al.* 2016). The design and implementation of a PWV device, using the POFpen technology, is also planned. Finally, the conception of new wearable sensing networks on physical parameters assessment such as plantar pressure, temperature, heart and respiratory rates, had also already started (Domingues *et al.* 2016).

References

Abrate *et al.* 2013	Abrate S, Gaudino R, Perrone G, “Step-index PMMA fibers and their applications”, in *Current Developments in Optical Fiber Technology*, Harum S and Arof H (eds), InTech (2013).
Abushagur *et al.* 2014	Abushagur A, Arsad N, Reaz M, Bakar A., “Advances in bio-tactile sensors for minimally invasive surgery using the fibre Bragg grating force sensor technique: a survey”, *Sensors*, 9 (14):6633-6665 (2014).
Adji and O’Rourke 2012	Adji A, O’Rourke M, “Brachial artery tonometry and the Popeye phenomenon: explanation of anomalies in generating central from upper limb pressure waveforms”, *Journal of Hypertension*, 30 (8):1540-1551 (2012).
Agabiti-Rosei *et al.* 2007	Agabiti-Rosei E, Mancia G, O'Rourke M, Roman M, Safar M, “Central blood pressure measurements and antihypertensive therapy: a consensus document”, *Hypertension*, 50 (1):154-160 (2007).
Agnoletti *et al.* 2014	Agnoletti D, Millasseau S, Topouchian J, Zhang Y, Safar M, Blache J, “Pulse wave analysis with two tonometric devices: a comparison study”, *Physiological Measurement*, 35 (9):1837-48 (2014).
Albert 2011	Albert J, “Fiber Bragg grating sensors: a look back”, Chapter in *Fiber Bragg Grating Sensors: Recent Advancements, Industrial Applications and Market Exploitation*, Cusano A, Cutolo A, Albert J (eds.), Bentham Science Publishers, USA (2011).
Alberto *et al.* 2013	Alberto N, Bilro L, Antunes P, Leitao C, Lima H, *et al.*, “Optical fiber technology for eHealthcare”, chapter in *Handbook of research on ICTs and management systems for improving efficiency in healthcare and social care*. Cruz-Cunha M, Miranda I, Goncalves P (eds.), IGI Global, USA (2013).
Alivon *et al.* 2015	Alivon M, Vo-Duc Phuong T, Vignon V, Bozec E, Khettab H, “A novel device for measuring arterial stiffness using finger-toe pulse wave velocity: Validation study of the pOpmètre®”, *Archives of Cardiovascular Disease*, 108 (4):227-234 (2015).
Allen 2007	Allen J, “Photoplethysmography and its application in clinical physiological measurement”, *Physiological measurement*, 28 R1-R39 (2007).
André *et al.* 2001	André P, Pinto J, Abe I, Kalinowski H, Frazão O, Araújo F, “Fibre Bragg grating for telecommunications applications : tuneable thermally stress enhanced OADM”, *Journal of Microwaves, Optoeletronics and*

	Electromagnetic Applications, 2 (3):32-45 (2001).
Antunes *et al.* 2012	Antunes P, Lima H, Varum H, André P, “Optical fiber sensors for static and dynamic health monitoring of civil engineering infrastructures: Abode wall case study”, *Measurement,* 45 (7):1695-1705 (2012).
Antunes *et al.* 2014	Antunes P, Dias J, Varum H, André P, “Dynamic structural health monitoring of a civil engineering structure with a POF accelerometer”, *Sensors review* 34 (1):36-41 (2014).
Aviva 2010	Structure and Function: The Blood Vessels. Available online in http://www.aviva.co.uk/health-insurance/home-of-health/medical-centre/medical-encyclopedia/entry/structure-and-function-the-blood-vessels/ (accessed in 10/6/2016).
Avolio *et al.* 2009	Avolio A, van Bortel L, Boutouyrie P, Cockcroft J, McEniery C, “Role of pulse pressure amplification in arterial hypertension: Experts' opinion and review of the data”, *Hypertension*, 54 375-383 (2009).
Avolio *et al.* 2010	Avolio A, Butlin M, and Walsh A, "Arterial blood pressure measurement and pulse wave analysis—their role in enhancing cardiovascular assessment," Physiological Measurement, 31 (1):R1-R47 (2010).
Balicki *et al.* 2011	Balicki M, Uneri A, Iordachita I, Handa J, Gehlbach P, Taylor R, “Micro-force sensing in robot assisted membrane peeling for vitreoretinal surgery”, *Medical Image Computing and Computer-Assisted Intervention*, 13 (Pt 3):303-310 (2010).
Bao *et al.* 2013	Bao B, Melo L, Davies B, Fadaei H, Sinton D, Wild P, “Detecting supercritical CO2 in brine at sequestration pressure with an optical fiber sensor”, *Environmental Science and Technology*, 47 (1):306-312 (2013).
Bartgaile 2012	Bartgaile G*,* “Arterial wall dynamics”*, Perspectives on medicine,* 1 (1-12):146-151 (2012).
Baulmann *et al.* 2008	Baulmann J, Schillings U, Rickert S, Uen S, Düsing R, *et al.* “A new oscillometric method for assessment of arterial stiffness: comparison with tonometric and piezo-electronic methods”, *Journal of Hypertension*, 26 (3):523-528 (2008).
BBC 2016	BBC, “William Harvey (1578-1657)”, in Historic Figures, 2016. Available online at www.bbc.co.uk/history/historic_figures/harvey_william.shtml (accessed in 10/10/2016).
Benetos *et al.* 2011	Benetos A, Salvi P, Lacolley P, “Blood pressure regulation during the aging process: the end of the 'hypertension era'?”, *Journal of Hypertension*, 29 (4):646-652 (2011).

Bilro *et al.* 2011	Bilro L, Alberto N, Sá L, Pinto J, Nogueira R, “Analytical analysis of side-polished plastic optical fiber as curvature and refractive index sensor”, *Journal of Lightwave Technology*, 29 (6):864-870 (2011).
Bilro *et al.* 2012	Bilro L, Alberto N, Pinto J, Nogueira R, “Optical sensors based on plastic fibres”, *Sensors*, 12 12184-12207 (2012).
Benetos *et al.* 1993	Benetos A, Laurent S, Hoeks A, Boutouyrie P, Safar M, “Arterial alterations with aging and high blood pressure. A noninvasive study of carotid and femoral arteries”, *Atherosclerosis and Thrombosis*, 13 (1):90-97 (1993).
Bortolotto and Safar 2006	Bortolotto L, Safar M, “Blood pressure profile along the arterial tree and genetics of hypertension”, *Arquivos Brasileiros de Cardiologia*, 86 (3) (2006).
Boutouyrie *et al.* 1999	Boutouyrie P, Bussy C, Lacolley P, Girerd X, Laloux B, Laurent S., “Association between local pulse pressure, mean blood pressure, and large-artery remodeling”, *Circulation,* 100 (13):1387-1393 (1999).
Boutouyrie *et al.* 2010	Boutouyrie P, Achouba A, Trunet P, Laurent S, “Amlodipine-valsartan combination decreases central systolic blood pressure more effectively than the amlodipine-atenolol combination: the EXPLOR study”, *Hypertension*, 55 (6):1314-1322 (2010).
Boutouyrie and Vermeersch 2010	Boutouyrie P, Vermeersch S, and remaining authors from the Reference Values for Arterial Stiffness’ Collaboration, “Determinants of pulse wave velocity in healthy people and in the presence of cardiovascular risk factors: ‘establishing normal and reference values’”, *European Heart Journal*, 31 (19):2338-2350 (2010).
Boutouyrie *et al.* 2014	Boutouyrie P, Macron L, Mousseaux E, Laurent S, “Determination of systemic and regional arterial structure and function”, chapter in *Blood Pressure and Arterial Wall Mechanics in Cardiovascular Diseases*, Safar M, O’Rourke M, Frohlich (eds.), Springer-Verlag, London (2014).
Bramwell and Hill 1922	Bramwell J, Hill A, "The velocity of the pulse wave in man", *Proceedings of the Royal Society of London. Series B, Containing Papers of a Biological Character (1905-1934)*, 93 298-306 (1922).
Briet *et al.* 2012	Briet M, Boutouyrie P, Laurent S, London G, “Arterial stiffness and pulse pressure in CKD and ESRD”, *Kidney International*, 82 388-400 (2012).
Byun *et al.* 2014	Byun D, Han S, Park J, Kim J, Baik J, Park J, “Relationship between augmentation index and acute ischemic stroke subtype”, *Journal of Clinical Neuroscience*, 21 1220-1224 (2014).
Cennamo *et*	Cennamo N, Pesavento M, Lunelli L, Vanzetti L, Pederzolli C, *et al.*,

al. 2015	"An easy way to realize SPR aptasensor: A multimode plastic optical fiber platform for cancer biomarkers detection", *Talanta*, (140):88-95 (2015).
Chethana *et al.* 2016	Chethana K, Guru Prasad A, Omkar S, Asokan S, "Fiber Bragg grating sensor based device for simultaneous measurement of respiratory and cardiac activities", *Journal of Biophotonics*, (Epub ahead of print) (2016).
Chirinos *et al.* 2005	Chirinos J, Zambrano J, Chakko S, Veerani A, Schob A, "Aortic pressure augmentation predicts adverse cardiovascular events in patients with established coronary artery disease", *Hypertension*, 45 (5):980-985 (2005).
Chirinos *et al.* 2012	Chirinos J, Kips J, Jacobs D, Brumback L, Duprez D, "Arterial wave reflections and incident cardiovascular events and heart failure: MESA (Multiethnic Study of Atherosclerosis)", *Journal of American Cardiology*, 60 (21):2170-2177 (2012).
Chu and Chuang 2015	Chu C, Chuang C, "Ratiometric optical fiber sensor for dual sensing of copper ion and dissolved oxygen", *Applied Optics*, 54 (36):10659-10665 (2015).
Clausen and Glott 2014	Clausen I and Glott T, "Development of clinically relevant implantable pressure sensors: perspectives and challenges", *Sensors*, 14 (9):17686-17702 (2014).
Consales *et al.* 2012	Consales M, Ricciardi A, Crescitelli A, Esposito E, Cutolo A, Cusano A., "Lab-on-fiber technology: toward multifunctional optical nanoprobes", *ACS Nano*, 6 (4):3163-3170 (2012).
Corning 2014	Corning Incorporated, "Corning® SMF-28e+® optical fibre" (2014). Available online at www.corning.com (accessed in 9/10/2016).
Cusano *et al.* 2015	Cusano A, Consales M, Crescitelli A, Ricciardi A, "Lab-on-fiber technology", Springer International Publishing, Switzerland (2015).
Darne *et al.* 1989	Darne B, Girerd X, Safar M, Cambien F, Guize L, "Pulsatile versus steady component of blood pressure: a cross sectional analysis and a prospective analysis on cardiovascular mortality", *Hypertension*, 13 392-400 (1989).
DGS 2015	Direção-Geral da Saúde, "A Saúde dos Portugueses - Perspetiva 2015", available online at www.dgs.pt (accessed in 9/8/2016).
Ding *et al.* 2011	Ding F, Fan W, Zhang R, Zhang Q, Wang J, "Validation of the non-invasive assessment of central blood pressure by the SphygmoCor and Omron devices against the invasive catheter measurement",

	American Journal of Hypertension, 24 (12):1306-1311 (2011).
Domingues *et al.* 2016	Domingues M F, Frizera-Neto A, Marques C, Leitão C, Lima R, *et al.*, "Implementation of an insole matrix of FBG sensors for plantar pressure monitor", *Advanced Laser Technologies*, Galway, Ireland, September (2016).
Drzewiecki *et al.* 1983	Drzewiecki M, Melbin J and Noordergraaf A, "Arterial tonometry: review and analysis", *Journal of Biomechanics*, (16):141–52, 1983.
European Score Memocard	EACPR and European Society of Cardiology, "European SCORE Memocard (Systematic Coronary Risk Evaluation) – Think total cardiovascular risk & act for better CVD prevention". Available online at www.escardio.org (accessed in 09/09/2016).
Fibercore 2013	Fibercore, "Boron Doped Photosensitive Fiber - datasheet" (2013). Available online at http://fibercore.com/product/boron-doped-photosensitive-fiber (accessed in 09/12/2016).
García-Ortiz *et al.* 2012	García-Ortiz L, Recio-Rodríguez J, Canales-Reina J, Cabrejas-Sánchez A, Gomez-Arranz A, "Comparison of two measuring instruments, B-pro and SphygmoCor system as reference, to evaluate central systolic blood pressure and radial augmentation index", Hypertension Research, 35 (6):617-623 (2012).
Ghatak and Thyagarajan 1998	Ghatak A and Thyagarajan K, "Introduction to fiber optics", Cambridge University Press, USA (1998).
Giannetti *et al.* 2015	Giannetti A,*, Barucci A, Franco Cosi F, Pelli S, Tombelli S, "Optical fiber nanotips coated with molecular beacons for DNA detection", *Sensors*, 15 (5):9666-9680 (2015).
Grassini *et al.* 2014	Grassini S, Ishtaiwi M, Parvis M, Vallan A, "Design and deployment of low-cost plastic optical fiber sensors for gas monitoring", *Sensors*, 15 (1):485-498 (2014).
Grattan and Sun 2000	Grattan K, Sun T, "Fiber optic sensor technology: an overview", *Sensors and Actuators*, 82 40-61 (2000).
Grillet *et al.* 2008	Grillet A, Kinet D, Witt J, Schukar M, Krebber K, *et al.*, "Optical fiber sensors embedded into medical textiles for healthcare monitoring", *IEEE Sensors Journal*, 8 (7):1215-1222 (2008).
Guo *et al.* 2016	Guo T, Liu F, Liang X, Qiu X, Huang Y, *et al.* "Highly sensitive detection of urinary protein variations using tilted fiber grating sensors with plasmonic nanocoatings", *Biosensors and Bioelectronics*, 78, 221-228 (2016).

Heng *et al.* 2016	Heng S, McDevitt C, Kostecki R, Morey J, Eijkelkamp B, *et al.*, "Microstructured optical fiber-based biosensors: reversible and nanoliter-scale measurement of zinc Ions", *ACS Applied Materials and Interfaces*, 8 (20):12727-12732 (2016).
Henken *et al.* 2012	Henken K, Van Gerwen D, Dankelman J, Van Den Dobbelsteen J, "Accuracy of needle position measurements using fiber Bragg gratings", *Minimally Invasive Therapy and Allied Technologies*, 21 (6):408–414 (2012).
Herbert *et al.* 2014	Herbert A, Cruickshank J, Laurent S, and Boutouyrie P, on behalf of The Reference Values for Arterial Measurements Collaboration, "Establishing reference values for central blood pressure and its amplification in a general healthy population and according to cardiovascular risk factors", *European Heart Journal*, 35 (44):3122-3133 (2014).
Hill *et al.* 1978	Hill K, Fujii Y, Johnson D, and Kawasaki B, "Photosensitivity in optical fiber waveguides: Application to reflection filter fabrication", *Applied Physics Letters*, 32 (10):647-649 (1978).
Hirata *et al.* 2006	Hirata K, Yaginuma T, O'Rourke M, Kawakami M, "Age-related changes in carotid artery flow and pressure pulses", *Stroke*, 37, (10):2552-2556 (2006).
Horváth *et al.* 2010	Horváth I, Németh A, Lenkey Z, Alessandri N, Tufano F, "Invasive validation of a new oscillometric device (Arteriograph) for measuring augmentation index, central blood pressure and aortic pulse wave velocity", *Journal of Hypertension*, 28 (10):2068-2075 (2010).
Jing *et al.* 2015	Jing N, Zheng J, Zhao X, Teng C, "Refractive index sensing based on a side-polished macrobending plastic optical fiber", *IEEE Sensors Journal*, 15 (5):2898-2901 (2015).
ISO 2003	Organization for Standardization, "ISO 13485:2003 Medical Devices - Quality Management Systems - Requirements for Regulatory Purposes", Geneva (2013).
Janeway 1904	Janeway T, "The study of clinical blood-pressure", D. Appleton and company, New York (1904).
Janner *et al.* 2010	Janner J, Godtfredsen N, Ladelund S, Vestbo J, Prescott E, "Aortic augmentation index: reference values in a large unselected population by means of the SphygmoCor device", *American Journal of Hypertension*, 23 (2):180-185 (2010).
Jonckheere *et al.* 2009	Jonckheere J, Jeanne M, Narbonneau F, Witt J, Paquet B, et al, "OFSETH: A breathing motions monitoring system for patients under MRI", Proceedings of the *Annual International Conference of the IEEE*

Engineering in Medicine and Biology Society, 2010 1016-1019 (2010).

Kaess *et al.* 2012 | Kaess B, Rong J, Larson M, Hamburg N, Vita J, *et al.*, "Aortic stiffness, blood pressure progression, and incident hypertension", *Journal of American Medical Association*, 309 (9):875-881 (2012).

Kahandawa *et al.* 2012 | Kahandawa G, Epaarachchi G, Wang H, and Lau K, "Use of FBG sensors for SHM in aerospace structures", *Photonic Sensors*, 3 (3):203-214 (2012).

Kalachev *et al.* 2005 | Kalachev A, Pureur V, Nikogosyan D, "Investigation of long-period fiber gratings induced by high-intensity femtosecond UV laser pulses", *Optics Communications*, 246 107-115 (2005).

Kannel *et al.* 1971 | Kannel W, Gordon T, Schwartz M, "Systolic versus diastolic blood pressure and risk of coronary heart disease: the Framingham study", *American Journal of Cardiology*, 27 335-346 (1971).

Kannel *et al.* 1981 | Kannel W, Wolf P, McGee D, "Systolic blood pressure, arterial rigidity and risk of stroke: the Framingham study", *Journal of the American Medical Association*, 245 1225-1229 (1981).

Keiser 2003 | Keiser G, "Optical fiber communications", *Encyclopedia of Telecommunications*, John Wiley & Sons (2003).

Keizer *et al.* 2015 | Keizer J, Martins M, Prats S, Santos L, Vieira D, *et al.*, "Assessing the performance of a plastic optical fibre turbidity sensor for measuring post-fire erosion from plot to catchment scale", *Soil*, 1 641-650 (2015).

Kelly *et al.* 1989 | Kelly R, Hayward C, Avolio A, O'Rourke M, "Noninvasive determination of age-related changes in the human arterial pulse", *Circulation*, 80 1652-1659 (1989).

Kips *et al.* 2010 | Kips J, Vanmolkot F, Mahieu D, Vermeersch S, Fabry I, *et al.*, "The use of diameter distension waveforms as an alternative for tonometric pressure to assess carotid blood pressure", *Physiological Measurement*, 31 (4):543-53 (2010).

Kips 2011 | Kips J, "Development and validation of non-invasive diagnostic tools for the assessment of arterial stiffness and wave reflections with application in sub-Saharan Africa", PhD Thesis, Gent University (2011).

Krejza *et al.* 2006 | Krejza J, Arkuszewski M, Kasner S, Weigele J, Ustymowicz A, *et al.*, "Carotid artery diameter in men and women and the relation to body and neck size", *Stroke*, 37 (4):1103-1105 (2006).

Laurent *et al.* 2001 | Laurent S, Boutouyrie P, Asmar R, Gautier I, Laloux B, "Aortic stiffness is an independent predictor of all-cause and cardiovascular mortality in hypertensive patients", *Hypertension*, 37 1236-1241 (2001).

Laurent *et al.* 2003	Laurent S, Katsahian S, Fassot C, Tropeano A, Gautier I, *et al.*, “Aortic stiffness is an independent predictor of fatal stroke in essential hypertension”, *Stroke*, 34 (5):1203-1206 (2003).
Laurent *et al.* 2006	Laurent S, Cockcroft J, Van Bortel L, Boutouyrie P, Giannattasio C, *et al.*, "Expert consensus document on arterial stiffness: methodological issues and clinical applications", *European Heart Journal*, 27 (21):2588-2605 (2006).
Leitão *et al.* 2013	Leitão C, Bilro L, Alberto N, Antunes P, Lima H, *et al.*, "Feasibility studies of Bragg probe for noninvasive carotid pulse waveform assessment", *Journal of Biomedical Optics*, 18 017006-017006 (2013).
Leitão *et al.* 2016	Leitão C, Antunes P, Marques C, Domingues M F, Pinto J, *et al.*, “Assessing central arterial pressure with a collar POF intensity sensor”, *The 25th International Conference on Plastic Optical Fibres* (*POF*), Birmingham-UK, September (2016).
Lewis 1994	Lewis O, “Stephen Hales and the measurement of blood pressure”, *Journal of Human Hypertension*, 8 (12):865-971 (1994).
Li *et al.* 2012	Li Q, Qiu T, Hao H, Zhou H, Wang T, *et al.*, “Rapid and on-site analysis of illegal drugs on the nano-microscale using a deep ultraviolet-visible reflected optical fiber sensor”, *Analyst*, 137 (7):1596-1603 (2012).
London *et al.* 2001	London G, Blacher J, Pannier B, Guérin A, Marchais S, “Arterial wave reflections and survival in end-stage renal failure”, *Hypertension*, 38 434-438 (2001).
London and Pannier 2010	London G, Pannier B, “Arterial functions: how to interpret the complex physiology”, *Nephrology Dialysis Transplantation*, 25 3815-3823 (2010).
Lorenz *et al.* 2007	Lorenz M, Markus H, Bots M, Rosvall M, Sitzer M, “Prediction of clinical cardiovascular events with carotid intima-media thickness: a systematic review and meta-analysis”, *Circulation*, 115 459–467 (2007).
Mahomed 1872	Mahomed F, “The physiology and clinical use of the sphygmograph”, *Medical Times Gazette*, II:62 (1872).
Mancia *et al.* 2013	Mancia G, Fagard R, Narkiewicz K, Redon J, Zanchetti A, *et al.*,“2013 ESH/ESC Guidelines for the management of arterial hypertension”, *European Heart Journal*, 34 2159-2219 (2013).
Marey 1863	Marey E, “Physiologie medicale de la circulation du sang”, Adrien Delahaye ed., France (1863).
Marieb and Hoehn 2012	Marieb E and Hoehn K, “The cardiovascular system: blood vessels”, in *Human Anatomy & Physiology*, Marieb E and Hoehn K (eds.), 9th

	edition, Pearson publishing, Cambridge (2012).
Marques 2013	Marques C*,* "Fiber-optic components for optical communications and sensing", PhD thesis, University of Aveiro (2013).
Marques *et al.* 2015	Marques C, Peng G, Webb D, "Highly sensitive liquid level monitoring system utilizing polymer fiber Bragg gratings", *Optics express*, 23 (5):6058-6072 (2015).
Martinez-Sanchez and Alexandrov 2013	Martinez-Sanchez P, Alexandrov A, "Ultrasonography of carotid plaque for the prevention of stroke", *Expert review of cardiovascular therapy*, 11 (10):1425-1440 (2013).
Massaroni *et al.* 2015	Massaroni C, Saccomandi P, Schena E, "Medical smart textiles based on fiber optic technology: an overview", *Journal of Functional Biomaterials*, 6 (2):204-221 (2015).
Masugata and Senda 2010	Masugata H, Senda S.," Clinical significance of central blood pressure measurement in antihypertensive treatment", *Expert Review on Cardiovascular Therapy*, 8 (6):763-765 (2010).
Matsui *et al.* 2004	Matsui Y, Kario K, Ishikawa J, Eguchi K, Hoshide S, Himada K, "Reproducibility of arterial stiffness indices (pulse wave velocity and augmentation index) simultaneously assessed by automated pulse wave analysis and their associated risk factors in essential hypertensive patients", *Hypertension Research*, 27 (11):851-857 (2004).
McEniery *et al.* 2008	McEniery C, McDonnell B, Munnery M, Wallace S, Rowe C, "Central pressure: variability and impact of cardiovascular risk factors - the Anglo-Cardiff collaborative trial II", *Hypertension*, 51 1476-1482 (2008).
McEniery *et al.* 2014	McEniery C, Cockcroft J, Roman M, Franklin S, Wilkinson I, "Central blood pressure: current evidence and clinical importance", *European Heart Journal*, 35 (26):1719-1725 (2014).
Meinders and Hoeks 2004	Meinders J, Hoeks A, "Simultaneous assessment of diameter and pressure waveforms in the carotid artery", *Ultrasound and Medicine and Biology*, 30 (2):147-154 (2004).
Meltz *et al.* 1989	Meltz G., Morey W, Glenn W, "Formation of Bragg gratings in optical fibers by a transverse holographic method", *Optics letters*, 14 (15):823-825 (1989).
Mesquita *et al.* 2016	Mesquita E, Paixão T, Antunes P, Coelho F, Ferreira P, "Groundwater level monitoring using a plastic optical fiber", *Sensors and Actuators A*, 240 (16):138-144 (2016).

Mesquita-Bastos *et al.* 2010	Mesquita-Bastos J, Bertoquini S, Polónia J, "Cardiovascular prognostic value of ambulatory blood pressure monitoring in a Portuguese hypertensive population followed up for 8.2 years", *Blood Pressure Monitoring*, 15 (4):240-246 (2010).
Mishra *et al.* 2011	Mishra V, Singh N, Tiwari U, Kapur P, "Fiber grating sensors in medicine: Current and emerging applications", *Sensors and Actuators A: Physical*, 167 (2):279-290 (2011).
Mitchell *et al.* 2004	Mitchell G, Parise H, Benjamin E, Larson M, Keyes M, *et al.*, "Changes in arterial stiffness and wave reflection with advancing age in healthy men and women: the Framingham Heart Study", *Hypertension*, 43 (6):1239-1245 (2004).
Mitchell *et al.* 2010	Mitchell G, Hwang S, Vasan R, Larson M, Pencina M, "Arterial stiffness and cardiovascular events – The Framingham Heart Study", *Circulation*, 121 (4):505-511 (2010).
Mitchell *et al.* 2011	Mitchell G, Buchem M, Sigurdsson S, Gotal J, Jonsdottir M, "Arterial stiffness, pressure and flow pulsatility and brain structure and function: the Age, Gene/Environment Susceptibility – Reykjavik Study", *Brain*, 134, 3398-3407 (2011).
Mitsubishi 2010	Mitsubishi Rayon Co., "ESKATM Premier Polyethylene Jacketed Optical Fiber Cord: GH4001", available online at i-fiberoptics.com/pdf/gh4001.pdf (accessed in 09/12/2016).
Muiesan *et al.* 2013	Muiesan M, Salvetti M, Rizzoni D, Paini A, Agabiti-Rosei C, "Pulsatile hemodynamics and microcirculation evidence for a close relationship in hypertensive patients", *Hypertension*, 61 130-136 (2013).
Murgo *et al.* 1980	Murgo J, Westerhof N, Giolma P, and Altobelli A, "Aortic input impedance in normal man: relationship to pressure wave shape". *Circulation*, 62 105-116 (1980).
Miyashita *et al.* 2012	Miyashita H, "Clinical assessment of central blood pressure", *Current Hypertension Reviews*, 8 (2):80-90 (2012).
Narbonneau *et al.* 2008	Narbonneau F, Kinet D, Paquet B, Depré A, Jonckheere J, *et al.*, "Smart textile embedding optical fibre sensors for healthcare monitoring during MRI", *Advances in Science and Technology*, 60, 134-143 (2008).
Nezhat 2011	Nezhat C, "History of endoscopy", Endo:Press, Germany (2011).
Nichols 1990	Nichols W, "Properties of arterial wall", in *McDonald's blood flow in arteries: theoretical, experimental and clinical principles*, Nichols W, O'Rourke M, Vlachopoulos C (eds), CRC Press, Boca Raton (1990).

Nichols 2005	Nichols W, “Clinical measurement of arterial stiffness obtained from noninvasive pressure waveforms”, *American Journal of Hypertension*, 18, 3S-10S (2005).
O’Keeffe *et al.* 2015	O'Keeffe S, McCarthy D, Woulfe P, Grattan M, Hounsell A, “A review of recent advances in optical fibre sensors for in vivo dosimetry during radiotherapy”, *The British Journal of Radiology*, 88 (1050):20140702 (2015).
Orłowska *et al.* 2015	Orłowska K, Słupski P, Świątkowski M, Kunicki P, Sankowska S, Gotszalk T, “Light intensity fibre optic sensor for MEMS displacement and vibration metrology”, *Optics & Laser Technology*, 65 159-163 (2015).
O’Rourke 1990	O’Rourke M, “Arterial stiffness, systolic blood pressure, and logical treatment of arterial hypertension”, *Hypertension*, 15 (4):339-47 (1990).
O’Rourke 1999	O’Rourke M, “Mechanical principles. Arterial stiffness and wave reflection”, *Pathology Biology*, 47 (6):623-633 (1999).
O’Rourke and Nichols 2005	O’Rourke M, Nichols W, “Aortic diameter, aortic stiffness, and wave reflection increase with age and isolated systolic hypertension”, *Hypertension*, 45 (part2):652-658 (2005).
O’Rourke *et al.* 2010	O’Rourke M, Safar and Victor Dzau, “The Cardiovascular Continuum extended: Aging effects on the aorta and microvasculature”, *Vascular Medicine*, 16 (6):146-468 (2010).
Othonos 1997	Othonos A, “Fiber Bragg gratings”, *Review of Scientific Instruments*, 68 (12):4309-4341 (1997).
Othonos and Kalli 1999	Othonos A, Kalli K, “Fiber Bragg gratings – Fundamentals and applications in telecommunications and sensing”, Artech House, USA (1999).
Park *et al.* 2010	Park Y-L, Elayaperumal S, Daniel B, Ryu S, Shin M, *et al.*, “Real-time estimation of 3-D needle shape and deflection for MRI-Guided interventions”, *IEEE/ASME Transactions on Mechatronics*, 15 (6):906-915 (2010).
Pauca and Wallenhaupt 1992	Pauca A, Wallenhaupt S, “Does radial artery pressure accurately reflect aortic pressure?”, *Chest*, 102 1193-98 (1992).
Pereira *et al.* 2014	Pereira T, Maldonado J, Coutinho R, Cardoso E, Laranjeiro M, *et al.*, “Invasive validation of the Complior Analyse in the assessment of central artery pressure curves: a methodological study”, Blood Pressure Monitoring, 19 (5):280-287 (2014).

Peters 2011	Peters K, “Polymer optical fiber sensors – a review”, *Smart Materials and Structures*, 20 (1):013002 (2011).
Petrovic *et al.* 2014	Petrovic M, Petrovic J,Danicic A, M. Vukcevic M, Bojovic B, “Non-invasive respiratory monitoring using long-period fiber grating sensors”, *Biomedical Optics Express*, 5 (4):1136 (2014).
Piepoli *et al.* 2016	Piepoli M, Hoes A, Agewall S, Albus C, Brotons C, “2016 European Guidelines on cardiovascular disease prevention in clinical practice”, *European Heart Journal*, ehw106, 1-78 (2016).
Pini *et al.* 2008	Pini R, Cavallini C, Palmieri V, Marchionni N, Di Bari M, “Central but not brachial blood pressure predicts cardiovascular events in an unselected geriatric population: the ICARe Dicomano study”, *Journal of American College of Cardiology*, 51 (25) 2432-2439 (2008).
Poeggel *et al.* 2015	Poeggel S, Tosi D, Duraibabu D, Leen G, McGrath D, Lewis Elfed, “Optical fibre pressure sensors in medical applications”, *Sensors*, 15 (7):17115-17148 (2015).
Polak *et al.* 2016	Polak J, Carter S, Pellerito J, “Hemodynamic considerations in peripheral vascular rand cerebrovascular disease”, available online at http://radiologykey.com/hemodynamic-considerations-in-peripheral-vascular-and-cerebrovascular-disease/ (accessed in 09/06/2016).
Pospíšilová *et al.* 2015	Pospíšilová M, Kuncová G and Trögl J, “Fiber-optic chemical sensors and fiber-optic bio-sensors”, *Sensors*, 15 (10): 25208-25259 (2015).
Powalowski *et al.* 2000	Powalowski T, Trawinski Z, Hilgertner L, “Common carotid wall elasticity and intima-media thickness, examinations by means of ultrasound”, *Archives of Acoustics*, 25 (2):205-212 (2000).
Prehn *et al.* 2009	Prehn J, Vincken K, Sprinkhuizen S, Viergever M, van Keulen J., “Aortic pulsatile distention in young healthy volunteers is asymmetric: analysis with ECG-gated MRI”, *European Journal of Vascular and Endovascular Surgery*, 37 168-174 (2009).
Pucci *et al.* 2013	Pucci G, Cheriyan J, Hubsch A, Hickson S, Gajendragadkar P, *et al.*, “Evaluation of the Vicorder, a novel cuff-based device for the noninvasive estimation of central blood pressure”, *Journal of Hypertension*, 31 (1):77-85 (2013).
Pucci *et al.* 2014	Pucci G, Battista F, Schillaci G, “Effects of antihypertensive drugs on central blood pressure: new evidence, more challenges”, *Hypertension Research*, 37 (1):10-12 (2014).
Qasem *et al.* 2008	Qasem A, Avolio A, “Determination of aortic pulse wave velocity from waveform decomposition of the central aortic pressure pulse”,

	Hypertension 51, 188-195 (2008).
Quandt *et al.* 2015	Quandt B, Scherer L, Boesel L, Wolf M, Bona G, Rossi R, "Body-monitoring and health supervision by means of optical fiber-based sensing systems in medical textiles", *Advanced Healthcare Materials*, 4 (3):330-355 (2015).
Redheuil *et al.* 2011	Redheuil A, Yu W, Mousseaux E, Harouni A, Kachenoura N, *et al.* "Age-related changes in aortic arch geometry: relationship with proximal aortic function and left ventricular mass and remodelling", *Journal of American College of Cardiology*, 58 (12):1262-1270 (2011).
Ricciardi *et al.* 2015	Ricciardi A, Crescitelli A, Vaiano P, Quero G, Consales M, *et al.* "Lab-on-fiber technology: a new vision for chemical and biological sensing", *The Analyst*, 140 (24):8068-79 (2015).
Riva-Rocci 1896	Riva-Rocci S, "Un nuovo sfigmomanometro", *Gazzetta medica di Torino*, 47 981-996, 1001-1017 (1896).
Rodríguez *et al.* 2014	Rodríguez A, Zamarreño C, Matías I, Arregui F, Cruz R, May-Arrioja D, "A fiber optic ammonia sensor using a universal pH indicator", *Sensors*, 14 (3):4060-4073 (2014).
Roman *et al.* 2007	Roman M, Devereux R, Kizer J, Lee E, Galloway J, *et al.* "Central pressure more strongly relates to vascular disease and outcome than does brachial pressure: the strong heart study", *Hypertension*, 50 197-203, (2007).
Roman *et al.* 2009	Roman M, Devereux R, Kizer J, Okin P, Lee E, "High central pulse pressure is independently associated with adverse cardiovascular outcome: the strong heart study", *Journal of American College of Cardiology*, 54 (18): 1730-1734 (2009).
Roman *et al.* 2010	Roman M, Okin P, Kizer J, Lee E, Howard B and Devereux R, "Relations of central and brachial blood pressure to left ventricular hypertrophy and geometry: the Strong Heart Study", *Journal of Hypertension*, 28 (2):384-388 (2010).
Roriz *et al.* 2013	Roriz P, Frazão O, Lobo-Ribeiro A, Santos J, Simões J, "Review of fiber-optic pressure sensors for biomedical and biomechanical applications", *Journal of Biomedical Optics*, 18 (5):050903 (2013).
Rothmaier *et al.* 2008	Rothmaier M, Luong M, Clemens F, "Textile Pressure Sensor Made of Flexible Plastic Optical Fibers", *Sensors*, 8 (7):4318-4329 (2008).
Rothwell 2000	Rothwell P, "Carotid artery disease and the risk of ischaemic stroke and coronary vascular events", *Cerebrovascular diseases*, 10 (5):21-33 (2000).

Safar *et al.* 2002	Safar M, Blacher J, Pannier B, Guerin A, Marchais S, *et al.* "Central pulse pressure and mortality in end-Stage renal disease", *Hypertension*, 39 735-738 (2002).
Safar *et al.* 2003	Safar M, Levy B, Struijker-Boudier H, "Current perspectives on arterial stiffness and pulse pressure in hypertension and cardiovascular diseases", *Circulation*, 107 (22):2864-9 (2003).
Safar 2007	Safar M, "Arterial stiffness: a simplified overview in vascular medicine", in *Atherosclerosis, Large Arteries and Cardiovascular Risk*, Safar M and Frohlich E (eds), S. Karger AG, Basel, 2007.
Safar and Jankowski 2009	Safar M, Jankowski P, "Central blood pressure and hypertension: role in cardiovascular risk assessment", *Clinical Science*, 116 (4):273-282 (2009).
Safar 2010	Safar M, "Arterial aging-hemodynamic changes and therapeutic options", *Nature Reviews Cardiology*, 7 (8):442-449 (2010).
Schena *et al.* 2016	Schena E, Tosi D, Saccomandi P, Lewis E, Kim T, "Fiber optic sensors for temperature monitoring during thermal treatments: an overview", Sensors, 16 (7):1144 (2016).
Sharath *et al.* 2014	Sharath U, Shwetha C, Anand K, Asokan S4., "Radial arterial compliance measurement by fiber Bragg grating pulse recorder", *Journal of Human Hypertension*, 28 736-742 (2014).
Sharath *et al.* 2015	Sharath U, Padma S, Ambastha S, Anand K, Asokan S, "Pulse transit time differential measurement by fiber Bragg grating pulse recorder", *Journal of Biomedical Optics*, 20 (5): 057005 (2015).
Silva *et al.* 2011	Silva A, Carmo J, Mendes P and Correia J, "Simultaneous cardiac and respiratory frequency measurement based on a single fiber Bragg grating sensor", *Measurement Science and Technology*, 22 (7):075801 (2011).
Silva *et al.* 2013	Silva A, Catarino A, Correia M, Frazão O, "Design and characterization of a wearable macrobending fiber optic sensor for human joint angle determination", *Optical Engineering*, 52 (12):126106 (2013).
Silvestri and Schena 2011	Silvestri S, Schena E, "Optical-fiber measurement systems for medical applications", Chapter 11 in *Optoelectronics - Devices and Applications,* Predeep, InTech (2011).
Song *et al.* 2011	Song H, Kim K, Lee J, "Development of optical fiber Bragg grating force-reflection sensor system of medical application for safe minimally invasive robotic surgery", *The Review of Scientific Instruments*, 82 (7):074301 (2011).

Srinivasan *et al.* 2016	Srinivasan R, Umesh S, Murali S, Asokan S, Siva Gorthi S. “Bare fiber Bragg grating immunosensor for real-time detection of Escherichia coli bacteria”, *Journal of Biophotonics*, (Epub ahead of print) (2016).
Stea *et al.* 2014	Stea F, Bozec E, Millasseau S, Khettab H, Boutouyrie P, *et al.*, “Comparison of the Complior Analyse device with Sphygmocor and Complior SP for pulse wave velocity and central pressure assessment”, *Journal of Hypertension*, 32 (4):873-880 (2014).
Stergiou *et al.* 2016	Stergiou G, Parati G, Vlachopoulos C, Achimastos A, Andreadis E, “Methodology and technology for peripheral and central blood pressure and blood pressure variability measurement: current status and future directions - Position statement of the European Society of Hypertension Working Group on blood pressure monitoring and cardiovascular variability”, *Journal of Hypertension*, 34 (9):1665-1677 (2016).
Sztrymf *et al.* 2013	Sztrymf B, Jacobs F, Chemla D, Richard C, Millasseau S, “Validation of the new Complior sensor to record pressure signals non-invasively”, *Journal of Clinical Monitoring and Computing*, 27 (6):613-619 (2013).
Tabassum *et al.* 2013	Tabassum R, Mishra S, Gupta B, “Surface plasmon resonance-based fiber optic hydrogen sulphide gas sensor utilizing Cu-ZnO thin films”, *Physical Chemistry Chemical Physics*, 15 (28):11868-11874 (2013).
Taffoni *et al.* 2013	Taffoni F, Formica D, Saccomandi P, Di Pino G and Schena E, “Optical fiber-based MR-Compatible sensors for medical applications: an overview”, *Sensors*, 13 (10):14105-14120 (2013).
Tawil *et al.* 2014	Tawil N, Sacher E, Mandeville R, Meunier M., “Bacteriophages: biosensing tools for multi-drug resistant pathogens”, *Analyst*, 139 (6):1224-1236 (2014).
Turkbey *et al.* 2013	Turkbey E, Jain A, Johnson C, Redheuil A, Arai A., *et al.*, “Determinants and normal values of ascending aortic diameter by age, gender, and race/ethnicity in the multi-ethnic study of atherosclerosis (MESA)”, *Journal of Magnetic Resonance Imaging*, (00):000-000 (2013).
Tosi *et al.* 2016	Tosi D, Saccomandi P, Schena E, Duraibabu D, Poeggel S, *et al.*, “Intra-tissue pressure measurement in ex vivo liver undergoing laser ablation with fiber-optic Fabry-Perot probe”, *Sensors*, 16 (4):544 (2016).
Ueda *et al.* 2004	Ueda H, Hayashi T, Tsumura K, Yoshimaru K, Nakayama Y, Yoshikawa J., “The timing of the reflected wave in the ascending aortic pressure predicts restenosis after coronary stent placement”, *Hypertension research*, 27 (8):523-540 (2004).
Van Bortel *et*	Van Bortel L, Balkestein E, van der Heijden-Spek J, Vanmolkot F, Staessen J, *et al.* “Non-invasive assessment of local arterial pulse

al. 2001	pressure: comparison of applanation tonometry and echo-tracking", *Journal of Hypertension*, 19 (6):1037-1044 (2001).
Van Bortel *et al.* 2012	Bortel L, Laurent S, Boutouyrie P, Chowienczyk P, Cruickshank J, "Expert consensus document on the measurement of aortic stiffness in daily practice using carotid-femoral pulse wave velocity", *Journal of Hypertension*, 30 (3):445-448 (2012).
Van Brakel *et al.* 2005	Van Brakel A, Swart P, Chtcherbakov A, Shlyagin M, "Blood pressure manometer using a twin Bragg grating Fabry-Perot interferometer", Proc. SPIE 5634, *Advanced Sensor Systems and Applications II*, 5634 595 (2005).
Vermeersch *et al.* 2008	Vermeersch S, Rietzschel E, De Buyzere M, De Bacquer D, De Backer G, *et al.* "Determining carotid artery pressure from scaled diameter waveforms: comparison and validation of calibration techniques in 2026 subjects", *Physiological Measurement*, 29 (11):1267-1280 (2008).
Vlachopoulos *et al.* 2000	Vlachopoulos C, O'Rourke M, "Diastolic pressure, systolic pressure, or pulse pressure?", *Current Hypertension Reports*, 2 (3):271-279 (2000).
Vlachopoulos *et al.* 2010	Vlachopoulos C, Aznaouridis K, O'Rourke M, Safar M, Baou K, Stefanadis C, "Prediction of cardiovascular events and all-cause mortality with central haemodynamics: a systematic review and meta-analysis", *European Heart Journal*, 31 (15):1865-1871 (2010).
Vosse and Stergiopulos 2011	Vosse F and Stergiopulos N, "Pulse wave propagation in the arterial tree", *Annual Review of Fluid Mechanics*, 43 467-499 (2011).
Wang *et al.* 2014	Wang D, Jia P, Ma Z, Xie L, Liang Q, "Tip-sensitive fibre-optic Bragg grating ultrasonic hydrophone for measuring high-intensity focused ultrasound fields", *Electronics letters*, 50 (9):649-650 (2014).
Wassertheurer *et al.* 2010	Wassertheurer S, Kropf J, Weber T, van der Giet M, Baulmann J, "A new oscillometric method for pulse wave analysis: comparison with a common tonometric method", *Journal of Human Hypertension*, 24 (8):498-504 (2010).
Weber *et al.* 2004	Weber T, Auer J, O'Rourke M, Kvas E, Lassnig E, *et al.*, "Arterial stiffness, wave reflections, and the risk of coronary artery disease", *Circulation*, 109 184-189 (2004).
Weber and Segers 2015	Weber T, Segers P, "Changes in central hemodynamics, wave reflection, and heart-vessel coupling with normal and accelerated aging", chapter in *Early Vascular Aging (EVA)*, Nilsson P, Olsen M, Laurent M (eds.), Academic Press, Elsevier (2015).
Weiss *et al.*	Weiss W, Gohlisch C, Harsch-Gladisch C, Tölle M, Zidek W, van der

2012	Giet M., "Oscillometric estimation of central blood pressure: validation of the Mobil-O-Graph in comparison with the SphygmoCor device", *Blood pressure monitoring*, 17 (3):128-131 (2012).
Westerhof *et al.* 2009	Westerhof N, Lankhaar J, Westerhof B, "The arterial Windkessel", *Medical & Biological Engineering & Computing*, 47 (2):131-141 (2009).
Wilkinson *et al.* 2000	Wilkinson I, MacCallum H, Flint L, Cockcroft J, Newby D, Webb D, "The influence of heart rate on augmentation index and central arterial pressure in humans", *The Journal of Physiology*, 525, (Pt1):263-270 (2000).
Wilkinson *et al.* 2010	Wilkinson I, McEniery M, Schillaci G, Boutouyrie P, Segers P, *et al.*, "ARTERY Society guidelines for validation of non-invasive haemodynamic measurement devices: Part 1, arterial pulse wave velocity", *Artery Research*, 4 (2):34-40 (2010).
Williams *et al.* 2006	Williams B, Lacy PS, Thom SM, Cruickshank K, Stanton A, et al, "Differential impact of blood pressure-lowering drugs on central aortic pressure and clinical outcomes: principal results of the Conduit Artery Function Evaluation (CAFE) study", *Circulation*, 113 1213-1225 (2006).
Williams *et al.* 2011	Williams B, Lacy P, Yan P, Hwee C, Liang C, Ting C, "Development and validation of a novel method to derive central aortic systolic pressure from the radial pressure waveform using an n-point moving average method", *Journal of American College of Cardiology*, 57 (8):951-961 (2011).
Wittliff *et al.* 2008	Wittliff J, Andres S, Kruer T, Kerr D, Smolenkova I, Erb J, "Biosensors for detecting estrogen-like molecules and protein biomarkers", *Advances in Experimental Medicine and Biology*, 614 315:322 (2008).
Wojciechowska *et al.* 2006	Wojciechowska W, Staessen J, Nawrot T, Cwynar M, Seidlerová J, *et al.*, "Reference values in white Europeans for the arterial pulse wave recorded by means of the SphygmoCor device", *Hypertension Research*, 29 (7):475-483 (2006).
Woodrow 2000	Woodrow P, "Intensive care nursing: a framework for practice", Ashworth P (ed.), Routledge, London (2000).
WHO 2011	World Health Organization, "Global atlas on cardiovascular disease prevention and control", Mendis S, Puska P, Norrving B (eds), Geneva, 2011. Available online at www.who.int (accessed in 09/09/2016).
WHO 2016	World Health Organization, "Hypertension", 2016. Available online at www.world-heart-federation.org/cardiovascular-health/cardiovascular-disease-risk-factors/hypertension/ (accessed in 10/10/2016).
Xiong *et al.*	Xiong Z, Peng G, Wu B, and Chu P., "Highly tunable Bragg gratings in

1999	single-mode polymer optical fibers", *IEEE Photonics Letters*, 11, (3):352-354 (1999).
Ye at el. 2009	Ye C, Dulieu-Barton J, Webb D, Zhang C, Peng G, *et al.*, "Applications of polymer optical fibre grating sensors to condition monitoring of textiles", Proceedings of the SPIE, *20th International Conference on Optical Fibre Sensors*, 7503 75030 (2009).
Yildirim *et al.* 2014	Yildirim N, Long F, He M, Shi H, Gu A, "A portable optic fiber aptasensor for sensitive, specific and rapid detection of bisphenol-A in water samples", *Environmental Science – Processes & Impacts*, 16 (6):1379-1386 (2014).
Yokoyama *et al.* 2008	Yokoyama K, Nakagawa H, Shah DC, Lambert H, Leo G, *et al.*, "Novel contact force sensor incorporated in irrigated radiofrequency ablation catheter predicts lesion size and incidence of steam pop and thrombus", *Circulation: Arrhytmia and Electrophysiology*, 1 (5):354-362 (2008).
Yuan et al. 2013	Yuan L, Xue D, Duan Y, Cao T, Zhou N, "Maternal carotid remodeling and increased carotid arterial stiffness in normal late-gestational pregnancy as assessed by radio-frequency ultrasound technique", *BMC pregnancy and childbirth*, 27 (13):122 (2013).
Zhang *et al.* 2013	Zhang Y, Agnoletti D, Safar M, Wang J, Topouchian J, *et al.*, "Comparison study of central blood pressure and wave reflection obtained from tonometry-based devices", *American Journal of Hypertension* 26 (1):34-41 (2013).
Zhong *et al.* 2011	Zhong Z, Fritzsche M, Pieper S, Wood T, Lear K, *et al.*, "Fiber optic monooxygenase biosensor for toluene concentration measurement in aqueous samples", *Biosensors and Bioelectronics*, 26 (5):2407-2412 (2011).
Ziemann *et al.* 2008	Ziemann O, Krauser J, Zamzow P, Daum W, "POF handbook - optical short range transmission systems", Springer-Verlag, Germany (2008).
Zuo *et al.* 2010	Zuo J, Li Y, Yan Z, Zhang R, Shen W, Zhu D, "Validation of the central blood pressure estimation by the SphygmoCor system in Chinese", *Blood pressure monitoring*, 15 (5):268-274 (2010).

Publications and communications

A1. Publications in scientific journals

J1. **Leitão C**, Bilro L, Alberto N, Antunes P, Lima H, et al., “Feasibility studies of Bragg probe for non-invasive carotid pulse waveform assessment,” Journal of Biomedical Optics, 18:017006 (2013).

J2. **Leitão C**, Antunes P, André P, Pinto J, Bastos J, “Central arterial pulse waveform acquisition with a portable pen-like optical fibre sensor”, *Blood Pressure Monitoring Journal*, 20 (1):43-6 (2015).

J3. **Leitão C**, Antunes P, Bastos J, Pinto J, André P, “Plastic Optical Fibre Sensor for Noninvasive Arterial Pulse Waveform Monitoring”, *IEEE Sensors Journal*, 15 (1):14-18, (2015).

J4. **Leitão C**, Antunes P, Pinto J, Bastos J, André P, “Optical fiber sensors for central arterial pressure monitoring”, *Optical and Quantum Electronics*, 48 (3):218 (2016).

J5. **Leitão C**, Antunes P, Afreixo V, Andre P, Pinto L, Fernandes R, Costa M, Bastos J, “Comparison study of carotid distension waves measured with a non-invasive optical fibre sensor and aortic invasive pressure waves”, *26th European Meeting on Hypertension and Cardiovascular Protection*, *Journal of Hypertension*, Vol 34, e-Supplement 2 (2016).

J6. **Leitão C**, Antunes P, Pinto J, Bastos J, André P, “Carotid distension waves acquired with a fiber sensor as an alternative to tonometry for central arterial systolic pressure assessment in young subjects”, *Measurement*, 95:45-49 (2017).

J7. **Leitão C**, Ribau V, Afreixo V, Antunes P, André P, Pinto J, Boutouyrie P, Laurent S, Bastos J, “Clinical evaluation of an optical fibre sensor in the assessment of the central arterial pulse waves”, to be submitted to *Journal of Hypertension* (2017).

A2. Book Chapters

B1. Antunes P, **Leitão C,** Rodrigues H, Travanca R, Pinto J L, *et al.*, "Optical Fiber Bragg Grating Based Accelerometers and Applications", Chapter in *Accelerometers: Principles, Structure and Applications*, André P and Varum H (eds), Nova Publisher, New York - USA (2013).

B2. Alberto N, Bilro L, Antunes P, **Leitão C**, Lima H, et al., "Optical Fiber Technology for eHealthcare", Chapter in *Handbook of Research on ICTs and Management Systems for Improving Efficiency in Healthcare and Social Care*, Cruz-Cunha M, Miranda I, Gonçalves P (eds), IGI global, Medical Information Science Reference,

USA (2013).

A3. Communications

C1. Bilro L, Alberto N, Antunes P, **Leitão C**, Lima H, *et al.*, “Photonics for healthcare”. *6º Congresso Luso-Moçambicano de engenharia*, Maputo - Moçambique (2011).

C2. **Leitão C**, Bilro L, Antunes P, Alberto N, Lima H, Pinto J, “Design of Bragg sensor for hemodynamic assessment”, *7th International conference on physics teaching in engineering education (SEFI-PTEE)*, Mannheim - Germany (2011).

C3. **Leitão C**, Lima H, Bilro L, Antunes P, Marques C, *et al.*, “Development and characterization of new sensors for hemodynamic evaluation: fibre Bragg sensor for arterial pulse waveform acquisition”, proceedings of the *2nd Portuguese meeting of Bioengineering* (Portuguese chapter of IEEE EMBS), Coimbra - Portugal (2012).

C4. **Leitão C**, Bilro L, Alberto N, Antunes P, Lima H, *et al.*, "Development of a FBG probe for non-invasive carotid pulse waveform assessment", *Photonics Europe - Biophotonics: Photonic Solutions for Better Health Care*, proceedings of SPIE 8427 1-4, Brussels - Belgium (2012).

C5. **Leitão C**, Novo C, Yang G, Tang C, Pinto J, “Fiber Bragg grating sensors novel applications”, Latin America Optics & Photonics conference (LAOP), The Optical Society of America (OSA), São Sebastião - Brasil (Invited talk) (2012).

C6. **Leitão C**, Antunes P, André P, Pinto J, Bastos J, “Monitorização do risco cardiovascular de uma população com hipertensão resistente e investigação clinica de novo sensor de fibra ótica para avaliar a pressão central”, 20as Jornadas da Cardiologia da Zona Centro, Aveiro – Portugal (Best poster award) (2012).

C7. **Leitão C**, Antunes P, André P, Pinto J, Bastos J, “Monitorização do risco cardiovascular de uma população hipertensa e investigação clinica de novo sensor de fibra ótica para avaliar a pressão central”, 7º Congresso português de hipertensão e risco cardiovascular global, Vilamoura - Portugal (2013).

C8. **Leitão C**, Antunes P, André P, Pinto J, Bastos J, “Cardiovascular risk evaluation of a resistant hypertensive population and clinical investigation of a new optical fibre sensor for central pressure assessment”, 23rd European meeting on hypertension & cardiovascular protection, Milan - Italy (2013).

C10. **Leitão C**, Antunes P, Bastos J, André P, Pinto J, "In the trail of a fiber Bragg grating sensor to assess the central arterial pressure wave profile", Fifth European Workshop on Optical Fibre Sensors, Proceedings of SPIE 8794, 87941C (Best student presentation in its session) Krakow - Poland (2013).

C11. **Leitão C**, Antunes P, Bastos J, Pinto J, André P, “Optical fiber sensors in arterial pulse waveform acquisition”, II International Conference on Applications of Optics and Photonics, Proceedings of SPIE 9286, 92864O-1 (1st Place for student presentation) Aveiro - Portugal (2014).

C12. Antunes P, **Leitão C**, Pinto J, Bastos J, André P, “Optical fiber sensors for blood pressure monitoring.” Advanced Laser Technologies (Invited talk), Faro - Portugal (2015).

C13. **Leitão C**, Gonçalves S, Antunes P, Bastos J, Pinto J, André P, “Central arterial pressure assessment with intensity POF sensor”, International Conference on Optical Fibre Sensors, Curitiba - Brazil (2015).

C14. **Leitão C**, Ribau V, Antunes P, André P, Pinto J, Bastos J, “Avaliação da pressão central usando a onde de distensão carotídea em jovens”, 10º Congresso Português de Hipertensão e risco cardiovascular, Vilamoura - Fevereiro (2016).

C15. **Leitão C**, Antunes P, Marques C, Domingues M F, Pinto J, *et al.*, “Assessing central arterial pressure with a POF intensity sensor placed in a collar”, the 25th International Conference on Plastic Optical Fibres, Birmingham - UK (2016).